2017

Succination Impairs Protein Folding and Promotes Chop Stability in the Adipocyte during Diabetes

Allison Manuel
University of South Carolina

SUCCINATION IMPAIRS PROTEIN FOLDING AND PROMOTES CHOP STABILITY IN THE ADIPOCYTE DURING DIABETES

by

Allison Manuel

Bachelor of Science
University of South Carolina, 2012

Submitted in Partial Fulfillment of the Requirements

For the Degree of Doctor of Philosophy in

Biomedical Science

School of Medicine

University of South Carolina

2017

Accepted by:

Norma Frizzell, Major Professor

James Fadel, Committee Member

Susan Wood, Committee Member

Angela Murphy, Committee Member

Ho-Jin Koh, Committee Member

Cheryl L. Addy, Vice Provost and Dean of the Graduate School

Dedication

I would like to dedicate this manuscript to my loving and supportive parents Nancy and Ernie Manuel who taught me the 5 P's. To my sister Laura and my brother Gregory for always being concerned about the status of my cell culture experiments. To Dr. Gerardo Piroli who has been invaluable to my research training and a wonderful person to work with in the laboratory. And my mentor Dr. Norma Frizzell who first introduced me to academic scientific research and without her I would not be where I am today.

Acknowledgements

First and foremost I would like to thank my mentor Dr. Norma Frizzell for allowing me to work under her guidance as an undergraduate student and further complete my Doctoral Degree in her laboratory. Thank you for your time and patience and willingness to allow me to pursue my own hypothesis and research ideas in the laboratory. I would like to give a special thanks to Dr. Gerardo Piroli and Dr. John Baynes for their expertise and advice throughout the past 6 years. I want to thank Dr. Mike Walla and Dr. Bill Cotham for all of their instruction in the mass spectrometry lab. I would also like to thank our former student Mrs. Sonia Wicker for teaching me new laboratory skills and making lab an enjoyable place to work. In addition, I would like to thank our current students Stephanie Martin and Tulsi Patel and lab technician Josh Wang along with every former Frizzell laboratory member for their dedication and assistance to my research throughout the course of their time in the laboratory.

Thank you to my committee members Drs. Jim Fadel, Susan Wood, Angela Murphy and Ho-Jin Koh for taking the time to participate on my committee and provide constructive advice to advance my scientific critical thinking skills and research projects. I would like to thank the PPN faculty and staff that I have had the pleasure of working with during my graduate career for all of their help and guidance and providing such an enjoyable work atmosphere.

Abstract

Type 2 diabetes mellitus has been diagnosed in ~21 million people in the United States and is closely correlated with obesity, prompting the need for a detailed understanding of adipocyte metabolism in the development of diabetes. The intake of excess nutrients surpasses the energy requirements of the cell and leads to increased mitochondrial stress in the adipocyte. We have shown that this is associated with increased levels of the mitochondrial metabolite fumarate. Fumarate can react with cysteine thiol groups to form the chemical modification S-(2-succino)cysteine (2SC), also termed protein succination. Succination is significantly increased in the adipose tissue of type 2 diabetic mouse models (*ob/ob* and *db/db*) and in adipocytes matured in high glucose medium, resulting in impaired protein function. The endoplasmic reticulum (ER) oxidoreductase protein disulfide isomerase (PDI) is succinated in adipocytes matured in high glucose, and we investigated if succination would alter PDI oxidoreductase activity, directly linking mitochondrial stress and ER stress. PDI is succinated by fumarate on both CXXC containing active sites, contributing to reduced enzymatic activity. In the presence of prolonged ER stress the unfolded protein response (UPR) triggers the production of the pro-apoptotic protein C/EBP homologous protein (CHOP). Succinated PDI has decreased reductase activity in adipocytes matured in high glucose, and in *db/db* epididymal adipose tissue, in association with increased levels of the ER stress marker CHOP. PDI succination

and ER stress were decreased, and PDI reductase activity was restored when exposure to chronic high glucose was limited, highlighting the importance of calorie restriction in the improvement of adipocyte metabolic function. The experiments completed in chapter 2 confirm succination of PDI as a novel biochemical mechanism linking altered mitochondrial metabolism to perturbed ER proteostasis in the adipocyte during diabetes.

Our observations in chapter 2 consistently demonstrated that CHOP levels are elevated in all cases where fumarate and protein succination are increased. Here we show that CHOP levels are significantly increased in adipocytes matured in high glucose in the absence of UPR signaling and with no sign of apoptosis. We propose that the post-translational modification S-2-succinocysteine may be an alternative physiological regulator of CHOP stability under diabetic conditions. Kelch-like ECH-associated protein 1 (Keap1) negatively regulates CHOP degradation in the adipocyte, and Keap1 is succinated in cancers where fumarate levels are elevated. We discovered that while Keap1 is directly succinated in the presence of excess fumarate derived from genetic knockdown methods, it is the oxidative modification of Keap1 that predominates in adipocytes matured in high glucose. Notably, we also determined that succination indirectly regulates CHOP stability through the induction of oxidative stress. The results shown in chapter 3 demonstrate that increased fumarate induces increased oxidative stress and that the oxidation of Keap1 contributes to sustained CHOP stability and adipocyte dysfunction during diabetes. The studies conducted in chapters 2 and 3 demonstrate that early

biochemical changes in mitochondrial metabolism have important implications for the development of sustained adipocyte stress.

Table of Contents

List of Figures

List of Abbreviations

$\Delta\Psi_m$ ..... mitochondrial membrane potential

2SC ..... S-2(succino)cysteine

4HNE 4-hydroxy-trans-2, 3-nonenal

ADP ..... adenosine diphosphate

AFHKO ..... adipose fumarase knockout

ATF6 ..... activating transcription factor 6

ATP ..... adenosine triphosphate

BMI ..... body mass index

CCCP ..... carbonyl cyanide m-chlorophenyl hydrazone

C/EBP ..... CCAAT-enhancer binding protein

CHOP ..... C/EBP homologous protein

CHX ..... cycloheximide

CK2 ..... casein kinase 2

CSN ..... COP9 signalosome

DAPI ..... 4',6-diamidino-2-phenylindole

DCF ..... dichlorofluorescein

DMF ..... Dimethyl fumarate

DNP 2,4-dinitrophenol

DPP-4 ..... dipeptidyl peptidase-4

DTPA ..... diethylenetriaminepentaacetic acid

eIF2α.....eukaryotic initiation factor α

ER..... endoplasmic reticulum

Ero1 ..... endoplasmic reticulum oxidoreductase 1

Fh..... fumarase protein

Fh1……..fumarase gene

FHKD ..... fumarase knockdown

GAPDH ..... glyceraldehyde-3 phosphate dehydrogenase

GLP-1 ..... glucagon-like peptide 1

GLUT ..... glucose transporter

GRP78 ..... 78 kDa glucose related protein

GSH ..... glutathione

HLRCC .....hereditary leiomyomatosis and renal cell carcinoma

HOX1 .....heme oxygenase 1

IB ..... immunoblot

IFN γ ..... interferon γ

IKKβ..... inhibitor of nuclear factor kappa-B kinase β

IL.....interleukin

IP ..... immunoprecipitation

IRE1..... inositol-requiring enzyme 1

IRS..... insulin receptor substrate

JNK ..... c-Jun N-terminal kinase

Keap1 ..... Kelch-like associated protein 1

MAM .....mitochondrial associated ER membrane

MCP1 ..... monocyte chemoattractant protein 1

MEFs ..... mouse embryonic fibroblasts

MMF ..... monomethyl fumarate

m/z ..... mass/charge ratio

NAC ..... n-acetylcysteine

NADH ..... nicotinamide adenine dinucleotide

NOX4 ..... NADPH oxidase 4

NRF2 ..... nuclear factor (erythroid-derived 2)-like 2

OCR ..... oxygen consumption rate

oxLDL ..... oxidized low density lipoprotein

PBA ..... sodium phenylbutyrate

PDI ..... protein disulfide isomerase

PE ..... pyridyl ethyl

PERK ..... protein kinase-like endoplasmic reticulum kinase

PKD ..... protein kinase D

PPARγ ..... peroxisome proliferator-activated receptor gamma

PPP ..... pentose phosphate pathway

Prx4 ..... peroxiredoxin 4

RFU ..... relative fluorescence units

RIPA ..... radioimmunoprecipitation assay buffer

ROS ..... reactive oxygen species

srebf1 ..... sterol regulatory element-binding protein1 gene

shRNA ..... short hairpin ribonucleic acid

Th.....T helper

TNFα.....tumor necrosis factor alpha

TLR.....toll-like receptor

UPR.....unfolded protein response

USP15 .....ubiquitin specific protease 15

VDAC..... voltage dependent anion channel

VEGF.....vascular endothelial growth factor

XBP.....x-box binding protein

Chapter 1

General Introduction

1.1 Epidemiology of Obesity and Type 2 Diabetes

A total of 29.1 million people or 9.3% of the United States population were documented to have diabetes in the Center for Disease Control 2014 National Diabetes Statistics Report. Within this group 21 million people have been clinically diagnosed with diabetes, and estimated 8.1 million people suffer from undiagnosed/uncontrolled diabetes (CDC 2014). Prediabetes, a condition that often precedes the development of Type 2 diabetes, is estimated to occur in 86 million people based on an irregular hemoglobin A1C (>6.5%) and elevated fasting blood glucose levels (>126 mg/dL or 7 mM). Type 2 diabetes is primarily diagnosed in adults aged 45 to 64 and is also called “adult onset” diabetes. Unfortunately, childhood obesity and type 2 diabetes are also on the rise with a shocking 5,089 individuals under the age of 20 reported to be newly diagnosed with type 2 diabetes from 2008-2009. In 2012 the estimated cost of treating clinically determined cases of type 2 diabetes was $245 billion, with direct medial costs totaling $176 billion. Comorbidities of diabetes such as cardiovascular disease, stroke, blindness, kidney disease and amputations worsen medical expenses and account for ~10% of the medical costs associated with treatment (CDC 2014).

Obesity is a major contributing factor to the development of type 2 diabetes with roughly 85.2% of diabetes patients described as overweight or obese. Obesity is characterized by the body mass index (BMI) scale used to categorize body mass based on a person’s weight to height ratio (BMI = kilograms/meters^2). A normal healthy person has a BMI range of 18.5 to 24.9

kg/m^2. A BMI between 25 to 29.9 kg/m^2 is classified as overweight and a BMI greater than 29.9 kg/m^2 defines the obese category. In 2011-2014 over one-third (36.5%) of adults and 17% of children in the U.S. were considered clinically obese. In addition, the annual medical expenditures of obese individuals are $1,429 higher than individuals of normal healthy weight due to obesity-related conditions including heart disease, stroke and type 2 diabetes (CDC 2014). With the prevalence of obesity and type 2 diabetes near epidemic proportions it is critical to understand the economic, environmental and biological factors that induce type 2 diabetes, and to establish more effective preventative and therapeutic strategies.

1.2 Insulin Signaling

In metabolically healthy people the pancreatic beta cell secretes insulin in response to carbohydrate intake after a meal, prompting the uptake of glucose into insulin sensitive tissues. The insulin tyrosine kinase receptor is a dimer comprised of an α subunit that binds insulin at the extracellular face of the plasma membrane and a transmembrane β subunit that facilitates intracellular signaling. Insulin binding instigates auto-phosphorylation of the β subunit and subsequent phosphorylation of the insulin receptor substrate (IRS) 1 and 2. Activated IRS-1 and -2 will bind phosphoinositide 3-kinase (PI3K) to generate the second messenger phosphatidylinositol (3,4,5)-triphosphate, leading to phosphorylation of Akt, also called protein kinase B. Insulin signaling via pAkt regulates the translocation of glucose transporter 4 (GLUT4) to the plasma membrane of skeletal muscle myocytes and adipose tissue adipocytes to

augment glucose uptake. Nutrients are then catabolized to produce energy, predominantly generating adenosine triphosphate (ATP). If there is a fuel surplus, insulin will facilitate increased glycogen synthesis in the liver and muscle, as well as lipogenesis in the adipose tissue to store glucose and fatty acids for use during fasting and exercise. In addition, insulin acts to suppress glucose production in the liver to restore homeostatic blood glucose levels after consuming a meal.

The development of Type 2 diabetes is characterized by initial hyperinsulinemia in response to insulin resistance when the muscle, liver and adipose tissues no longer respond properly to insulin signaling, discussed below. Impaired insulin sensitivity prompts pancreatic beta cells to produce and secrete increasing amounts of insulin in an attempt to boost insulin signaling and lower blood glucose levels. Over time, the beta cells fail to meet the insulin demand to invoke a normal response in the peripheral insulin sensitive tissues. This results in the accumulation of glucose in the blood stream due to the lack of glucose uptake by the muscle and adipose tissue, and sustained glucose output by the liver.

1.3 Symptoms and Treatments for Type 2 Diabetes

Impaired tissue glucose uptake increases fasting blood glucose levels in type 2 diabetic patients, causing a variety of symptoms including recurrent urination, increased thirst and fatigue. Further systemic complications are common with chronic hyperglycemia and disease progression including diabetic retinopathy, peripheral nerve damage and diabetic nephropathy. This is due to

exacerbated GLUT-1 mediated glucose uptake into the non-insulin dependent capillary beds of the retina and kidneys, as well as the GLUT-3 mediated uptake of glucose in nerve cells. Glucose oxidation and the generation of reactive metabolic intermediates are proposed to induce mitochondrial dysfunction, oxidative stress and intracellular damage in these tissues (Brownlee, 2005). Living with type 2 diabetes requires inconvenient and consistent monitoring of blood glucose levels that fluctuate with meal to meal caloric intake and daily physical activity. The primary treatment for these patients is to closely monitor blood glucose levels throughout the day, and micromanage food consumption and physical activity coupled to a variety of pharmacological approaches. Pharmacological agents such as metformin, which reduces hepatic gluconeogenesis (Miller *et al*. 2013) and lipid metabolism (Fullerton *et al*. 2013), are prescribed if lifestyle interventions do not result in sufficient glycemic control. Sulfonylureas that stimulate the pancreas to release insulin (Thulé and Umpierrez, 2014), and the peroxisome proliferator-activated receptor (PPAR) agonist group thiazolidinediones (Hauner, 2002) are supplementary clinical therapeutic agents employed to aid metformin in the reduction of blood glucose levels. Exenatide and liraglutide are glucagon-like peptide 1 (GLP-1) analogs, also called ‘incretin mimics’, and bind the glucagon-like 1 receptor on the islets of Langerhans cells to stimulate insulin and inhibit glucagon release. These result in moderately lower blood glucose levels in prolonged diabetes (Campbell *et al*. 2013, Fehse *et al.* 2005). Dipeptidyl peptidase-4 (DPP-4) is the incretin inactivating enzyme, and DPP-4 inhibitors or gliptins have also been considered,

but with limited evidence of efficacy, as a treatment for type 2 diabetes. In addition, both GLP-1 agonists and DPP-4 inhibitors are under investigation as perpetuators of pancreatitis, pancreatic cancer and heart failure (Rehman *et al.* 2017). Although these drugs can help to improve fasting blood glucose levels there is still no cure for type 2 diabetes.

1.4 Adipocyte Metabolism

Preadipocytes are dispersed throughout the adipose tissue of metabolically healthy individuals, and can differentiate into mature adipocytes allowing flexibility in the adipose tissue storage capacity.. Insulin signaling promotes adipogenesis through suppression of forkhead transcription factor O1 leading to upregulation of peroxisome proliferator-activated receptor gamma (PPARγ), a key regulator of the mature adipocyte phenotype. In a state of caloric excess white adipose tissue expands to accommodate the surplus energy in the form of triglycerides. De novo triglyceride synthesis, also known as lipogenesis, is mediated by insulin signaling in the adipose tissue; relieving phosphorylation mediated inhibition of acetyl-CoA carboxylase to promote fatty acid synthesis and triglyceride production. Insulin signaling also prevents phosphorylation and activation of hormone sensitive lipase to inhibit lipolysis when blood glucose levels are high. During fasting or in response to a pronounced increase in energy expenditure, the stored triglycerides in white adipose tissue are hydrolyzed to release free fatty acids to be used as fuel in metabolically active tissues. Adipocyte hypertrophy and obesity occurs when the balance between energy intake and energy expenditure is disproportionate due to excessive fuel intake.

Adipose tissue is the healthiest site for the deposition of additional caloric energy in the form of triglycerides (Unger *et al.* 2013). However, when adipose tissue expansion reaches its threshold, triglycerides will begin to accumulate in other organs such as the liver, resulting in non-alcoholic fatty liver disease (Schwenger and Allard, 2014, Rosen and Spiegelman, 2014).

In addition to its role as an energy storage depot, adipose tissue is an important endocrine organ that secretes a variety of hormones known as adipokines. Perturbation in the levels of several adipokines is closely associated with obesity and type 2 diabetes. Adiponectin is produced and secreted from the adipocyte in an insulin sensitizing manner and acts to increase fatty acid oxidation in the skeletal muscle and suppress gluconeogenesis in the liver. Decreased circulating levels of adiponectin are an established hallmark in obese type 2 diabetic patients (Cao *et al.* 2014). Leptin is another key adipokine that functions in caloric regulation by binding to the leptin receptor on proopiomelanocortin-cocaine amphetamine regulated transcript (POMC-CART) neurons in the arcuate nucleus of the hypothalamus. This stimulates the release of melanocortins that mediate appetite suppression. Leptin also regulates satiety by binding its receptor on the agouti related peptide (AgRP) neurons in the arcuate nucleus, inhibiting the release of neuropeptide Y and orexins (Abizaid and Horvath, 2008, Hakansson *et al.* 1999, Stephens *et al.* 1995). Leptin secretion is directly proportional to adipose tissue mass; yet despite the hyperleptinemina in obese individuals, the hormonal response in the hypothalamus is attenuated due to leptin resistance (Cao *et al.* 2014).

Diabetes is a complex multi-organ disease involving hormonal and metabolic mediators, and it is clear that compromised adipose tissue functionality is a significant component of Type 2 diabetes (Cusi, 2010, Lee *et al*. 2016, Smith and Kahn, 2016). The following sections highlight the recognized and proposed contributors to adipocyte stress and dysfunction in the development of Type 2 diabetes.

1.5 Adipocyte Stress in Type 2 Diabetes

1.5a Inflammation and Insulin Resistance

Type 2 diabetes is closely correlated with increased obesity and a state of chronic low grade inflammation in the adipose tissue, in association with lifestyle factors such as a poor diet and lack of exercise. Adipose tissue was typically regarded as a unassuming reservoir for triglyceride storage within adipocytes, but is now valued as a complex organ encompassing a variety of interacting cell types including adipocytes, macrophages, eosinophils, neutrophils, endothelial cells, fibroblasts, stem cells and neuronal projections (Cohen and Spiegelman, 2016). While some adipose tissue is necessary for lipid storage and hormone production, the accumulation of excess adipose tissue is associated with the secretion of pro-inflammatory cytokines. Several intracellular inflammatory signaling responses are activated in the adipocyte including Toll-like receptor (TLR)-4 and -2, inflammasome activation, c-Jun N-terminal kinase (JNK) and inhibitor of nuclear factor kappa-B kinase-β (IKKβ) signaling, and the production of inflammatory cytokines due to metabolic stress (Gregor and Hotamisligil, 2011, Solinas *et al.* 2010). The increased production and secretion

of potent cytokines including tumor necrosis factor α (TNFα), interferon (IFN)-γ, interleukin (IL)-6, IL-β and monocyte chemoattractant protein 1 (MCP1) occurs in parallel with adipocyte hypertrophy (Berg *et al*. 2005). MCP1 acts to recruit monocytes and macrophages to the site of cellular distress (Kanda et al. 2006), resulting in the accumulation of macrophages in the subcutaneous adipose tissue of obese type 2 diabetic patients, and in the visceral adipose tissue of *ob/ob* and *db/db* type 2 diabetic mice (Amano *et al*. 2014, Haase *et al.* 2013, Weisberg *et al.* 2003). Macrophages tend to congregate at sites of adipocyte cell death forming crown-like structures surrounding the cellular debris and lipid droplets for removal (Cinti *et al*. 2005). Importantly, obese adipose tissue resident macrophages significantly contribute to the production of pro-inflammatory cytokines, e.g., TNFα and IL1β, in the adipose tissue microenvironment of diabetic *ob/ob* and *db/db* mice (Xu *et al*. 2003). This is due to the M1 or "classically activated" pro-inflammatory phenotype of macrophages localized in obese adipose tissue compared to the anti-inflammatory M2 or "alternatively activated" polarized macrophages found in lean adipose tissue (Lumeg *et al*. 2007). Suzuki *et al*. recently described that the loss of T-helper (Th) 2 cytokine signaling from adipocytes regulates macrophage polarity and this promotes the M1 phenotype in insulin resistant mice fed a high fat diet (Suzuki *et al.* 2017). The reduced quantity of anti-inflammatory cytokines in the adipose tissue microenvironment is also attributed to decreased resident Th2 and T regulatory cells and a buildup of CD8+ T cells and Th1 cells that contribute to macrophage recruitment and prolonged inflammation (Solinas *et al.* 2010).

Importantly, adipose tissue inflammation is recognized as being present when there is decreased systemic insulin sensitivity, prior to the development of Type 2 diabetes (Samuel and Shulman, 2012, Solinas *et al.* 2010, Suzuki *et al*. 2017, Tanti *et al.* 1994).

Pro-inflammatory cytokines impair insulin sensitivity in tissues through activation of JNK and IKKβ pathways (Solinas *et al.* 2010, Solinas and Becattini, 2016). JNK activation leads to increased phosphorylation of IRS-1 at the Ser307 residue and IRS-2 at Thr348, inhibiting the interaction and activation of IRS by the insulin receptor via tyrosine phosphorylation in response to insulin (Aguirre *et al.* 2000, Aguirre *et al.* 2002, Solinas *et al.* 2006). Under normal conditions, IRS-1 activity is diminished by mammalian target of rapamycin (mTOR) and its downstream effector ribosomal S6 kinase 1 (S6K1) via direct phosphorylation at residues Ser636, Ser639 and Ser307 that results in desensitization of insulin signaling (Ozes *et al.* 2001). Lee *et al.* described that TNFα stimulation of IKKβ induces hyperactivation of mTOR signaling and consequent insulin resistance in hepatocytes of mice fed a high fat diet and *ob/ob* mice (Lee *et al*. 2008). Pro-inflammatory cytokines also increase adipose lipolysis (Kawakami *et al.* 1987) by suppressing the lipolysis inhibitor fat specific protein 27 (Ranjit *et al.* 2011), contributing to high levels of circulating free fatty acids. Saturated fatty acids are able to bind TLR4 culminating in heightened IKKβ/NFkB signaling to produce additional pro-inflammatory cytokines (Shi *et al.* 2006), perpetuating a positive feedback loop to sustain systemic insulin resistance (Jauhiainen *et al.* 2011). Interestingly, adipose tissue specific deletion of the phosphatase PTEN

(phosphatase and tensin homolog), a known negative regulator of insulin signaling, is sufficient to improve serum adiponectin levels, systemic insulin sensitivity, hepatic p-Akt and reduce TNFα production in subcutaneous adipose tissue (Morley *et al.* 2015). Therefore, reducing adipose tissue inflammation is imperative to re-establish insulin sensitivity and normal hormonal control over glucose homeostasis.

1.5b Endoplasmic Reticulum Stress

The endoplasmic reticulum (ER) is the intracellular organelle where proteins designated for secretion or incorporation into the plasma membrane are translated, folded and processed. Several chaperone and oxidoreductase proteins reside in the ER lumen to assist with protein folding. Protein disulfide isomerase (PDI) is an ER chaperone protein that aids in the formation of correctly configured substrate disulfide bonds via a series of redox reactions. PDI contains two CGHC sequence active site motifs and each cysteine plays a crucial role in the reduction and oxidation of substrate disulfide bonds (Appenzeller-Herzog *et al.* 2008). The N-terminal cysteines (Cys55 and Cys399) in both active sites have a lower pK_a (~4.5) compared to the high pK_a of the C-terminal cysteines (Cys58 and Cys402) (pK_a ~9.5) (Hawkins and Freedman, 1991, Karala *et al*. 2010, Lappi *et al.* 2004). This promotes the increased nucleophilicity of the N-terminal cysteines and the reduction of PDI active site cysteines, accompanied by the oxidation and formation of a substrate disulfide bond (Hawkins and Freedman, 1991, Karala *et al.* 2010, Lappi *et al.* 2004). ER oxidoreductin 1 (Ero1) acts in conjunction with FAD^+ to re-oxidize PDI through

the shuffling of electrons via similar CXXC regulatory sites. This facilitates the recycling of PDI active site cysteines to continue protein folding (Tu *et al*. 2002). Excess reactive peroxides are produced in the ER via Ero1 re-oxidation and these are quenched by peroxiredoxin-4 (Prx4) (Tavender *et al.* 2008, Tavender *et al.* 2010). PDI reduces the oxidized form of Prx-4, salvaging its active site cysteines and facilitating continued regulation of potentially harmful reactive peroxide levels in the ER (Tavender *et al.* 2010, Zito *et al.* 2010).

A disturbance to ER homeostasis, alterations in the oxidative environment or the accumulation of misfolded proteins, is taxing to the ER organelle and denotes a state of ER stress. The unfolded protein response (UPR) is activated in adipocytes during diabetes in an effort to prevent the development of ER stress (Özcan *et al.* 2004). The UPR is comprised of three separate pathways; protein kinase-like endoplasmic reticulum kinase (PERK), inositol-requiring enzyme 1 (IRE1), and activating transcription factor 6 (ATF6). The accumulation of misfolded proteins is first sensed by glucose related protein 78 (GRP78) causing it to dissociate from IRE1, PERK and/or ATF6. This allows for the homodimerization and phosphorylation of the IRE1 and PERK protein complexes. pIRE1 possesses spliceosome activity and cleaves X-box binding protein 1 (XBP1) in the cytosol to generate the truncated isoform spliced-XBP1 (sXBP1) a transcription factor that forms homodimers or heterodimers with other UPR proteins. Dissociation of GRP78 from ATF6 results in translocation of ATF6 from the ER membrane to the golgi apparatus where ATF6 is also cleaved. The spliced form of ATF6 translocates into the nucleus and forms transcription factor

complexes with sXBP1 to promote the production of additional ER chaperone proteins to aid in protein folding (Figure 1.1). The PERK pathway serves to temporarily inhibit protein translation via phosphorylation of eukaryotic initiation factor α (eIF2α), this arm of the UPR is prominently activated in the 3T3-L1 adipocyte cultured in diabetic conditions (Han *et al*. 2013a). If the UPR is persistent and ER stress develops, the UPR signaling will result in the production of the pro-apoptotic protein C/EBP homologous protein (CHOP). Acute CHOP expression induces growth arrest and DNA damage-inducible protein (GADD34) and results in dephosphorylated eIF2α and reinstatement of protein synthesis (Han *et al.* 2013b), contributing further to the already defective proteostatic environment. The activation of the UPR and presence of ER stress in diabetes has been well documented (Boden *et al.* 2008, Özcan *et al.* 2006) however, there is limited mechanistic insight on the direct initiator of ER stress in the adipocyte. In chapter 2 we investigate a novel biochemical mechanism contributing to the development of sustained ER stress in the adipocyte during diabetes.

1.5c Oxidative Stress

Hydroxyl radicals, superoxide, hydrogen peroxide, ketoaldehydes, and hydroxynonenal are chemically reactive molecules characterized as reactive oxygen species (ROS). ROS are endogenously generated during cellular metabolism and may be beneficial or detrimental, dependent upon the concentration produced in the tissue. ROS such as hydrogen peroxide have a physiological role in redox signaling, however, excessive production of ROS leads to the damaging oxidative modification of cellular macromolecules (Circu *et*

al. 2010). Similar to extracellular inflammatory cytokine signaling, intracellular ROS accumulation can activate JNK and IKKβ to impair insulin signaling (Tiganis, 2011), aiding the development of type 2 diabetes.

Mitochondria are a premier site of ROS production with the electron transport chain, pyruvate dehydrogenase and α-ketoglutarate dehydrogenase complexes able to generate superoxide anion (Fisher-Wellman *et al.* 2013, Starkov *et al.* 2004). Superoxide produced via the transfer of electrons through complexes I and III of the electron transport chain to molecular oxygen is metabolized by manganese superoxide dismutase to hydrogen peroxide. Hydrogen peroxide can be oxidized to form a hydroxyl radical in the presence of ferrous iron, leading to lipid peroxidation to generate reactive unsaturated lipid aldehydes such as 4-hydroxy-trans-2,3-nonenal (4-HNE) (Grimsrud *et al.* 2008). These highly reactive aldehydes irreversibly modify protein side chains of cysteine, lysine and histidine residues, termed protein carbonylation (Curtis *et al.* 2012). Total protein carbonylation positively correlates with growing adiposity and increasing serum free fatty acid levels in obese adults (Frohnert *et al.* 2011), highlighting oxidative protein damage as a severe consequence of glucotoxicity. Importantly, a significant increase in protein carbonylation underlies the development of insulin resistance in human adipose tissue after just 6 days of excess caloric intake (Boden *et al.* 2015). Specifically, the identification of GLUT4 carbonylation in response to acute gluco-lipotoxicity (Boden *et al.* 2015) implied that oxidative stress is a major contributor to the observed deficiency in glucose uptake and decreased adipose tissue insulin sensitivity.

Nicotinamide adenine dinucleotide phosphate (NADPH) oxidase (NOX) 4 is an abundant adipose tissue protein and has been attributed to initiate ROS production during early stages of obesity (Han *et al.* 2012). Excess nutrients increase pentose phosphate pathway (PPP) activity and NADPH levels in 3T3-L1 adipocytes (Han *et al.* 2012). Located in the mitochondria, NOX4 transfers electrons from NADPH to oxygen, thus generating the radical superoxide (Block *et al.* 2009). Intracellular superoxide signaling has been shown to activate the pro-inflammatory NF-κB pathway promoting adipose tissue insulin resistance (Kaul and Forman, 1996). Interestingly, adipose tissue specific NOX4 deficiency lowered ROS production and inflammation, and delayed the onset of insulin resistance in mice fed a high fat and high sucrose diet (Den Hartigh *et al*. 2017). However, reduced NADPH levels due to slower PPP flux are observed when the adipocyte has reached its maximum triglyceride storage capacity, which may limit NOX4 driven ROS generation in later stages of obesity (Han, 2016). Overall, sustained ROS production in the adipose tissue appears to be a significant factor in obesity associated inflammation and insulin resistance (Houstis *et al.* 2006) contributing to the onset of type 2 diabetes. Thus, it is important to understand the mechanisms that mediate prolonged ROS production and oxidative stress in the adipose tissue.

The cell is equipped with several redox systems including the glutathione and thioredoxin systems in order to combat chronic oxidative stress. The antioxidant response element (ARE) is located within the promoter region of several antioxidant genes and regulates the facilitation of the antioxidant

response (Rushmore *et al*. 1991). Nuclear factor (erythroid-derived 2)-like 2 (Nrf2) is a transcription factor that translocates to the nucleus and binds to the ARE. Nrf2 up-regulates the transcription of several detoxification enzymes and antioxidant genes including heme oxygenase-1, NAD(P)H: quinone oxidoreductase 1, glutathione peroxidase and glutathione S-transferase. Under normal conditions the negative regulator Kelch-like ECH-associated protein 1 (Keap1) binds the Cullin3-based E3 ligase complex and sequesters Nrf2 in the cytosol to be tagged with ubiquitin and degraded by the proteasome (Akira *et al.* 2004, Kobayashi *et al.* 2004). Keap1 contains at least 3 cysteine residues confirmed to be sensitive to oxidative stress (Levonen *et al*. 2004, McMahon *et al.* 2010). The covalent modification of these cysteine residues is crucial for Nrf2 activation, disturbing Keap1/Nrf2 binding and stimulating Nrf2 stabilization and transcriptional activity during cellular stress (Kobayashi *et al.* 2006). Activation of Nrf2 is generally considered beneficial for a variety of cells as it invokes the protective antioxidant response. Nrf2 activation upon sulforaphane modification, that targets Keap1 redox sensitive cysteines, reduces the concentration of ROS in endothelial cells exposed to hyperglycemic conditions (Xue *et al.* 2008). Nrf2 also stimulates the transcription of glyoxalase 1 leading to reductions in methyglyoxal induced protein damage in endothelial (HMEC-1) and hepatic (HepG2) cell lines (Xue *et al.* 2012).

Although Nrf2 activation is considered protective in the defense against glycemic stress during diabetes, the enhancement of Nrf2 activity in the adipose tissue of diabetic mice is controversial and is associated with negative metabolic

effects. Constitutive Nrf2 activation via *Keap1* knockdown decreases glucose tolerance, lipogenic gene expression and lipid accumulation while simultaneously increasing insulin resistance in the adipose tissue of *ob/ob* type 2 diabetic mice (Xu *et al.* 2012). The pharmacological enrichment of Nrf2 with sulforaphane inhibits adipogenesis in mouse embryonic fibroblasts (MEFs) *in vitro* (Xu *et al.* 2012) which is often proposed as a beneficial means to combat obesity. However, impaired adipogenesis and lipid storage in the adipose tissue contributes to hepatic steatosis during type 2 diabetes and after high fat diet feeding (More *et al.* 2013, Xu *et al.* 2012). Therefore enhanced Nrf2 activity due to defects in the Keap1 degradation pathway may actually induce harmful effects as decreased adipogenesis does not offer any benefit when the lipid is instead stored in other tissues such as liver and muscle.

In addition, Keap1 has also been described as a negative regulator of the ER stress protein CHOP in adipocytes (Huang *et al.* 2012), as CHOP is also degraded by the ubiquitin proteasome system (Diaz *et al.* 2015, Li *et al.* 2006). Keap1 binding to CHOP results in polyubiquitination of CHOP due to the recruitment of ubiquitin by the COP9 signalosome/cullin3-based E3 ligase complex (Figure 1.2), while knockdown of Keap1 expression results in upregulation of CHOP in adipocytes (Huang *et al.* 2012). In addition to oxidative modification, Keap1 cysteines are susceptible to modification by other electrophiles including a range of xenobiotic compounds. In chapter 3 we propose an alternative mechanism regulating CHOP degradation and stability in the adipocyte in response to glucotoxicity.

1.6 C/EBP Homologous Protein

Although adipogenesis is regulated by several transcription factor families (White *et al.* 2010), this section will discuss the CCAT/enhancer binding protein (C/EBP) transcription factors as this family is highly regulated by CHOP signaling. The C/EBP family has a firmly established regulatory role in the development of adipocyte differentiation. In response to hormonal stimuli in adipocyte culture conditions (insulin, dexamethasone and isobutylmethylxanthine), the C/EBP isoforms δ and β dimerize and upregulate transcription of C/EBPα (Cao, 1991, Yeh, 1995) by attaching to the C/EBP binding site in the gene promoter region (Christy *et al*. 1991). In turn, C/EBPα stimulates transcription of the master adipogenic regulator peroxisome proliferator-activated receptor gamma (PPAR-γ) (Rosen *et al.* 2002) that promotes lipogenesis (Tontonoz *et al.* 1994). Deletion of the C/EBP δ, β or α genes can be fatal and effectively stunts white adipose tissue development in surviving mice (Tanaka *et al.* 1997, Wang *et al.* 1995). Recent evidence suggests a significant role for the direct interaction of transcriptional cofactor cyclin C with C/EBPα to activate adipogenesis of brown adipose tissue (Song *et al.* 2017). In addition, knocking down the expression of cyclin C in 3T3-L1 fibroblasts inhibits adipogenesis, detectable as reduced lipid accumulation and expression of the adipogenic genes PPARγ, C/EBPα, adiponectin and fatty acid binding protein 4 (Song *et al*. 2017). Overall this demonstrates the importance of C/EBP signaling for proper adipose tissue function, as enhanced adipogenesis is essential to accommodate the lipid overload due to excessive nutrient consumption.

C/EBP homologous protein (CHOP) is a basic leucine zipper transcription factor known to form heterodimers with C/EBPα and C/EBPβ family members. Unlike C/EBPα and C/EBPβ, CHOP contains glycine and proline substitutions in the conserved C/EBP-DNA binding region. Therefore, CHOP binding of C/EBP isoforms suppresses gene transcription due to the inability of the complex to interact with normal C/EBP binding sequences on the target gene (Ubeda *et al.* 1996). The production of CHOP is known to be upregulated in response to cellular stress, e.g., ER stress, DNA damage, glucose starvation, hypoxia and oxidative stress (Carriére *et al.* 2004, Han *et al.* 2013a, Luethy and Holbrook, 1992, Mihai *et al.* 2015). Importantly, ectopic expression of CHOP following retrovirus transfection, glucose starvation, hypoxia or the induction of ER stress reduces C/EBPα and PPARγ production and downstream signaling to prevent adipogenesis (Batchvarova *et al.* 1995, Han *et al.* 2013a). Consistent with these findings, CHOP knockout mice display larger adipocytes and fat pads compared to wild mice fed a high fat diet (Maris *et al.* 2012). The inhibition of adipogenesis due to elevated CHOP expression may be detrimental in obesity, forcing the accumulation of lipids in peripheral tissues due to the inability to differentiate new adipocytes for energy storage.

It is increasingly recognized that CHOP has additional physiological roles beyond its ability to regulate adipogenesis. CHOP controls the induction of cell cycle arrest between the G1/S phase in fibroblasts (Barone *et al.* 1994), and the regulation of Bcl-2 family members to promote apoptosis in cardiomyocytes, hepatocytes, podocytes and pancreatic beta cells (Kim *et al.* 2008, Li *et al.* 2014,

Malhi *et al.* 2013). Jauhiainen *et al*. reported that tunicamycin induced CHOP accumulates in the cytoplasm, in addition to the nucleus, of human fibroblasts and GOT3 sarcoma cells (Jauhiainen *et al.* 2012). Further gene expression profiling by microarray and ontology analysis revealed that cytoplasmic CHOP indirectly controls the expression of 94 different genes related to cellular movement, development, proliferation and growth, cell cycle, cell death and gene expression (Jauhiainen *et al.* 2012).

In addition, CHOP has been shown to directly bind the DNA promoter/enhancer region of *Ppara, Srebf1* and *Cebpα* in hepatocytes culminating in the suppression of metabolic gene expression during stress (Chika *et al*. 2013). Prasad *et al*. have described a novel role for CHOP as an important mediator of phosphate movement into the mitochondria in adrenal cells. This results in increased steroid synthesis by stabilizing 3β-hydroxysteroid dehydrogenase type-2 protein conformation and its association with Translocase Outer Membrane-22 during periods of stress due to cold temperatures (Prasad *et al.* 2016). CHOP mRNA and protein levels are also increased in the tumors of a genetic mouse model of hepatocellular carcinoma generated by mobilized T2/Onc3 transposon and human hepatocellular carcinoma (DeZwaan-McCabe *et al.* 2013). Here CHOP promotes hepatocyte cell death that provokes a pro-inflammatory response and fibrotic deposition. Additionally, tumorigenesis is reduced by 50% in *CHOP* knockout mice treated with diethylnitrosamine compared to wild type animals (DeZwaan-McCabe *et al.* 2013, Scaiewicz *et al.* 2013) suggesting a prominent role for CHOP to stimulate oncogenesis.

In considering alternative roles for CHOP function beyond the suppression of adipogenesis, we have noted an increase in CHOP as adipocytes progress through maturation in high glucose (similar to Han *et al.* 2013a). In contrast, this increase in CHOP is not sustained in adipocytes in normal glucose despite the fact that they also progress normally through adipogenesis, nor is it present in the adipose tissue of healthy mice versus diabetic mice. Since our *in vitro* studies specifically compared adipocytes simultaneously undergoing adipogenesis and maturation in either normal or high glucose, it suggests that sustained CHOP unique to high glucose conditions may have an alternative role during diabetes. Two studies examining CHOP knockout mice distinguish CHOP as an important component of inflammation mediated insulin resistance in mice fed a high fat diet (Maris *et al.* 2012, Suzuki *et al.* 2017).

CHOP knockout mice show a significant improvement in fasting blood glucose levels and insulin sensitivity compared to wild type mice after high fat diet feeding (Suzuki *et al.* 2017). Interestingly, while the degree of macrophage infiltration does not change between wild type and CHOP knockout mice (Maris *et al.* 2012, Suzuki *et al.* 2017), CHOP deficiency specifically in the adipose tissue induces anti-inflammatory M2 macrophage polarization (Suzuki *et al.* 2017). In addition, the absence of CHOP in adipose tissue promotes eotaxin production and eosinophil recruitment in the adipose tissue microenvironment of mice fed a high fat diet (Suzuki *et al.* 2017). Overall, increased or sustained CHOP levels in the absence of increased apoptosis in the adipose tissue appears to be detrimental during diabetes. The exact mechanism by which

CHOP regulates inflammation and insulin resistance in the adipose tissue remains to be explored.

1.7 Protein Succination

Cysteine is one of the least common amino acids incorporated into the primary sequence of a protein, however, it is most often included as an important structural or active site residue governing protein function or regulation. The thiol group of cysteine has a pK_a ~8.5, while the pK_a of an active site cysteine may range from 3-6. The lower pK_a value of the active site thiolate indicates the increased reactivity of the nucleophilic cysteine residue. Our laboratory was first to describe the Michael addition reaction between the Krebs cycle intermediate fumarate and the thiolate group of cysteine to form a thioether bond and the chemical modification S-(2-succino)cysteine (2SC). This enzymatically irreversible reaction is termed succination (Figure 1.3) (Alderson *et al.* 2006). 2SC was first identified *in vivo* in human plasma proteins where fumarate modifies ~3.5% of total albumin from healthy individuals (Alderson *et al.* 2006). We assessed the kinetics of succination *in vitro* after incubating fumarate with N-acetylcysteine (pK_a ~9.5) and commercial glyceraldehyde-3 phosphate dehydrogenase (GAPDH) (pK_a ~6) (Alderson *et al.* 2006, Blatnik *et al.* 2008). As predicted the succination of GAPDH was ~250 times faster than N-acetylcysteine due to the lower pK_a and increased reactivity of GAPDH cysteine residues (Alderson *et al*. 2006). The degree of protein succination directly correlates with the concentration of fumarate, and since succination is a slow chemical reaction, the cysteines must be exposed to reasonably high levels of fumarate for a

prolonged period (Alderson *et al.* 2006, Blatnik *et al*. 2008, Frizzell *et al.* 2009, Nagai *et al.* 2007). Consistent with this data, decreasing intracellular fumarate levels directly reduces protein succination (Frizzell *et al.* 2012, Tanis *et al.* 2015).

Protein succination increases ~3.5 fold in the skeletal muscle of streptozotocin-induced type 1 diabetic rats (Blatnik *et al.* 2008). Matrix assisted laser desorption/ionization – time of flight (MALDI-TOF) and ultra-performance liquid chromatography electrospray ionization tandem mass spectrometry (UPLC ESI-MS/MS) analysis of GAPDH isolated from the gastrocnemius muscle confirmed a pronounced increase in the relative amount of succinated peptides to control peptides containing active site Cys149 and peripheral Cys244 in diabetic versus control rats (Blatnik *et al.* 2008). Interestingly, modification of GAPDH by fumarate correlates indirectly with GAPDH enzymatic activity in a dose dependent manner *in vitro*, and in the muscle of diabetic rats (Blatnik *et al*. 2008). This study was the first to describe the targeted effect of succination to inhibit enzyme activity via direct cysteine modification by fumarate. A number of additional functional studies on specific succinated proteins have since been conducted in adipocytes (Frizzell *et al.* 2009), neurons (Linker *et al*. 2011), fibroblasts (Adam *et al.* 2011, Ternette *et al.* 2013), T cells (Blewett *et al.* 2016), as well as purified protein *in vitro* (Piroli *et al.* 2014). Beyond the original identification of endogenous succination of plasma albumin, increased protein succination has been documented in the context of several diverse disease settings including; type 2 diabetes (Merkley *et al.* 2014), Leigh syndrome (Piroli *et al.* 2016), renal cell carcinoma (Yang *et al.* 2014), tuberculosis management

(Ruecker *et al.* 2017) and the pharmacological modulation of autoimmune disorders (Blewett *et al.* 2016, Piroli *et al*. 2017 in preparation).

1.7a Type 2 Diabetes

As discussed in Section 1.4, the hyperglycemic/hyperinsulinemic state observed during type 2 diabetes exceeds the energy needs of adipocytes. This creates a build-up of ATP, relative to ADP, in adipocytes matured in high glucose (Frizzell *et al*. 2012). Respiratory control prevents further ATP production, reducing ATP synthase activity and the translocation of hydrogen ions back into the mitochondrial matrix. The accumulation of hydrogen ions in the inner membrane space increases the mitochondrial membrane potential and contributes to reductive stress, i.e. the accumulation of increased NADH relative to NAD^+. A consequence of this 'pseudohypoxic' state is the temporary inhibition of the NAD^+-dependent Krebs cycle enzymes and the accumulation of Krebs cycle intermediates (Frizzell *et al.* 2012). Lai and Goldman reported that 3T3-L1 adipocytes matured in high glucose will release elevated concentrations of several Krebs cycle intermediates, including fumarate, into the cell culture medium (Lai and Goldman, 1992). We have established that intracellular fumarate levels increase ~2.5-4 fold in adipocytes matured in high (30 mM) versus normal (5 mM) glucose concentrations as a direct result of this glucotoxicity driven mitochondrial stress (Nagai *et al.* 2007, Frizzell *et al*. 2012)(Figure 1.4). The presence of excess fumarate results in a pronounced increase in protein succination in both adipocytes matured in 30 mM glucose, and in the adipose tissue from diabetic *ob/ob* and *db/db* mice (Nagai *et al.* 2007,

Frizzell *et al.* 2009, Thomas *et al.* 2012). Notably, when compared with other tissues in the *db/db* model (kidney medulla and cortex, lungs, skeletal muscle, cardiac muscle, liver and spleen) this increase in 2SC seems to be selective for the adipose tissue (Thomas *et al.* 2012). This may be due to elevated fumarate in the relatively compressed cytoplasmic volume of the adipocyte in comparison with the total cell size, or that total tissue protein analyses cannot detect subtle cell-type specific changes. Protein succination was not detected in the catabolic adipose tissue of type 1 diabetic rats, and only subtle succination is observed in the adipose tissue from mice fed a high fat diet for 12 weeks (Thomas *et al*. 2012). This suggests that succination is distinctly associated with the presence of type 2 diabetes, rather than insulin resistance alone, in adipose tissue. A list of 38 total protein targets of elevated fumarate in adipocytes matured in high glucose have been identified by strong cation exchange or high pH fractionation followed by capillary LC-MS/MS mass spectrometry (Merkley *et al.* 2014). However, the stoichiometry, structural and function significance of 2SC remains to be determined for many of these adipocyte target proteins.

To date, we have characterized the effect of protein succination on the function of two proteins in the adipocyte; adiponectin (Frizzell *et al.* 2009) and tubulin (Piroli *et al.* 2014). Adiponectin is a homopolymeric protein assembled in the endoplasmic reticulum (Liu *et al.* 2008, Liu and Liu, 2010) and secreted into circulation where it regulates fatty acid beta oxidation in the skeletal muscle and glucose homeostasis in the liver. Type 2 diabetic patients consistently exhibit decreased plasma levels of both total and high molecular weight (HMW)

adiponectin, and this has been linked to the development of insulin resistance (Chang *et al.* 2009). Cys39 of the monomeric adiponectin isoform has been confirmed as the site of succination, preventing the formation of adiponectin multimers. Consistent with this, the succinated adiponectin is not secreted into the medium of adipocytes matured in high glucose (Frizzell *et al.* 2009). Similar to the *in vitro* profile, the succination of intracellular adiponectin was also increased in the epididymal adipose tissue from *db/db* mice and was not detected in the plasma (Frizzell *et al.* 2009). This study confirms that the site specific succination of adiponectin inhibits the formation and secretion of HMW species from adipocytes, consistent with the reduced levels of plasma adiponectin observed in type 2 diabetes (Frizzell *et al.* 2009).

α and β tubulin form heterodimers that generate the basic subunits of cytoskeletal microtubule polymers. The tubulin heterodimer is comprised of 20 cysteine residues and is consistently the most prominent succinated protein detected by our unique anti-2SC antibody in the brain, adipose tissue, cardiac and skeletal muscle and lung tissue from *db/db* mice, as well as 3T3-L1 adipocytes and C2C12 myocytes (Thomas *et al.* 2012 and Piroli *et al.* 2014). Consistent with our previous study (Thomas *et al.* 2012) the degree of tubulin succination increases only in the adipocyte under diabetic conditions and succination of tubulin remains unaltered between control and diabetic conditions in all other tissues examined to date (Thomas *et al.* 2012, Piroli *et al.* 2014). Assessment of the effect of succination on tubulin polymerization *in vitro* showed that physiological levels of fumarate do not influence polymerization. Using

MS/MS mass spectrometry I identified Cys347 and Cys376 on α tubulin and Cys12 and Cys303 on β tubulin from purified porcine brain tubulin as the precise sites of succination. Interestingly, succination of these cysteine residues impairs the detection ability of antibodies targeting tubulin epitopes that contain Cys347, Cys376 or Cys303 (Piroli *et al.* 2014). The observed decrease in antigen-antibody binding with increasing succination suggests that succination may alter the interaction of tubulin with microtubule associated proteins (MAPs) within these regions. In addition, these results underscore the importance of validating antibodies with cysteine containing epitopes to ensure succination does not affect antibody recognition.

The progressive increase in protein succination over 8 days of adipocyte maturation occurs in parallel with increased CHOP levels and enhanced inflammatory cytokine secretion (Tanis *et al.* 2015). Intriguingly, we have observed that the ER proteins glucose related protein 78 (GRP78) and protein disulfide isomerase (PDI) are targets of succination in 3T3-L1 adipocytes matured in high glucose (Nagai *et al.* 2007). In chapter 2 we investigate the functional significance of succination on the oxidoreductase PDI and how this contributes to adipocyte dysfunction during diabetes. Sodium phenylbutyrate (PBA) is a small chemical chaperone known to reduce ER stress and inhibit adipogenesis (Basseri *et al.* 2009, Özcan *et al.* 2006). We discovered that PBA acts to lower protein succination by reducing glucose uptake and the mitochondrial membrane potential in adipocytes cultured in 30 mM glucose (Tanis *et al.* 2015), independent of any effect on ER stress. Despite claims that

PBA acts to reduce ER stress in diabetic animals (Özcan *et al.* 2006), we detected no change in protein succination, UPR markers and greater CHOP levels in the adipose tissue of *db/db* mice treated with PBA (unpublished observations). In chapter 3 we further pursue the relationship between protein succination and CHOP stability, independent of the UPR and ER stress, in the adipocyte matured in high glucose.

Elimination of the *fumarase* gene in mouse embryonic fibroblasts significantly increases protein succination (Adam *et al.* 2011) due to the inability of fumarase to convert fumarate to malate. Our collaborators Yang *et al*. recently developed and characterized the phenotype of a unique adipose tissue specific fumarase knockout mouse (AFHKO) (Yang *et al*. 2016). This novel mouse model permits the investigation of the systemic implications of increased fumarate alone in the adipose tissue. Deletion of the *fumarase* gene under control of adiponectin-Cre specifically in the adipose tissue resulted in severe mitochondrial dysfunction in the perigonadal white adipose tissue, as evidenced by swollen mitochondria with reduced or absent cristae and insufficient ATP production (Yang *et al*. 2016). Cell death, cytoplasmic degeneration, lipid extrusion into the interstitial space and adipose tissue macrophage accumulation was also documented to occur in the white adipose tissue of these AFHKO mice (Yang *et al.* 2016). Unexpectedly, the AFHKO mice exhibited lower fat mass compared to controls, remained insulin sensitive and glucose tolerant and showed no change in liver mass or liver triglyceride levels after consuming a high fat diet over 9-11 weeks (Yang *et al.* 2016). Surprisingly, the absence of fumarase in the adipocyte

appeared to be protective against high fat diet induced obesity, insulin resistance and hepatic steatosis.

The aP2(adipocyte protein 2)-Cre and adipo(adiponectin)-Cre models are the most effective tools available to target adipose tissue specific deletions *in vivo*. An unfortunate limitation of both the aP2-Cre and adipo-Cre models is the inability to distinguish between white adipose tissue and brown adipose tissue as both aP2 and adiponectin are expressed in each adipose subtype. Therefore, the consequences of defective brown adipose tissue also have to be considered when explaining the overall phenotype of the AFHKO mouse. Brown adipose tissue demonstrated irregular and elongated mitochondria, decreased uncoupling protein 1 and β3 adrenergic receptor mRNA expression and impaired adaptive thermogenesis were present in the AFHKO mouse (Yang *et al.* 2016). The failure of brown adipose tissue to contribute to heat production in AFHKO mice housed at ~22ºC resulted in active skeletal muscle-mediated shivering thermogenesis (Yang *et al.* 2016). Shivering thermogenesis increases skeletal muscle energy expenditure in AFHKO mice housed at 22ºC and results in minimal lipid accumulation and improved insulin sensitivity, even during high fat diet feeding. Significantly, equilibration of AFHKO mice thermoneutral conditions (30ºC) reversed the unexpected protective effect of adipose tissue fumarase deficiency. Further experiments in this model at thermoneutral temperatures will provide more meaningful information on the homeostatic significance of adipose tissue *fumarase* deficiency, and validates the importance of thermoneutral housing for metabolic studies (Stemmer *et al.* 2015, Tian *et al.* 2016, Yang *et al.* 2016).

1.7b Leigh Syndrome

Leigh Syndrome is distinguished by progressive neurodegeneration and the production of lesions in the brainstem and basal ganglia (Finsterer, 2008, Rahman *et al.* 1996). This fatal mitochondrial disease develops due to mutations in the genes encoding protein subunits of complex I and VI of the electron transport chain (Ruhoy and Saneto, 2014). Ndufs4 is an 18 kDa protein that aids in the final assembly of complex I and was one of the first mutated genes identified to cause Leigh Syndrome. The loss of Ndufs4 leads to a form of complex I that lacks the NADH dehydrogenase unit, and is associated with the accumulation of NADH and impaired movement of electrons through the electron transport chain. Similar to glucotoxicity driven mitochondrial stress and succination in the adipocyte, pseudohypoxia drives the accumulation of fumarate in Ndufs4 deficient neurons. We have recently described elevated protein succination in the brainstem and cerebellar nuclei of Ndufs4 knockout mice (Piroli *et al.* 2015), particularly in the vestibular nucleus where most of the pathology is observed. The Ndufs4 knockout mouse displays many of the clinical and neurological symptoms detected in human Leigh syndrome (Quintana *et al*. 2010). We propose the fumarate accumulation and subsequent protein modification may provide a novel biochemical link to the underlying pathology.

Voltage dependent anion channel (VDAC) 1 and 2 are transmembrane proteins in the outer mitochondrial membrane and function as the primary channels for the movement of ADP, ATP and other ions and metabolites between the mitochondria and the cytosol. We confirmed that both VDAC 1 and

2 are novel targets of succination in the brainstem of Ndufs4 knockout mice by mass spectrometry and western blotting (Piroli *et al.* 2015). Further analysis by LC-MS/MS mass spectrometry identified Cys77 and Cys48 as the endogenous targets of succinated VDAC2 in the brainstem (Piroli *et al.* 2015). Current investigations aim to understand if succination of VDAC impairs channel activity as this may contribute further to the mitochondrial bioenergetic deficit observed in Leigh Syndrome, potentially by reducing mitochondrial ATP export.

1.7c Cancer

Fumarase is responsible for the hydration of fumarate to malate in the mitochondria. Genetic loss-of-function mutations in a *fumarase* allele predisposes patients to hereditary leiomyomatosis and renal cell carcinoma (HLRCC) (Tomlinson *et al.* 2002), further loss of heterozygosity specifically precedes the development of the aggressive renal carcinoma and results in a significant increase in fumarate levels (Pollard *et al*. 2005). Fumarate has since gained recognition as an oncometabolite, a small molecule component of normal metabolism whose accumulation signifies metabolic dysregulation and subsequently leads cells to oncogenesis (Yang *et al.* 2012). As expected, the substantial increase in fumarate leads to a pronounced increase in the amount of succinated proteins in kidney cells of a renal specific *fumarase* knockout mouse model (Pollard *et al*. 2007). MS/MS analysis has identified 94 succinated proteins in *fumarase* knockout mouse embryonic fibroblasts (MEF) and renal cysts (Ternette *et al.* 2013), and 60 confirmed protein targets of 2SC in human UOK262 and NCC-FH-1 cells and tumors (Yang *et al.* 2014). Selective

evaluation of the role of 2SC in *fumarase* deficient cancers identified the redox sensitive Cys151 and Cys288 of Keap1 as prominent targets of succination (Adam *et al*. 2011, Ooi *et al*. 2011). Modification of these precise cysteine residues impairs Keap1/Nrf2 binding and activates the Nrf2 anti-oxidant response. Continuous with the inhibitory effects of 2SC on protein functionality, succination of the mitochondrial enzyme aconitase at Cys385, Cys448 and Cys451, which are crucial for iron-sulfur cluster binding, significantly reduces enzyme activity *in vitro* and in *fumarase* knockout MEFs (Ternette *et al*. 2013). Kerins *et al*. have determined iron regulatory protein 2 is a target protein of succination in UOK262 cells, and that this allows for ferritin activation to promote the production of the pro-mitotic transcription factor Forkhead box protein M1 (Kerins *et al.* 2017). Additionally, fumarate inhibits demethylation of miR-200ba429, an anti-metastatic miRNA cluster, promoting the expression of epithelial-to-mesenchymal related transcription factors in fumarase deficient MEFs (Sciacovelli *et al*. 2016). These studies demonstrate protein succination is a critical link between *fumarase* deficiency and cell malignancy in HLRCC (Kerins *et al.* 2017). Unlike non-malignant cells, protein succination is advantageous to the cancer cell by boosting its antioxidant response and promoting metastasis, as well promoting metabolic plasticity in fuel utilization, e.g. decreased aconitase activity may force alternate anaplerotic fuel usage. Future investigations will continue to focus on the contribution of 2SC in HLRCC pathology progression. Interestingly, as fumarate is increasingly accepted as a novel oncometabolite (Yang *et al*. 2012), protein succination is also actively being pioneered as a

reliable early disease stage diagnostic marker (Chen *et al.* 2014, Llamas-Velasco *et al*. 2016).

1.7d Fumaric Acid Esters

Fumarate esters dimethyl fumarate (DMF) and monomethyl fumarate (MMF) (Figure 1.5) have been used to treat symptoms of autoimmune diseases, such as psoriasis, for more than fifty years (Ghoreschi *et al.* 2011, Gold *et al*. 2012, Papadopoulou *et al.* 2010). In 2013 the U.S. Food and Drug Administration approved DMF for multiple sclerosis treatment as an oral pharmaceutical drug marketed as Tecfidera® (Linker *et al.* 2013). Elucidation of the complete biochemical mechanism underlying the therapeutic benefits and side effects of DMF and MMF has received heightened attention (Ghoreschi *et al.* 2011, Blewett *et al.* 2016, Wu *et al.* 2017, Schloder *et al*. 2017). Fumarate esters enter the cell where they react rapidly with available thiols, including intracellular glutathione (Ghoreschi *et al.* 2011, Schmidt *et a*l. 2010, Thiessen *et al.* 2010, Manuel and Frizzell, 2013). The depletion of glutathione levels by fumarate esters increases heme-oxygenase 1 expression and STAT1 activation that amplifies IL-10 and impairs IL-12 and IL-23 production promoting the type II dendritic cell phenotype (Ghoreschi *et al.* 2011). This induces a switch from the pro-inflammatory Th1 profile towards a favorable Th2 profile in the experimental autoimmune encephalomyelitis (EAE) mouse model (Ghoreschi *et al.* 2011). Linker *et al*. showed that DMF stimulates the Keap1/Nrf2 antioxidant pathway by direct modification of Keap1 redox sensitive cysteines (Linker *et al.* 2011). The induction of the antioxidant response by Nrf2 preserved neuronal health and

axonal myelination in the myelin oligodendrocyte glycoprotein induced EAE mouse model of multiple sclerosis (Linker *et al.* 2011). While Nrf2 activation remains the dominant accepted mechanism of action of DMF, recent studies demonstrate that DMF can act independent of Nrf2 and is therapeutically beneficial for the treatment of multiple sclerosis models in Nrf2 knockout mice (Peng *et al.* 2016). A thorough proteomic approach has uncovered 40 DMF modified cysteines in primary human T cells, elucidating the reactivity of this potent electrophile with immunomodulatory proteins including IKKβ, tumor necrosis factor-α-induced protein 3 (TNFAIP3) and IL-16 (Blewett *et al.* 2016). Blewett *et al*. further established that DMF prevents T cell activation and IL-2 production via succination of a CXXC motif on protein kinase Cθ that disrupts its interaction with CD28 at the immunological synapse (Blewett *et al.* 2016).

Our laboratory has conducted a new extensive proteomics study to investigate new neuronal targets of fumarate esters that may be affected by treatment with Tecfidera®. I utilized bottom-up shotgun proteomics with the Orbitrap Velos Pro to identify an additional mass of 144.1270 Da or 130.0262 Da indicating the DMF or MMF cysteine modification on the fragment ion, respectively (Figure 1.5). In total, we identified 4 cysteine containing peptides in primary mouse neurons, 11 cysteines in primary rat astrocytes and 13 novel cysteine containing peptides in differentiated N1E-115 neuroblastoma cells that were succinated by DMF or MMF. Cofilin-1 was identified in primary astrocytes to be succinated by MMF at Cys139. Cofilin-1 modulates the actin cytoskeleton by depolymerizing filamentous actin and producing monomeric actin that can be

used to reorganize the actin cytoskeleton in response to cellular dynamics. Analysis of Colifin-1 depolymerization activity *in vitro* suggests that the chemical modification of Cys139 by fumarate esters reduces its capacity to regulate actin dynamics (data not published). We are continuing to examine the effect of fumarate esters on additional protein targets, both *in vitro* and *in vivo*,to better understand the positive therapeutic mechanism of DMF during multiple sclerosis.

While these diverse scenarios for fumarate accumulation provide new information on the role of succination, the studies in this dissertation will focus on the early mechanism of adipocyte dysfunction in diabetes. I propose that succination of the important ER oxidoreductase protein PDI inhibits PDI reductase activity, contributing to an accumulation of misfolded proteins and ER stress. I also investigate succination of Ero1 that contains a similar active site motif to PDI and may also be a prominent target for succination. In addition, I hypothesize that decreasing protein succination with mild mitochondrial uncouplers will relieve ER stress, identifying a new mechanism of glucotoxicity induced adipocyte dysfunction. In chapter 3 I propose that Keap1 is succinated in adipocytes matured in high glucose and that modification of Keap1 promotes CHOP stability. I confirmed that CHOP accumulates in the nuclear fraction of adipocytes matured in high glucose corresponding to decreased secretion of IL-13 and that IL-13 secretion is rescued by reducing oxidative stress and CHOP levels.

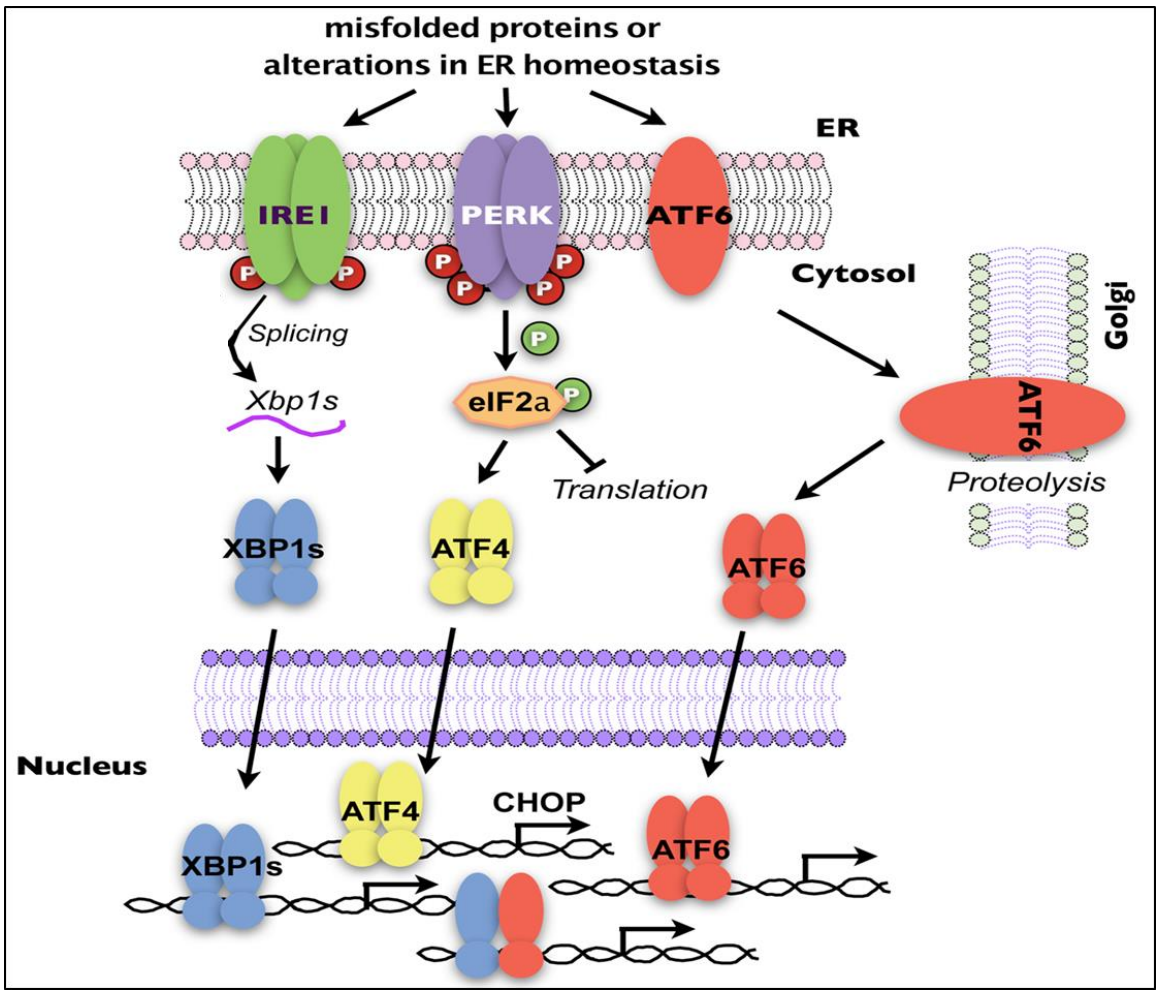

Figure 1.1: The unfolded protein response (UPR) pathway. Homeostatic imbalance initiated by the accumulation of misfolded proteins in the endoplasmic reticulum (ER) activates the UPR. The UPR is comprised of three separate pathways (1) IRE1 will splice XBP1 and (2) cleaved ATF6 in the golgi act as transcription factors to up-regulate ER chaperone proteins. The PERK pathway acts to attenuate translation via phosphorylation of eIF2a and continued activation of the PERK arm results in transcriptional up-regulation of C/EBP homologous protein (CHOP) as a terminal response to ER stress. (http://www.human.cornell.edu/dns/qilab/research.cfm)

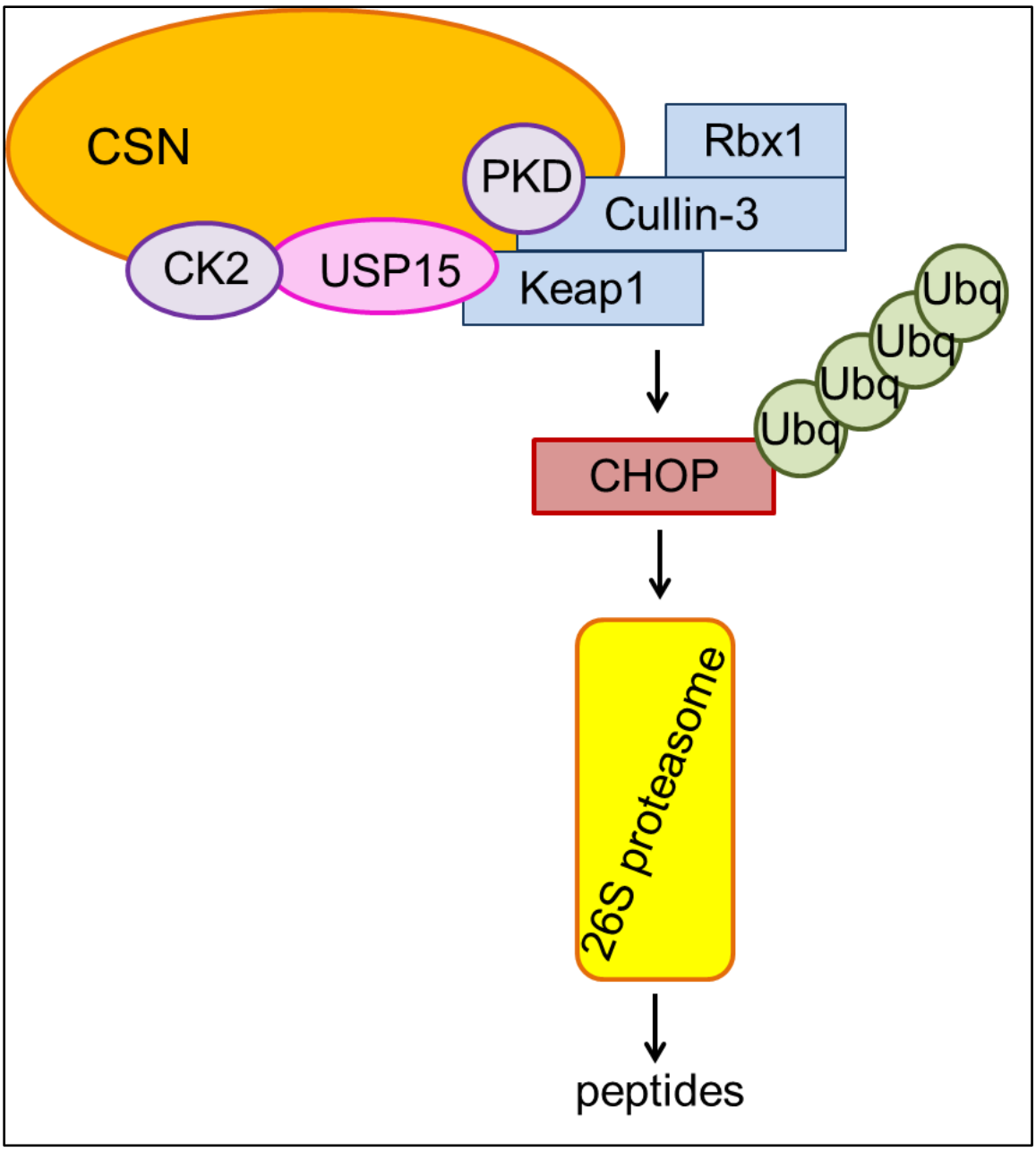

Figure 1.2: C/EBP homologous protein (CHOP) degradation pathway.
The COP9 signalosome (CSN) removes the ubiquitin-like protein Nedd8 from cullin-3 to inhibit cullin-3 activity. The CSN associated protein ubiquitin specific protease 15 (USP15) protects Keap1 from auto-ubiquitination and degradation. The degradation supercomplex will bind CHOP and CSN associated kinases, casein kinase 2 (CK2) and protein kinase D (PKD), phosphorylate CHOP to promote ubiquitination and degradation (Huang *et al*. 2012).

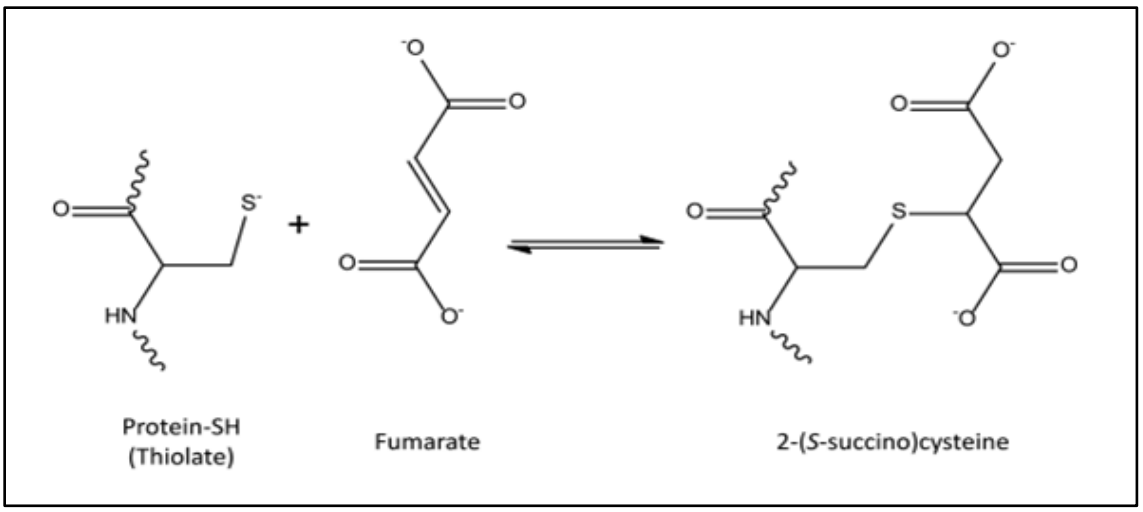

Figure 1.3: Formation of 2-(S-succino)cysteine (2SC). The Michael addition reaction of fumarate with cysteine residues on proteins to form 2SC (Alderson *et al.* 2006).

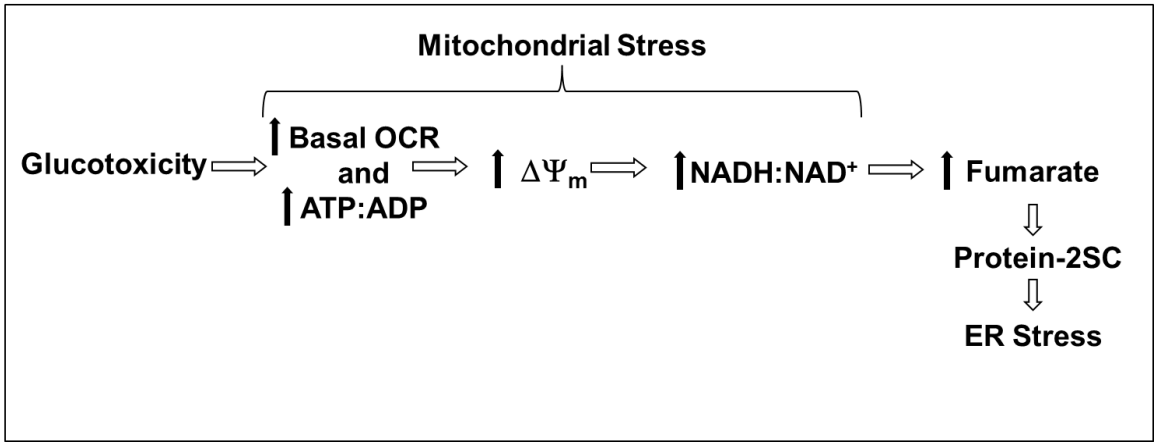

Figure 1.4: Schematic of how glucotoxicity derived mitochondrial stress drives the increase in protein succination and potentially endoplasmic reticulum (ER) stress in the adipocyte during diabetes. Elevated carbohydrate fuel supply exceeds the metabolic needs of the adipocyte leading to an increase in the basal oxygen consumption rate and ATP: ADP ratio. The decrease in mitochondrial ADP concentrations inhibits ATP synthase and results in a high mitochondrial membrane potential. Electron transport is inhibited with the accumulation of H^+ in the inner membrane space of the mitochondria and the cellular redox status shifts towards an increase in NADH concentration. The increase in NADH: NAD^+ causes an increase in fumarate and malate, consistent with feedback inhibition of the NAD^+ -dependent dehydrogenases of the tricarboxylic acid cycle. Excess fumarate is available to react with cysteine residues, including the succination of the ER oxidoreductase PDI. Sustained increases in fumarate directly contribute to an increase in ER stress.

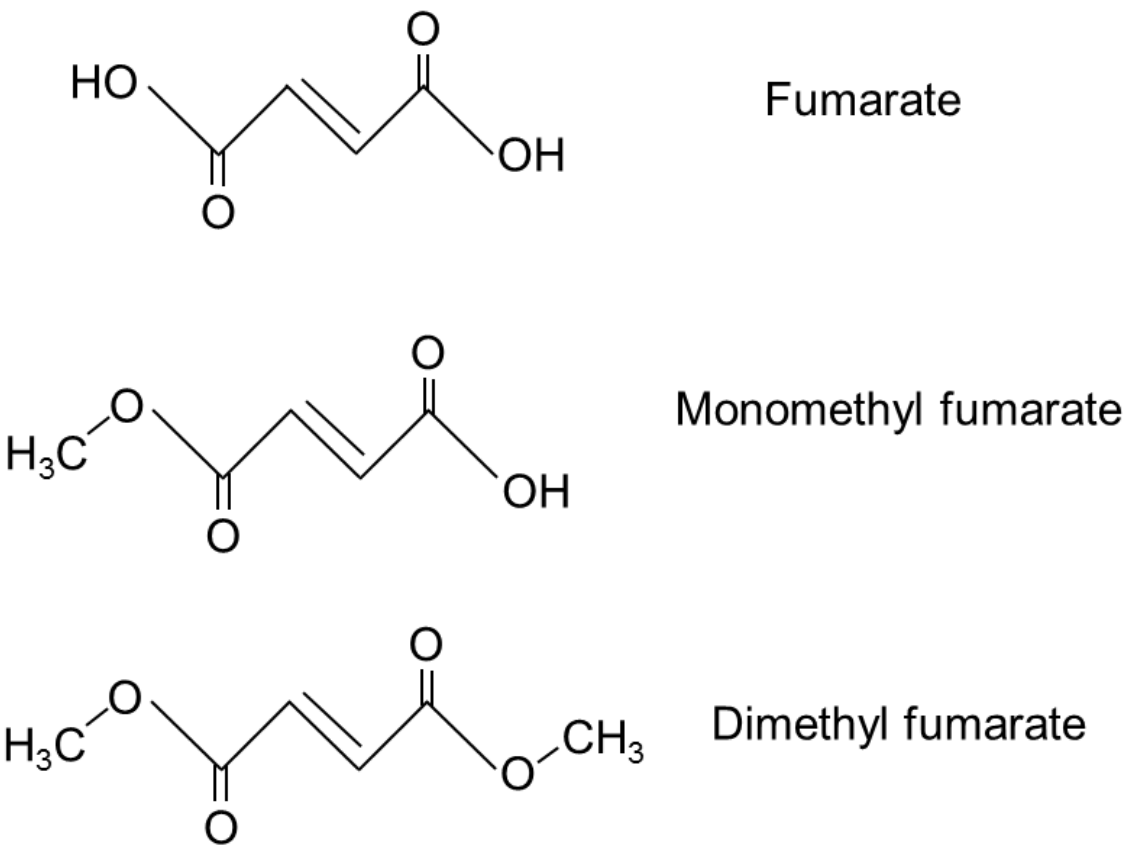

Figure 1.5: Fumarate and fumaric acid esters structures. Chemical structures of fumarate (116.07 Da), monomethyl fumarate (130.0262 Da) and dimethyl fumarate (144.1270 Da).

Chapter 2

Succination of Protein Disulfide Isomerase Links Mitochondrial Stress and Endoplasmic Reticulum Stress in the Adipocyte During Diabetes[1]

[1]Manuel AM, Walla MD, Faccenda A, Martin SL, Tanis RM, Piroli GG, Adam J, Kantor B, Mutus B, Townsend DM, Frizzell N. Accepted by *Antioxidants and Redox Signaling* Reprinted here with permission of publisher, 4/3/2017.

2.1 Introduction

Proper protein folding and disulfide bond arrangement requires the concerted activities of endoplasmic reticulum (ER) chaperones and isomerases, particularly during the correction of non-native disulfide bond configurations. Consequently, if the ER accessory protein response is compromised this will result in an accumulation of misfolded proteins in the ER, prompting the Unfolded Protein Response (UPR) in an attempt to maintain ER proteostasis (Kim *et al.* 2008, Ron *et al*. 2007). The continued accumulation of misfolded proteins eventually culminates in ER stress and the well characterized upregulation of the pro-apoptotic protein C/EBP homologous protein (CHOP) (Schröder *et al*. 2005). ER stress has been documented in the adipose tissue of type 2 diabetic patients (Boden *et al.* 2008, Boden *et al*. 2014a, Sharma *et al*. 2008), and is reduced following weight loss (Gregor *et al.* 2009). Hyperinsulinemia, hypoxia and inflammation have been proposed to initiate the development of ER stress in human adipose tissue (Boden *et al*. 2014b, Hosogai *et al.* 2007). ER stress has also been described in 3T3-L1 adipocytes (particularly through protein kinase RNA-like endoplasmic reticulum kinase signaling) and in the adipose tissue of type 2 diabetic mice (Han *et al.* 2013a, Kawasaki *et al.* 2012, Lefterova *et al*. 2009, Özcan *et al*. 2004). The treatment of adipocytes from obese subjects with lipopolysaccharides, high glucose concentrations or free fatty acids has been shown to promote ER stress *in vitro* (Alhusaini *et al.* 2010, Jiao *et al.* 2011). While all of these may be physiologically relevant contributors to ER stress, there remains limited insight on the mechanistic processes that directly cause

disturbed protein folding in the adipocyte (Sha *et al.* 2011, Sun *et al.* 2012). In this study we identify a novel biochemical mechanism responsible for reduced protein folding and increased ER stress in the adipocyte during diabetes.

Protein disulfide isomerase (PDI) is the most abundant ER oxidoreductase that facilitates the formation of correctly configured substrate disulfide bonds (Hatahet *et al.* 2009, Rutkevich *et al*. 2010). PDI contains two active sites with the sequence motif -CGHC- in the *a* and *a*' domains, and both of these play crucial roles in the reduction and oxidation of substrate disulfide bonds in the ER (Appenzeller-Herzog *et al*. 2008, Hawkins et al. 1991, Karala et al. 2010, Lappi *et al.* 2004). ER oxidoreductin 1α (Ero1) functions in re-oxidizing PDI using similar CXXC active sites, to sustain oxidative protein folding (Tu *et al.* 2002). S-glutathionylation of PDI active-site cysteines in both HL60 leukemia cells and SKOV3 ovarian cancer cells alters PDI protein structure and inhibits PDI isomerase activity *in vitro*, leading to stimulation of the UPR and the production of CHOP (Townsend *et al*. 2009, Xiong *et al.* 2012). In addition, nitrosative stress induced S-nitrosylation of PDI promotes UPR activation, ER stress and eventual cell death in cerebrocortical neurons (Uehara *et al*. 2006). These models demonstrate that the post-translational modification of PDI active-site cysteines precedes the development of ER stress. Oxidized low density lipoprotein (oxLDL) treatment of HMEC-1 cells augments CHOP mRNA levels and ER stress specifically due to decreased PDI reductase activity (Muller *et al.* 2013). However, HMEC-1 cells that over-express native PDI are immune to the induction of ER stress with oxLDL treatment (Muller *et al.* 2013). Importantly, the

restoration of functional ER chaperone levels is sufficient to decrease CHOP protein expression and ameliorate ER stress in the adipocyte (Liu *et al.* 2015, Zhou *et al.* 2010), therefore it is critical to mechanistically understand how chaperone function is altered under diabetic conditions.

We have previously confirmed that the ER residents PDI and glucose-regulated protein 78 (GRP78) are succinated by endogenously produced fumarate in the adipocyte under high glucose conditions (Nagai *et al.* 2007). Protein succination occurs when fumarate reacts non-enzymatically with cysteine thiols to produce the irreversible modification S-2-succino-cysteine (2SC) (Alderson *et al.* 2006, Frizzell *et al.* 2009, Nagai *et al.* 2007). The analysis of proteomic targets identified to date suggests that low pK_a thiols that may also be susceptible to oxidation as well as those with increased solvent accessibility may be most likely to react with endogenously produced fumarate (Merkley *et al.* 2014, Miglio *et al.* 2016) Protein succination is increased in the adipose tissue of *db/db* mice and in 3T3-L1 adipocytes matured in high glucose (10-30 mM) (Frizzell *et al.* 2009, Nagai *et al.* 2007). We previously demonstrated that the ATP:ADP ratio, NADH:NAD^+ ratio and the mitochondrial membrane potential are significantly increased in 3T3-L1 adipocytes matured in high (30 mM) glucose versus normal (5 mM) glucose concentrations (Frizzell *et al.* 2012, Tanis *et al.* 2015). In the metabolically challenged adipocyte the intracellular fumarate levels are elevated due to glucotoxicity driven mitochondrial stress and this results in the accumulation of succinated proteins (Figure 1.3)(Frizzell *et al.* 2012). Considering that protein succination occurs as a direct result of mitochondrial

stress in the adipocyte, and that functional PDI is critical to maintain ER proteostasis, we propose that the succination of PDI active-site thiols would inhibit its oxidoreductase activity, contributing to ER stress.

Mitochondrial uncouplers lower the inner mitochondrial membrane potential, created during glucose oxidation, by shuttling protons back into the mitochondrial matrix without generating additional ATP. Mitochondrial uncouplers are increasingly being investigated as therapeutic strategies to protect against coronary heart disease, ischemia-reperfusion injury, nonalchoholic steatohepatitis, obesity and diabetes (Kenwood *et al.* 2013, Long *et al.* 2016, Perry *et al.* 2015, Zhang *et al.* 2016). We have previously shown that the treatment of adipocytes matured in high glucose with mitochondrial uncouplers, 2,4-dinitrophenol (DNP) and carbonyl cyanide m-chlorophenyl hydrazone (CCCP), reduces both the intracellular fumarate concentration and the degree of protein succination (Frizzell *et al.* 2012). While DNP and CCCP are effective *in vitro,* both drugs are considered toxic and are unsuitable therapeutics. Niclosamide is a mild mitochondrial uncoupler (Satoh *et al.* 2016, Tao *et al.* 2014), approved by the US Food and Drug Administration as an anthelmintic drug for treating intestinal infections of tapeworms. Importantly, Tao *et al.* have demonstrated the beneficial outcomes of niclosamide in *db/db* mice after two months of oral administration, where niclosamide lowered both blood glucose and glycated hemoglobin levels and normalized plasma insulin levels (Tao *et al.* 2014). We investigated if targeting mitochondrial stress using niclosamide or a model of simple caloric restriction would subsequently reduce protein succination

and eliminate ER stress in the adipocyte matured in high glucose. The results of this study provide a novel mechanistic link between mitochondrial stress and the development of sustained ER stress, as evidenced by increased CHOP production, in the adipocyte during diabetes.

2.2 Results

The development of mitochondrial stress as a direct result of increased glucose oxidation (Figure 1.4) is expected to increase the basal oxygen consumption rate (OCR) of the adipocyte under diabetic conditions. We matured 3T3-L1 adipocytes in glucose and insulin concentrations that we have previously shown are physiologically representative of normal versus hyperglycemic/hyperinsulinemic conditions (5 mM glucose/0.3 nM insulin versus 30 mM glucose/3 nM insulin) (Tanis *et al.* 2015). We observed a ~90% increase in the basal oxygen consumption rate (OCR) of adipocytes matured in 30 mM glucose compared to 5 mM glucose after 2 days of maturation (Figure 2.2B). Our previous analyses of uncoupled respiration in adipocytes cultured in high glucose demonstrated that the cells are operating close to their maximal respiratory capacity, a manifestation of mitochondrial stress (Tanis *et al.* 2015). Metabolomic analyses confirmed that Krebs cycle intermediates, including fumarate, were increased in concert in high glucose conditions as a consequence of respiratory control and the inhibition of NAD^+-dependent dehydrogenases (Figure 2.1A)(Figure 2.2B, 2.2E). The increase in malate as well as fumarate confirms that the adipocyte is overwhelmed due to excessive ATP production (Frizzell *et al*. 2012), and immunoblotting using the anti-2SC antibody verifies that protein

succination is significantly increased in adipocytes matured in high versus normal glucose concentrations (Figure 2.2C)(Nagai *et al.* 2007). Adipocytes were matured in 5 mM glucose and treated with 0, 2 or 4 mM dimethyl succinate (DMS), an esterified form of the Krebs cycle intermediate succinate, to confirm that the anaplerotic supply of an alternative intermediate could augment endogenous fumarate production and protein succination. An anti-2SC immunoblot confirms increased succination of target proteins in the succinate supplemented adipocytes (Figure 2.2A). These results emphasize that adipocytes matured in high glucose exhibit features of mitochondrial stress early in maturation, with a subsequent increase in protein succination after 8 days of maturation (Figure 1.3). In contrast, adipocytes that mature and accumulate lipid normally in 5 mM glucose show no evidence of mitochondrial stress and have limited protein succination.

Protein succination occurs as a direct result of mitochondrial respiratory control in the metabolically challenged adipocyte (Figure 1.3)(Frizzell *et al.* 2012) therefore, we hypothesized that uncoupling the inner mitochondrial membrane using niclosamide would lower fumarate and 2SC levels. 3T3-L1 adipocytes were matured in 5 mM or 30 mM glucose or 30 mM glucose and treated with 2 µM niclosamide for 8 days. Metabolomic analyses substantiated the data that uncoupling the inner mitochondrial membrane, demonstrated by the acute increase in the basal oxygen consumption rate (Figure 2.2D)(Tao *et al.* 2014), prevents the accumulation of Krebs cycle intermediates in adipocytes matured in high glucose concentrations (Figure 2.1A)(Figure 2.2E). Immunoblotting with the

anti-2SC antibody demonstrates that niclosamide treatment reduces the degree of protein succination in adipocytes matured 30 mM glucose concentrations (Figure 2.1B). The lower panels depict shorter exposure times of the same anti-2SC immunoblot and highlight the decreased succination of several higher molecular weight proteins (50-150 kDa) (Figure 2.1B). Examining the relationship between protein folding, ER stress and glucose concentration we assessed the levels of CHOP, Ero1 and PDI in adipocytes matured in 5 mM or 30 mM glucose. The levels of CHOP were pronouncedly increased in adipocytes matured in high glucose compared to normal glucose (Figure 2.2C), confirming that persistent ER stress is selectively present in adipocytes matured under hyperglycemic conditions (Tanis *et al.* 2015). It is important to note that we did not detect differences in the protein levels of GRP78 or any components of the PERK, IRE1 or ATF6 branches of the UPR in adipocytes in normal/high glucose as the UPR is induced as a normal function of adipocyte maturation in the presence of insulin (Han *et al.* 2013a, Minard *et al.* 2016, Tanis *et al.* 2015). In order to establish a novel link between mitochondrial stress and the sustained ER stress, we examined CHOP protein expression levels in adipocytes matured in 5 mM, 30 mM or 30 mM glucose treated with 2 µM niclosamide for 8 days (Figure 2.1C). The data confirms that alleviating mitochondrial stress prevents the presence of prolonged ER stress generated by high glucose conditions. Although the transcription of ER chaperones may be up-regulated in parallel with ER stress, we did not detect any changes in the total protein levels of Ero1 or PDI between groups (Figure 2.1C)(Figure 2.2C). Importantly, alleviation of both mitochondrial

and ER stress with niclosamide corresponds to improved adiponectin secretion (Figure 2.1D), confirming that mitochondrial stress and succination impair adiponectin processing in the ER (Frizzell *et al.* 2009). These data confirm that mitochondrial stress and protein succination influence the development of ER stress and reduce adiponectin secretion from the adipocyte.

Lentiviral delivery of fumarase shRNA to adipocytes matured in normal glucose was used to increase fumarate levels in the adipocyte independent of glucotoxicity, since this prevents the hydration to malate and permits fumarate accumulation. The successful transduction of both the scrambled control and *fumarase* knockdown (FHKD) lentivirus was evaluated by monitoring green fluorescent protein (GFP) positive adipocytes 6 days post transduction (Figure 2.4A). Adipogenesis proceeded normally in FHKD cells and was confirmed by the elevated expression of adiponectin and peroxisome proliferator-activated receptor gamma (PPARγ) isoforms (Figure 2.3A). Reduced serum adiponectin species are a hallmark of type 2 diabetes. We observed a decrease in secreted adiponectin profiles from the FHKD adipocytes versus the scrambled controls (Figure 2.4D), similar to Yang *et al.* that reported lower circulating adiponectin levels in the plasma of adipose tissue specific *fumarase* knockout mice compared to control mice (Yang *et al.* 2016). These data again verify that elevated fumarate and succination lead to reduced serum adiponectin levels (Frizzell *et al.* 2009, Yang *et al.* 2016). The quantification of the triglyceride content in control and FHKD adipocytes matured in 5 mM or 30 mM glucose (Figure 2.3B), as well as the documented lipid accumulation by Oil Red O

staining (Figure 2.4B) verified that knocking down the expression of fumarase does not interfere with adipogenesis. The ~50% knockdown of fumarase levels observed was sufficient to increase protein succination in the adipocytes (Figure 2.3A). The pronounced escalation in protein succination in the FHKD adipocytes is directly proportional to the dramatic increase in the intracellular fumarate production. Analysis of mitochondrial metabolites from control and FHKD adipocytes matured in 5 mM glucose reveals a ~30 fold increase in fumarate compared to controls (Figure 2.3C)(Figure 2.4C). FHKD adipocytes displayed significant increases in the secretion of the pro-inflammatory cytokines TNFα, IL-1α and IL-1β, as well as VEGF, versus control adipocytes (Figure 2.3D) (Figure 2.4E). This similar to the significant increases in TNFα, MCP-1 and VEGF that we observed previously in adipocytes matured in 30 mM versus 5 mM glucose (Tanis *et al.* 2015). These data suggest that elevated fumarate and protein succination may play a role in the chronic low grade inflammatory state of adipose tissue observed during diabetes. Elevated CHOP levels were observed in both 30 mM glucose and FHKD adipocytes matured in 5 mM glucose (Figure 2.3E), confirming that protein succination alone functionally contributes to both the development of ER stress and the pro-inflammatory state of adipocytes, independent of other glucose derived metabolic stressors. In order to mechanistically understand how succination might contribute to ER stress, we examined the succination of PDI in adipocytes during glucotoxicity. PDI was immunoprecipitated from adipocytes matured in 5 mM or 30 mM glucose and examined by 2D-immunoblotting to detect succination, (Figure 2.3F, top panels)

followed by re-probing with anti-PDI (Figure 2.3F, lower panels). Compared to the total levels of immunoprecipitated PDI, there was significantly more succinated PDI in adipocytes matured in high glucose. We also confirmed increased PDI succination in *fumarase* knockout ($Fh^{-/-}$) mouse embryonic fibroblasts (MEFs), whose endogenous fumarate concentrations are ~5 mM (Ternette *et al*. 2013) (Figure 2.5). Overall, the results confirm that PDI is succinated in the presence of excess fumarate, potentially interfering with protein folding.

We were also interested in determining if Ero1, the thiol-dependent protein responsible for re-oxidizing PDI active-site cysteines, is also susceptible to succination by fumarate. Since mammalian Ero1 also contains redox-sensitive cysteine thiols (Inaba *et al.* 2010), we hypothesized that Ero1 might be a novel target of succination in the adipocyte. We incubated recombinant Ero1α (Araki *et al.* 2011) with increasing concentrations of fumarate *in vitro* to investigate if Ero1 is susceptible to succination. 1D-immunoblotting with anti-2SC and anti-Ero1 antibodies confirmed that Ero1 is succinated when incubated with 5 mM or 25 mM fumarate (Figure 2.6A). We next immunoprecipitated Ero1 from adipocytes matured in 5 mM or 30 mM glucose and immunoblotted with the anti-2SC antibody. However, Ero1 succination was not detected in the adipocytes (Figure 2.6B). The blot was re-probed with an anti-Ero1 antibody to confirm the presence of Ero1 in the immunoprecipitates (Figure 2.6B). Therefore, while recombinant Ero1 could be succinated *in vitro*, there were no detectable increases in the endogenous succination of Ero1 in adipocytes.

The succination of catalytically important thiols in the metabolic enzymes GAPDH and aconitase have been shown to reduce their enzymatic activity (Blatnik *et al.* 2008, Ternette *et al.* 2013). We hypothesized that succination at the active-site cysteines of PDI might also reduce enzymatic activity. Incubation of recombinant wild-type PDI (PDI-WT) with either 5 or 25 mM fumarate increased succination of PDI compared to the unmodified control (Figure 2.7A). Succination of PDI *in vitro* functionally decreased PDI reductase activity by 15% and 21% for 5 and 25 mM fumarate respectively (n=5, **p< 0.01) (Figure 2.7A, B). In addition, we used a mutant form of PDI (PDI^{FLFL}) to determine if succination of PDI active-site cysteines is essential for inhibition of PDI reductase activity. The residues His and Lys, adjacent to either side of the C-terminal active-site cysteines, are mutated to Phe and Leu (H55ΔF:K57ΔL and H399ΔF:K401ΔL), respectively in both the a and a' domains of the mutant form of PDI (Xiong *et al.* 2012). While remaining enzymatically functional, these simultaneous mutations are predicted to alter the active-site thiol pK_a, and prevent S-gluthionylation of PDI (Xiong *et al.* 2012). In contrast to the data obtained with PDI-WT, the mutant PDI could not be succinated in the presence of increasing fumarate concentrations *in vitro*, and its reductase activity was unaffected (Figure 2.7C, D), indicating that active-site cysteine modification by fumarate is necessary for inhibition of PDI reductase activity.

We confirmed that direct succination of active-site cysteines was mechanistically responsible for the inhibition of PDI reductase activity by LC-MS/MS mass spectrometry. Recombinant PDI that had been incubated in the

presence or absence of fumarate (Figure 2.8A) was alkylated with 4-vinylpyridine to produce a control pyridylethyl modification (C^{PE}, +105.058 Da) on the remaining free thiols. The tryptic precursor ion masses for control (C^{PE}, C^{PE}) and succinated (C^{PE}, C^{2SC}, +116.011 Da) peptides were analyzed by LC-MS/MS in order to determine the specific site of succination. We identified the MS/MS spectrum corresponding to the succinated peptide $^{45}YLLVEFYAPWC^{PE}GHC^{2SC}K^{59}$ ($[M+3H]^{3+}$: 683.9882 m/z) and $^{388}KNVFVEFYAPWC^{PE}GHC^{2SC}K^{403}$ ($[M+3H]^{3+}$: 717.0033 m/z) in the recombinant PDI sample modified by fumarate (Figure 2.8B, D), as well as each analogous control peptide ($Cys55^{PE}$, $Cys58^{PE}$) ($Cys399^{PE}$, $Cys402^{PE}$) in the unmodified recombinant PDI sample (Figure 2.8C, 2.8E). In the case of both active-site peptides the succination site was confirmed to be the second (C-terminal) cysteine, and was only detected in the PDI samples incubated with fumarate *in vitro*.

While succination of PDI active-site cysteines inhibits reduction of insulin disulfide bonds *in vitro* (Figure 2.8) the assay is not specific for PDI activity in cell lysates due to the presence of other oxidoreductases. Di-Eosin-GSSG is a fluorescent self-quenching synthetic PDI specific substrate (Klett *et al.* 2010, Raturi, 2007) frequently utilized to evaluate PDI reductase activity in protein lysates (Muller *et al.* 2013, Xiao *et al.* 2011). PDI reductase activity was decreased by ~36% (Figure 2.9A, 2.9D n=3, *$p<0.05$) in adipocytes matured in high glucose versus normal glucose, and increased succination was detected at the molecular weight of PDI (~57 kDa, arrow, Figure 2.9B) where the total levels

of PDI remained similar between all samples (Figure 2.9B). 1D-immunoblotting of PDI immunoprecipitates with anti-2SC verified that succination of PDI increased in FHKD versus control adipocytes (Figure 2.9C). The evaluation of PDI reductase activity in FHKD adipocytes demonstrated specifically that succination of PDI accounted for a 15% decrease in PDI reductase activity versus controls (Figure 2.9D, n=3, *p<0.05).

PDI was enriched from adipocytes matured in 5 mM or 30 mM glucose and analyzed by LC-MS/MS to confirm the endogenous sites of succination. A fragment ion (y13) representative of both control precursor ions containing active-site cysteines was detected in both adipocytes matured in 5 mM ($[M+3H]^{3+}$: 680.3434 m/z) ($[M+3H]^{3+}$: 670.6406 m/z) or 30 mM ($[M+3H]^{3+}$: 680.3387 m/z) ($[M+3H]^{3+}$: 670.6228 m/z) glucose (Figure 2.9E, 2.9F; panels 1 and 3). In contrast, the mass of the representative y13 fragment ion from each succinated precursor ion containing active-site cysteines ($[M+3H]^{3+}$: 683.3942 m/z) ($[M+3H]^{3+}$: 674.3534 m/z) was only detected in adipocytes matured in 30 mM glucose (Figure 2.9E, 2.9F; panel 2 versus 4). While the fragment ion profile was unique to these succinated peptides, the N-terminal or C-terminal location of the succinated cysteine could not be assigned, however, modification of either cysteine is sufficient to impair PDI function as both thiols participate in the oxidoreductase mechanism of PDI. Importantly, these measurements confirm that the endogenous succination of active-site cysteines in PDI selectively occurs in adipocytes matured in high glucose.

Control and *db/db* mice at 15 weeks of age were used for the analysis of

protein succination. The total epididymal fat pad weight, fasting blood glucose and plasma triglyceride levels of the *db/db* mice were all elevated compared to age matched control mice (Figure 2.10A). In order to establish if succination impacts PDI functionality *in vivo* we examined PDI enzymatic activity in the epididymal adipose tissue of *db/db* diabetic mice. Succinated PDI is found only in the epididymal adipose tissue of *db/db* mice and is absent in the epididymal adipose tissue of the control mice (Figure 2.10B, upper panels). Total PDI is detectable in both the control and *db/db* adipose tissue samples ~57 kDa (Figure 2.10B, lower panels). Assessment of PDI reductase activity using Di-Eosin-GSSG in control and *db/db* adipose tissue demonstrated that activity was reduced by 52.6% in the diabetic mice (n=4, *p<0.05, Figure 2.10C), while immunoblotting demonstrated equal amounts of PDI (Figure 2.10C). Immunoblotting with anti-GRP78 antibody verified our *in vitro* results that emphasize no alteration in the protein levels of GRP78 in the adipose tissue during diabetes however, probing with anti-CHOP confirmed the existence of ER stress in the epididymal adipose tissue from *db/db* mice versus controls, (Figure 2.10C) (Zhou *et al.* 2010). The succination of PDI occurs in parallel with reduced PDI reductase activity and the development of ER stress in the epididymal adipose tissue of *db/db* mice.

We have reported that decreasing glucotoxicity prevents the accumulation of succinated proteins in adipocytes (Frizzell *et al.* 2012), alleviating mitochondrial stress and permitting the turnover of succinated proteins. In the current study, we examined if limiting chronic glucose exposure

would be beneficial for recovery from ER stress in adipocytes. The accumulation of succinated proteins after 4 days of maturation (Tanis *et al.* 2015) was prevented when the high glucose medium was removed and replaced with normal glucose concentrations (30→5, Figure 2.11A). Notably, CHOP levels were also restored to those observed in normal glucose concentrations (Figure 2.11A), suggesting that limiting chronic high glucose exposure is sufficient to ameliorate ER stress in the adipocyte. To determine the mechanism of ER stress reduction, PDI was immunoprecipitated from adipocytes matured in 5 mM, 30 mM or 30→5 mM glucose. Immunoblotting verified that succination of PDI was greatest in adipocytes matured in 30 mM glucose for all 8 days of maturation, whereas 4 days of recovery under normal glucose concentrations rescued the amount of succinated PDI (Figure 2.11B). PDI reductase activity was 60% lower in adipocytes matured in 30 mM glucose versus 5 mM glucose, whereas the adipocytes matured in 30→5 mM glucose displayed a 46% decrease in PDI reductase activity (Figure 2.11C), indicating that a significant fraction of PDI functionality had been restored. The rescue of PDI reductase activity due to reduced succination of PDI contributes to an improved protein folding capacity, and diminished levels of ER stress in the adipocyte.

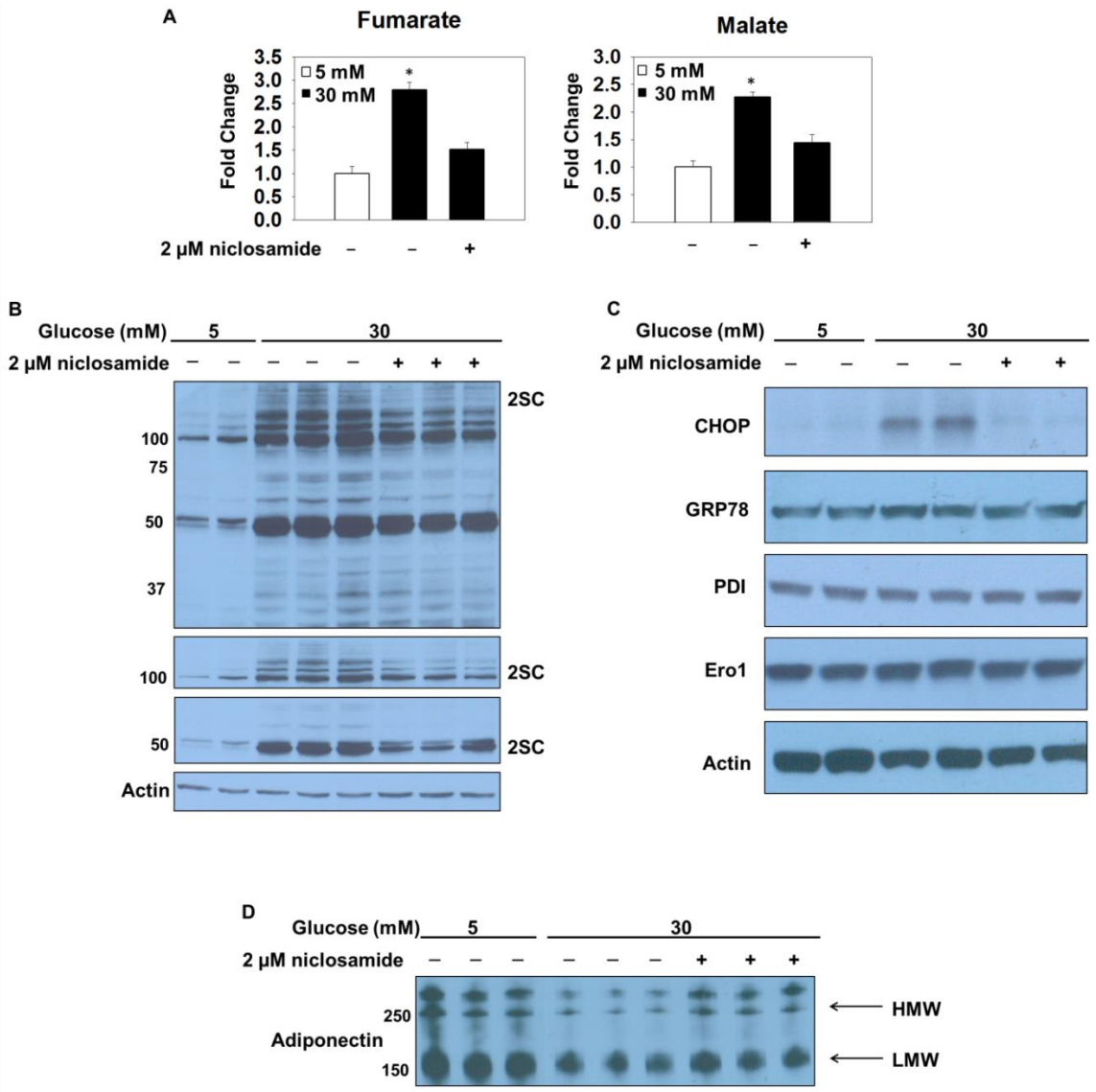

Figure 2.1: Mitochondrial stress drives ER stress in adipocytes matured in high glucose. (A) Krebs cycle metabolites were extracted from adipocytes matured in 5 mM or 30 mM glucose or 30 mM glucose and 2 μM niclosamide for 3 days prior to quantification by GC-MS. High glucose concentrations result in significantly increased levels of both fumarate and malate relative to the levels quantified in 5 mM glucose (n=3/group, mean +/- SEM, *p< 0.05). **(B)** Adipocytes were matured in 5 mM or 30 mM glucose for 8 days. A western blot was performed with 30 μg of protein from duplicate representative samples using anti-2SC antibody to detect succinated proteins. Molecular weight markers are shown on the far left. **(C)** Adipocytes were matured in 5 mM or 30 mM glucose 30 mM glucose with 2 μM nicolsamide for 8 days. Western blots were performed with 30 μg of protein to detect ER stress markers with anti -CHOP, -GRP78, -Ero1, and -PDI antibodies. Coomassie blue stain of the blot confirms equal loading of all samples. **(D)** An immunoblot probed with anti-adiponectin antibody shows the levels of secreted adiponectin assessed in the conditioned medium collected

after 4 hours from adipocytes matured in 5 mM or 30 mM glucose treated with 2 μM niclosamide. This is a merged image (merged between lanes 3 & 4). Immunoblots are representative of n=3 experiments.

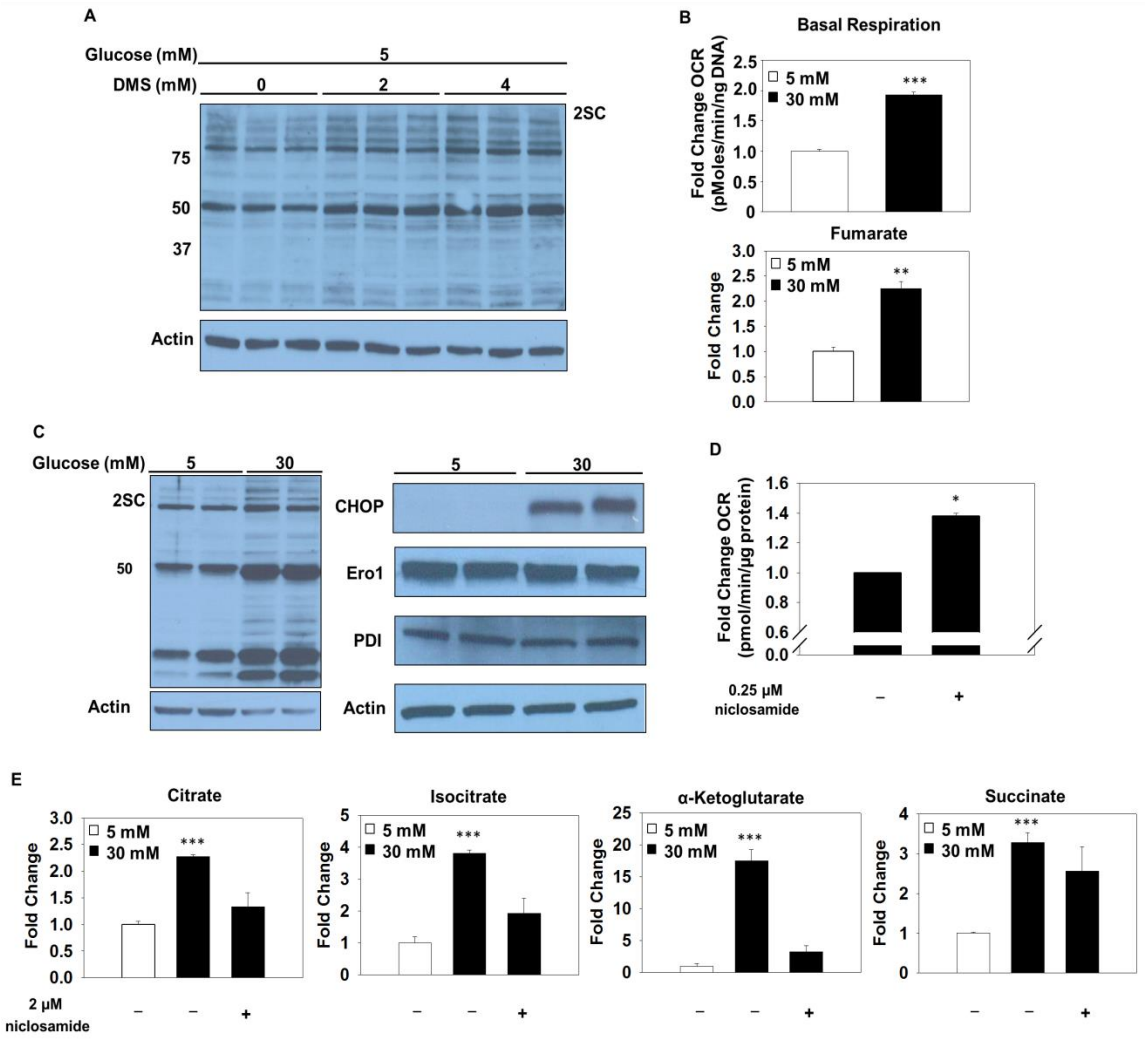

Figure 2.2: Quantification of additional Krebs cycle metabolites and confirmation of increased adipocyte metabolism, the uncoupling mechanism of niclosamide and ER stress in adipocytes matured in high glucose. (A) 3T3-L1 adipocytes were matured in 5 or 30 mM glucose and treated with 0, 2 or 4 mM dimethylsuccinate for 8 days. A 1D-immunoblot probed with anti-2SC antibody displays increased protein succination, specifically ~57kDa (black arrow). Re-probing with anti-actin antibody represents equal protein loading and molecular weight markers are shown of the left. **(B and E)** Krebs cycle metabolites were extracted from adipocytes matured in 5 mM or 30 mM glucose treated with or without 2 μM niclosamide for 3 days and derivatized prior to quantification by GC-MS. High glucose concentrations result in significantly increased the levels of all metabolites. The increases are expressed relative to the levels quantified in 5 mM glucose (n=3/group, mean +/- SEM, *p<

0.05). **(C)** Adipocytes were matured in 5 mM or 30 mM glucose for 8 days. Western blots were performed with 30 µg of protein to detect ER stress markers with anti -CHOP, -Ero1, and -PDI antibodies. Anti-actin immunoblot confirms equal loading of all samples. Immunoblots are representative of n=6 experiments. **(D)** The acute change in the oxygen consumption rate of adipocytes matured in 30 mM glucose for 2 days when niclosamide is added. 0.25 µM niclosamide was used in the acute 2 hour period to confirm uncoupling activity. The rate of oxygen consumption in adipocytes was measured by XF Flux Analyzer (Seahorse Biosciences) and the data was normalized to the total DNA content of the cells (n=5/group, mean +/- SEM, *p< 0.05).

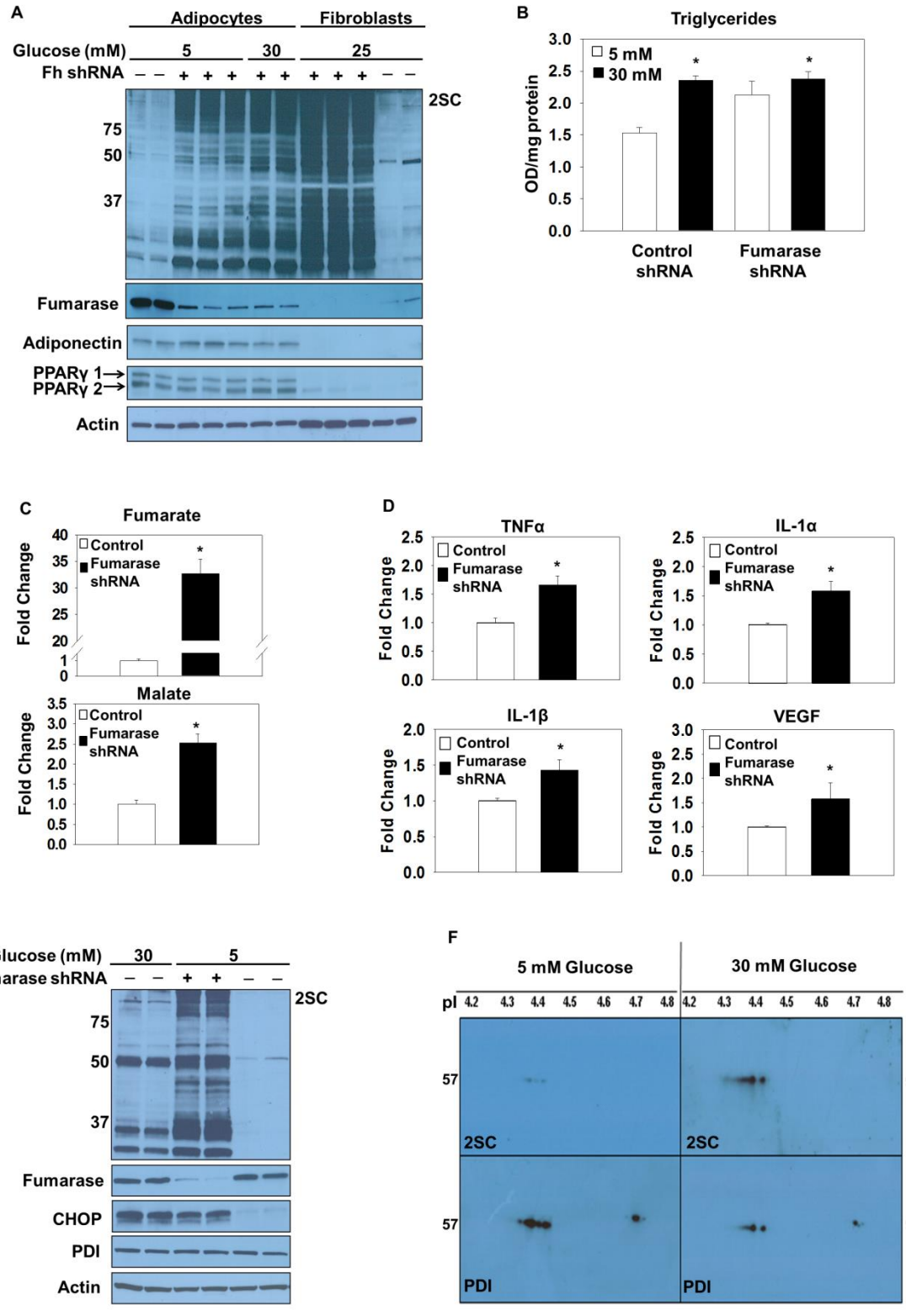

Figure 2.3: Protein succination induces ER stress independent of glucose levels. **(A)** Fibroblasts were transduced with scrambled (control) or *fumarase* (Fh) knockdown (FHKD) shRNA and grown to confluence. FHKD or control

adipocytes were matured in 5 mM or 30 mM glucose for 8 days. A merged image of the same 1D-immunoblot probed with anti-2SC and -Fh antibodies display increased protein succination in both fibroblasts and adipocytes when Fh expression is knocked down. The blot was stripped and reprobed with anti-PPARγ antibody to confirm that FHKD 3T3-L1 fibroblasts differentiate normally to adipocytes. The blot was reprobed with anti-α tubulin antibody as a protein loading control. **(B)** Control or FHKD adipocytes were matured in 5 mM or 30 mM glucose for 8 days. The triglyceride content was measured as described in Materials and Methods (n=3/group, mean +/- SEM, *p<0.05). **(C)** Krebs cycle metabolites were extracted from adipocytes transduced with scrambled control or FHKD lentivirus and matured in 5 mM glucose for 3 days and derivatized prior to quantification by GC-MS. Limited Fh expression result in significantly increased the levels of all metabolites. The increases are expressed relative to the levels quantified in control adipocytes that have normal levels of Fh present (n=3/group, mean +/- SEM, *p< 0.05). **(D)** Secreted levels of pro-inflammatory cytokines were measured by a mouse obesity ELISA as described in the Materials and Methods (n=4/group, mean +/- SEM, *p<0.05). **(E)** Adipocytes transduced with FHKD or scrambled control lentivirus were matured in 5 mM or 30 mM glucose for 8 days. 1D-immunoblots of duplicate samples probed with anti-2SC and -Fh antibodies show that knocking down Fh levels increases protein succination in adipocytes to the greatest degree versus both 5 mM and 30 mM glucose treatments when Fh is present. Western blotting with anti-CHOP antibody confirms that ER stress is present in both adipocytes matured in 30 mM glucose and FHKD adipocytes matured in 5 mM glucose. **(F)** Protein (500 µg) from adipocytes matured in 5 mM or 30 mM glucose was immunoprecipitated with anti-PDI antibody. The antibody-antigen complex was captured with Protein G beads. The eluted complex was isoelectrically focused on strips with a pI range 3.9-5.1. After 2D electrophoresis and protein transfer a western blot was performed to detect succination using anti-2SC (upper panel), followed by re-probing with anti-PDI to verify PDI immunoprecipitation (lower panel).

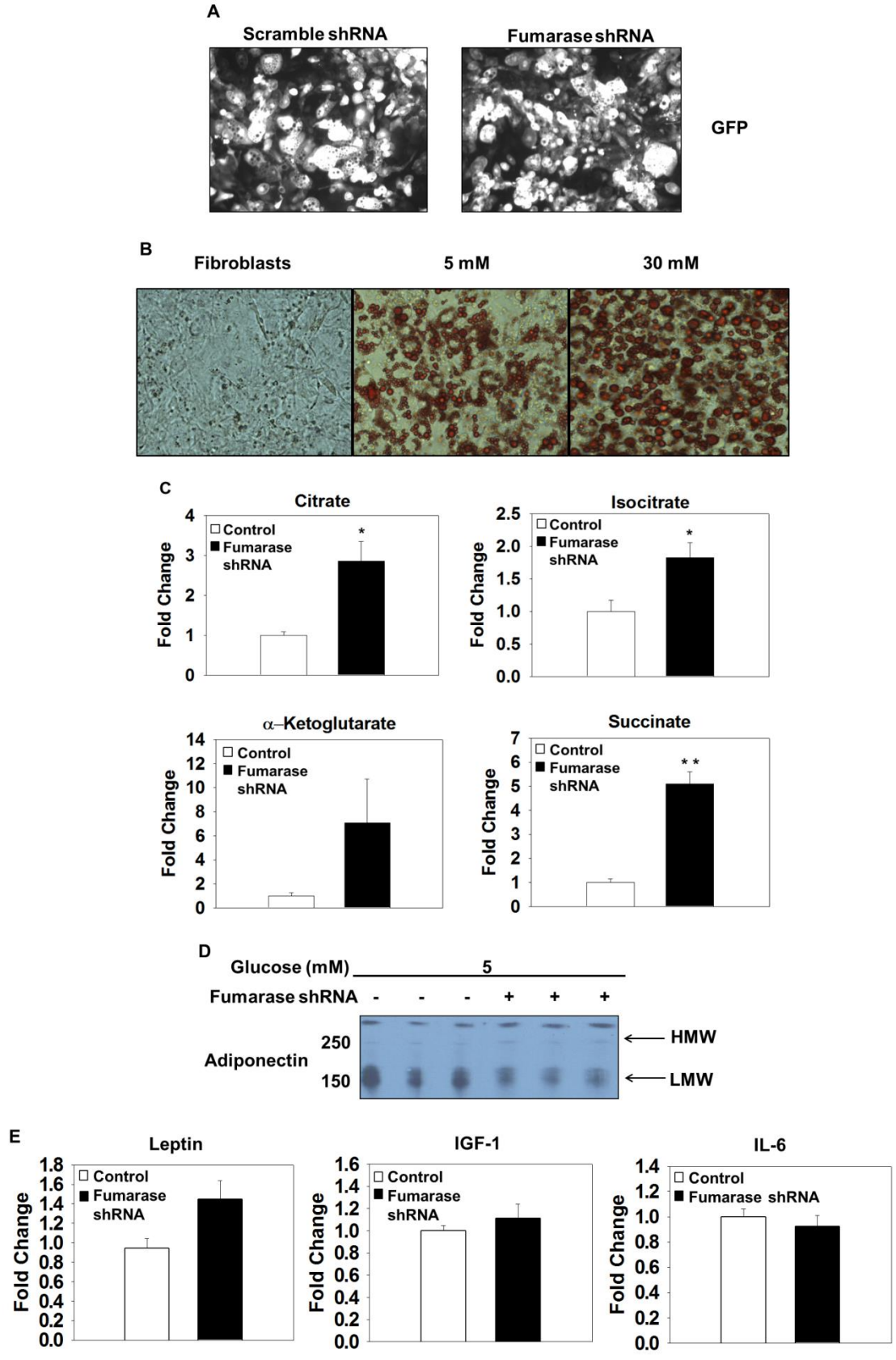

Figure 2.4: Verification of lentivirus transduction and adipocyte differentiation and quantification of Krebs cycle metabolites and secreted adipokines in control and FHKD adipocytes. (A) 3T3-L1 adipocytes were transduced with a scrambled (control) vector or FHKD shRNA coupled to green fluorescent protein expression. Positive green fluorescent protein (GFP) expression within adipocytes matured in 30 mM glucose for 8 days confirms scramble (left) or FHKD (right) viral expression. **(B)** 3T3-L1 fibroblasts and FHKD adipocytes matured in 5 mM or 30 mM glucose were stained with Oil Red O and representative images (n=3) of lipid droplet accumulation are documented by brightfield microscopy. **(C)** Krebs cycle metabolites were extracted from adipocytes transduced with scrambled control or FHKD lentivirus and matured in 5 mM glucose for 3 days and derivatized prior to quantification by GC-MS. Limited fumarase expression result in significantly increased the levels of all metabolites. The increases are expressed relative to the levels quantified in control adipocytes that have normal levels of fumarase present (n=3/group, mean +/- SEM, *p< 0.05). **(D)** An immunoblot probed with anti-adiponectin antibody shows the levels of secreted adiponectin analyzed in the conditioned medium collected from control and FHKD adipocytes. **(E)** Secreted levels of pro-inflammatory cytokines were measured by a mouse obesity ELISA as described in the Materials and Methods.

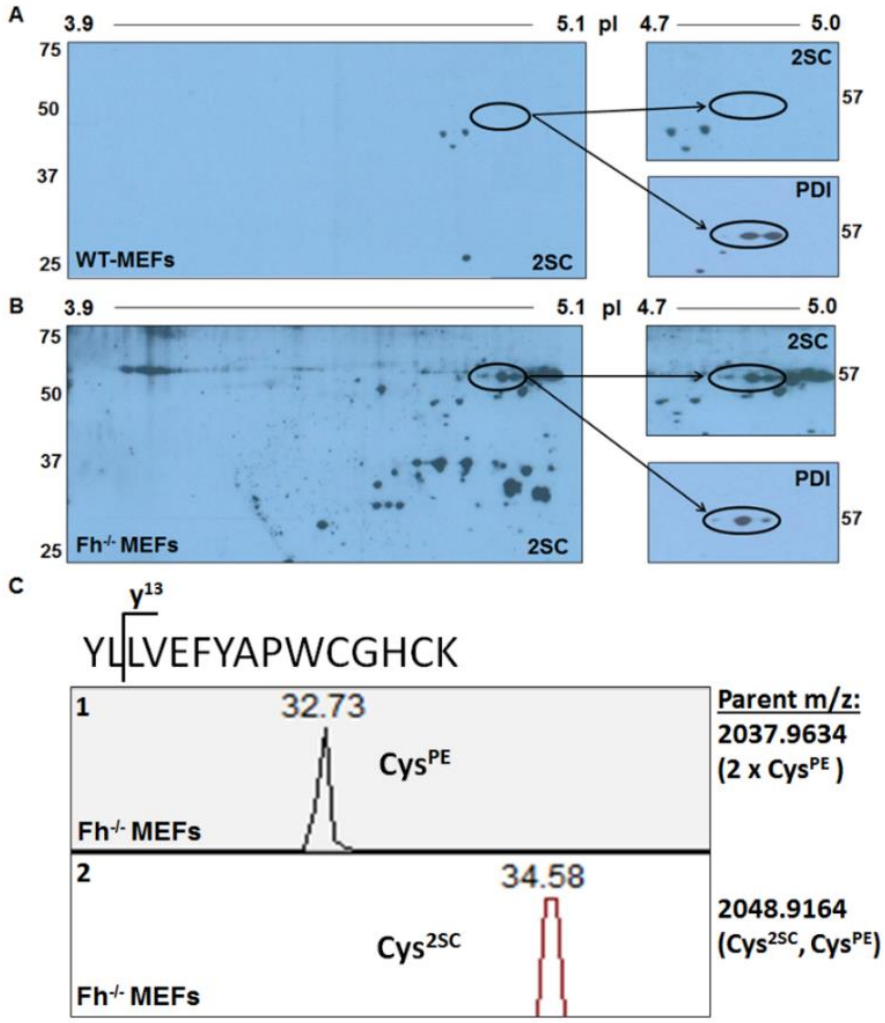

Figure 2.5: Succination of endogenous PDI in *Fh1*$^{-/-}$ MEFs. 200 µg of cell lysate protein from (**A)** wild-type (WT) and (**B)** *Fh1*$^{-/-}$ MEFs (1,2) was isoelectrically focused on strips with a pI range 3.9-5.1. After 2D electrophoresis & protein transfer a western blot was performed to detect succination using anti-2SC (left panels). Enlarged 2D-immunoblot images in the pI 4.7-5.0 region of the WT **(A)** and *Fh1*$^{-/-}$ **(B)** MEFs depict the presence of PDI at 57 kDa (pI ~4.8) in each sample. *Fh*$^{-/-}$ MEFs contain a significant amount of succinated PDI (note 3 distinct spots in the oval region corresponding to the 3 spots labeled with anti-PDI below), while there is no detectable succinated PDI in WT MEFs. Molecular weight markers are shown on the far left. **(C)** *Fh1*$^{-/-}$ MEFs were matured in 25 mM glucose for 4 days. The active site peptide of PDI containing Cys55 and Cys58 were analyzed by LC-ESI-MS/MS. The detection of the y13 fragment ion at retention time ~32.73 minutes represents the presence of the control (Cys^{PE}, Cys^{PE}) active site peptide in PDI (panel 1). The detection of the analogous y13 fragment ion at the retention time ~34.58 minutes represents the presence of the succinated (Cys^{PE}, Cys^{2SC}) active site peptide (panel 2). WT, wild type; Fh$^{-/-}$, fumarase gene knockout; MEFs, mouse embryonic fibroblasts.

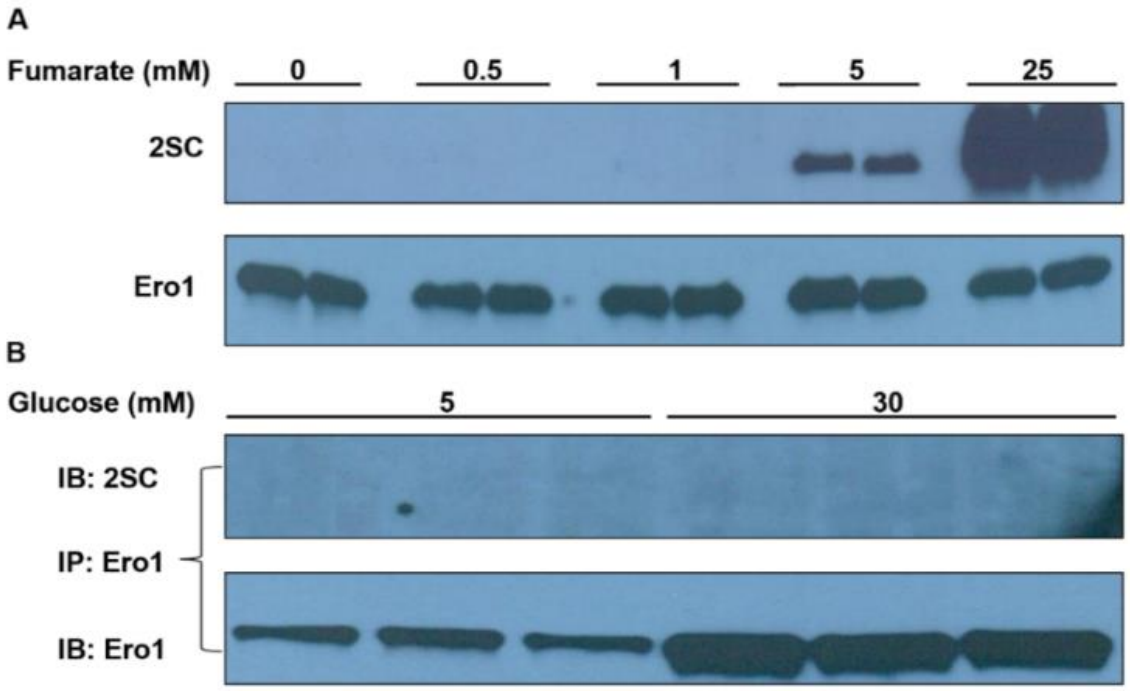

Figure 2.6: Succination of Ero1α *in vitro*. (A) 2.77 µg of recombinant Ero1α (3) was incubated in the presence or absence of the indicated fumarate concentrations for 24 hrs. A western blot with 2.77 µg of protein was probed with anti-2SC antibody confirmed a concentration-dependent increase in Ero1 succination when incubated with 5 mM or 25 mM fumarate. The blot was reprobed with anti-Ero1α antibody to verify equal protein loading. (**B)** Protein (500 µg) from adipocytes matured in 5 mM or 30 mM glucose was immunoprecipitated with anti-Ero1α antibody. The antibody-antigen complex was captured with Protein A beads. The eluted complex was subjected to 1D-immunoblotting with anti-2SC antibody to detect succination of Ero1. However, Ero1 succination was not detected in the adipocytes, independent of glucose concentration. The blot was reprobed with anti-Ero1α antibody to confirm the presence of Ero1 in the immunoprecipitated samples. Therefore, although recombinant Ero1 could be succinated *in vitro*, we were not able to detect any endogenous succination of Ero1 in the adipocytes. Immunoblots are representative of n=4 experiments.

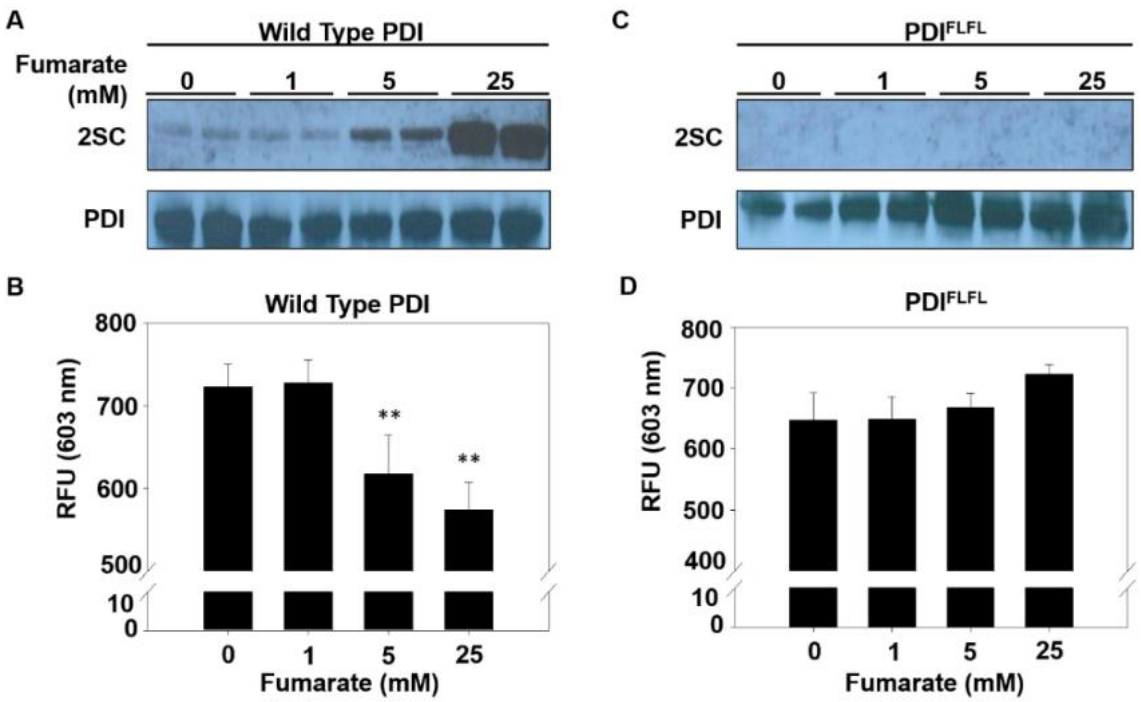

Figure 2.7: Succination inhibits PDI reductase activity *in vitro*. (A and B) Both the wild type and mutant recombinant PDI were incubated with indicated fumarate concentrations for 24 hrs. A western blot with 2.77 µg of protein was probed with anti-2SC and anti-PDI antibodies. Immunoblots are representative of n=5. **(C and D)** 2.77 µg of wild type or mutant recombinant PDI were incubated in the presence or absence of the indicated fumarate concentrations for 24 hrs. PDI reductase activity of control and succinated PDI was assayed as described in *Materials and Methods* using a fluorescent insulin turbidity assay. Fluorescence was measured at λ_{ex} = 500 nm and λ_{em} =603 nm (n=5/group, mean +/- SEM, **p< 0.01).

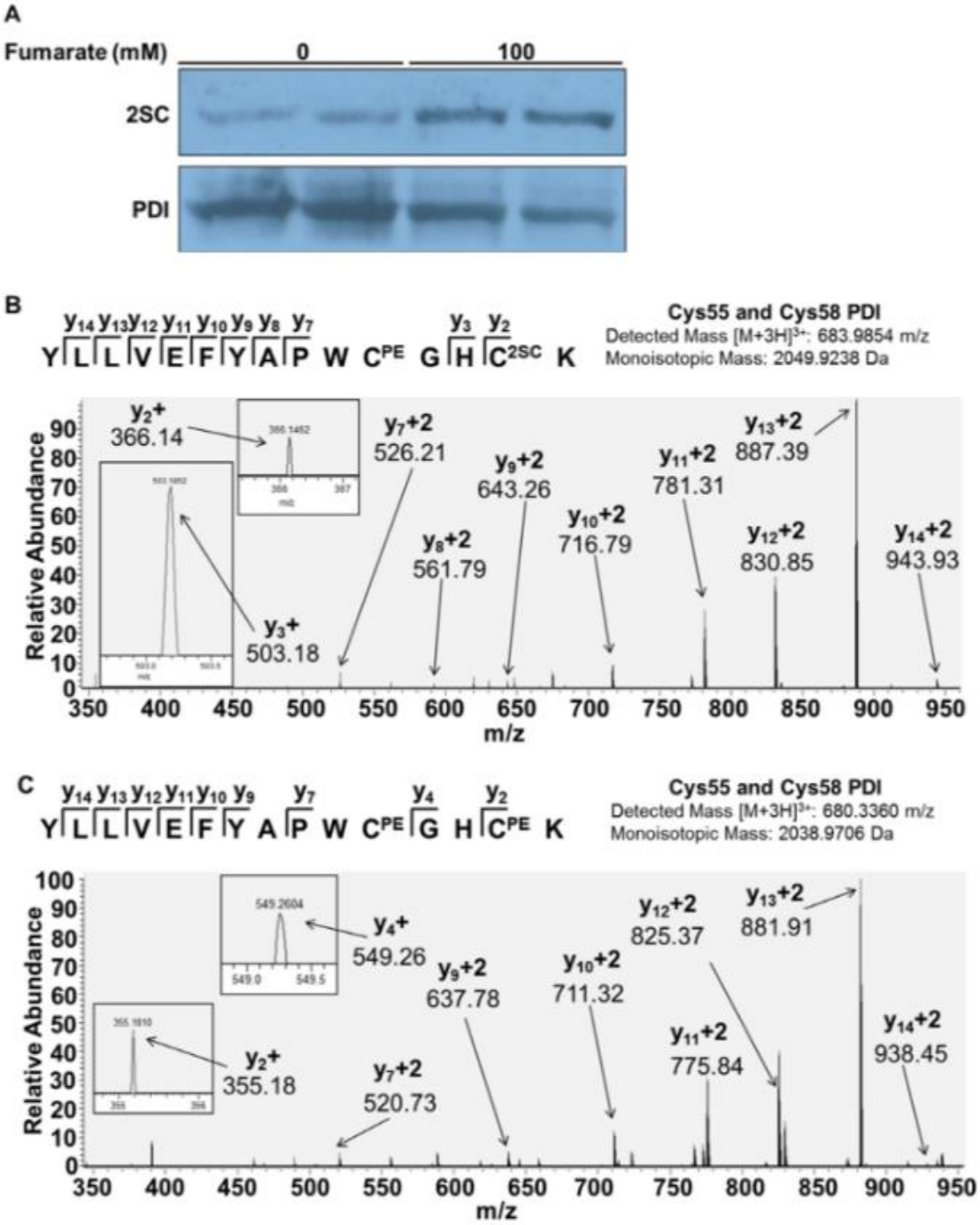

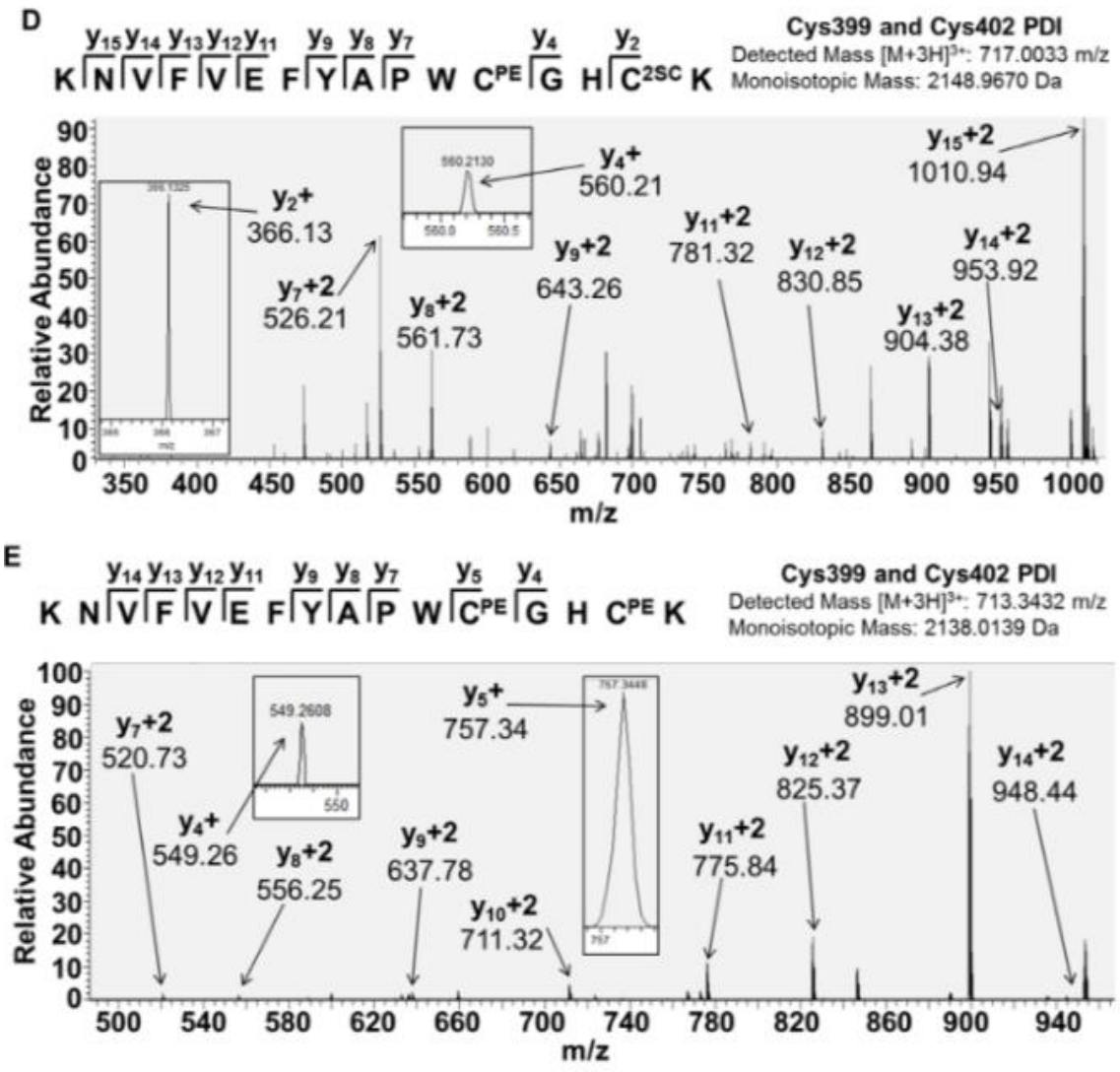

Figure 2.8: Identification of succination sites in PDI. (A) 2.77 µg of recombinant human PDI (PDI-WT) was incubated with 0 or 100 mM fumarate at 37°C for 24 hrs. A 1D-immunoblot probed with anti-2SC antibody followed by reprobing with anti-PDI antibody shows enhanced succination of PDI when incubated with 100 mM fumarate. **(B-E)** 3 µg of recombinant PDI was incubated in the presence **(B and D)** or absence **(C and E)** of 100 mM fumarate to maximize succinated peptides for LC-MS detection, resolved by SDS-PAGE and stained with Coomassie Brilliant Blue. The protein corresponding to 57 kDa was excised from the gel, digested with trypsin and the active site peptides were analyzed by LC-ESI-MS/MS mass spectrometry. (**B and D)** MS/MS spectra showing that the C-terminal cysteines in both active site peptides ^{45}YLLVEFYAPW**C^{PE}**GH**C^{2SC}**K^{59} and ^{389}KNVFVEFYAPW**C^{PE}**GH**C^{2SC}**K^{403} are the target of succination *in vitro*. **(C and E)** MS/MS spectra showing the unmodified peptides ^{45}YLLVEFYAPW**C^{PE}**GH**C^{PE}**K^{59} and ^{389}KNVFVEFYAPW**C^{PE}**GH**C^{PE}**K^{403} after alkylation with 4-vinylpyridine. m/z, mass/charge ratio; PE, pyridyl ethyl.

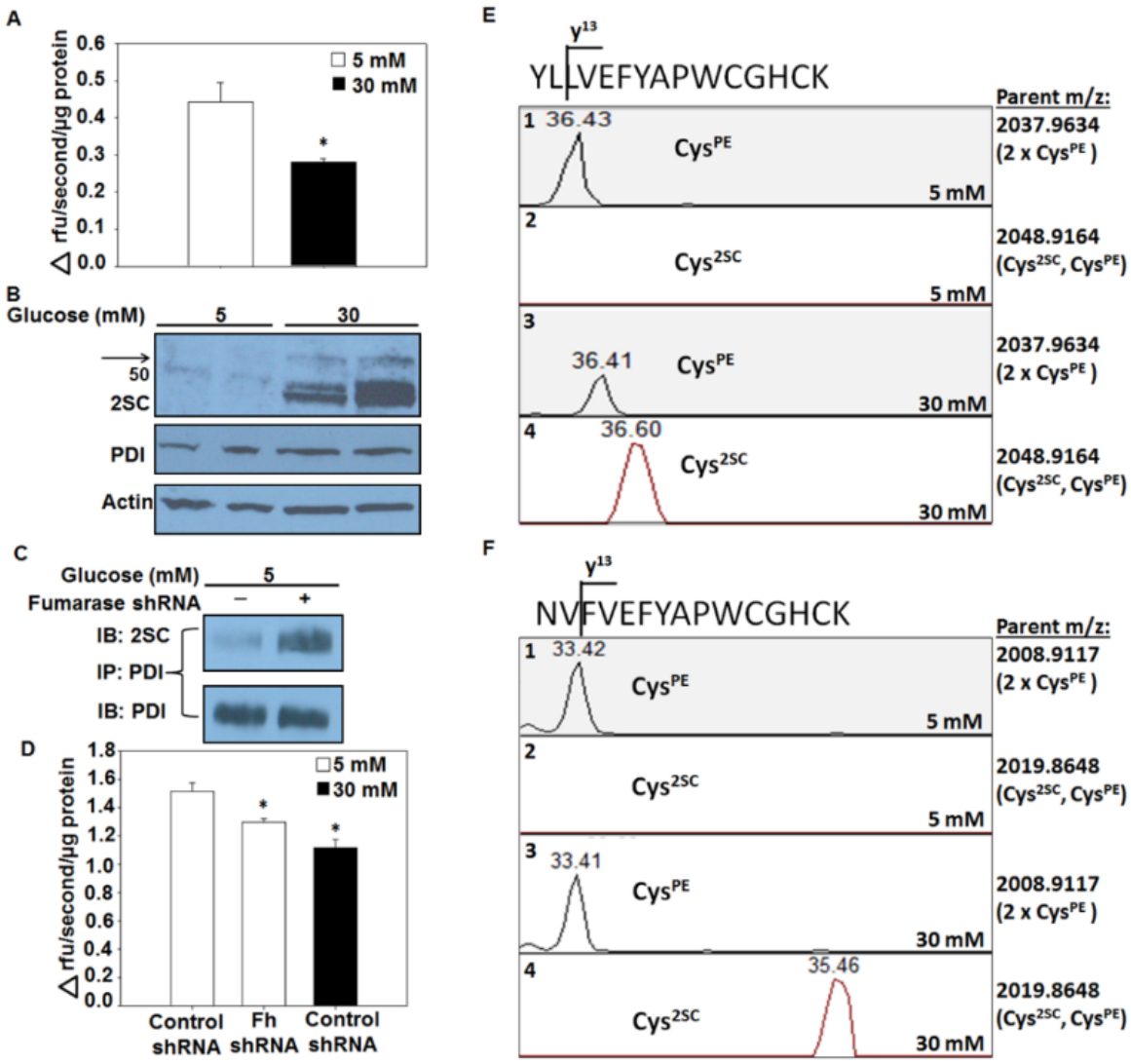

Figure 2.9: Succination of PDI active-site cysteines inhibits PDI reductase activity in 3T3-L1 adipocytes. (A) Adipocytes were matured in 5 mM or 30 mM glucose for 7 days. 6 µg of adipocyte cell lysate protein was incubated with 1.08 µM Di-Eosin-GSSG for 1 hr. Fluorescence was measured at λ_{ex}= 510 nm and λ_{em}= 550 nm and the initial rate of reaction calculated (n=4/group, mean +/- SEM, *p< 0.05). **(B)** Western blots with anti-2SC and -PDI antibodies show succination of PDI in the adipocytes matured in 30 mM glucose (black arrow) and representative equal amounts of PDI in each sample. An immunoblot with anti-actin antibody displays equal protein loading. **(C)** Protein (400 µg) from control or FHKD adipocytes matured in 5 mM glucose was immunoprecipitated with anti-PDI antibody and the antibody-antigen complex was captured with Protein G beads. The eluted complex was subjected to 1D-immunoblotting and probed with anti-2SC (upper panel) and anti-PDI (lower panel) antibodies. **(D)** 6 µg of adipocyte cell lysate protein was incubated with 1.08 µM Di-Eosin-GSSG for 1 hr. Fluorescence was measured at λ_{ex}= 510 nm and λ_{em}= 550 nm (n=3/group, mean

+/- SEM, *p< 0.05). **(E)** The active-site peptides of PDI from adipocytes matured in 5 mM or 30 mM glucose for 8 days were analyzed by LC-ESI-MS/MS. The detection of the y13 fragment ion at retention time ~36.4 minutes represents the presence of the control ($C55^{PE}$, $C58^{PE}$) PDI active-site peptide from adipocytes matured in both 5 mM (panel 1) and 30 mM (panel 3) glucose. The detection of the y13 fragment ion at the retention time ~36.6 minutes represents the presence of the succinated ($C55^{PE}$, $C58^{2SC}$) active-site peptide in adipocytes matured in 30 mM glucose (panel 4) and the absence of the succinated peptide in adipocytes matured in 5 mM glucose (panel 2). **(F)** The detection of the y13 fragment ion at retention time ~33.4 minutes shows the presence of the control ($C399^{PE}$, $C402^{PE}$) active-site peptide in PDI from adipocytes matured in both 5 mM (panel 1) and 30 mM (panel 3) glucose. The detection of the y13 fragment ion at the retention time ~35.5 minutes indicates the presence of the succinated ($C399^{PE}$, $C402^{2SC}$) active-site peptide in adipocytes matured in 30 mM glucose (panel 4) and the absence of the succinated peptide in adipocytes matured in 5 mM glucose (panel 2).

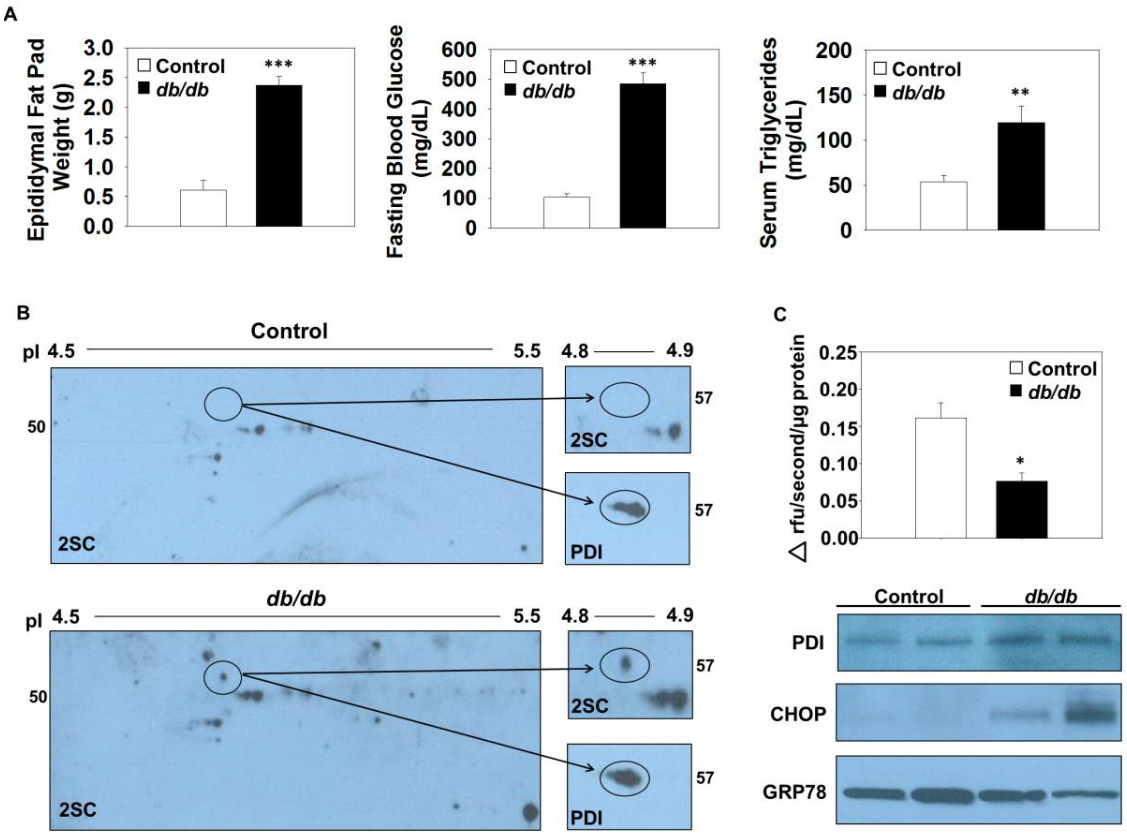

Figure 2.10: Succination inhibits PDI reductase activity in adipose tissue of *db/db* mice. (A) Epididymal fat pads were removed and weighed at the time of sacrifice. Fasting blood glucose was measured from the tail vein and serum triglyceride levels were measured (n=5-6 mice/group, mean +/- SEM, **p<0.01, ***p<0.001). All *in vivo* analysis were performed at 15 weeks of age**. (B)** 200 µg of protein from control (top) and *db/db* (lower) mouse epididymal adipose tissue was isoelectrically focused on a pI range 4-7. After 2D electrophoresis & protein transfer a western blot was performed to detect succination using anti-2SC antibody, followed by reprobing to verify PDI. Enlarged 2D-immunoblot images in the pI 4.7-4.9 region of the control and *db/db* adipose tissue depict the presence of PDI at 57 kDa (pI ~4.85) in each sample. Molecular weight markers are shown on the far left and right. **(C)** 6 µg of protein from control and *db/db* mouse epididymal adipose tissue was incubated with 1.08 µM Di-Eosin-GSSG for 1 hr. Fluorescence was measured at λ_{ex} = 510 nm and λ_{em} = 550 nm (n=3/group, mean +/- SEM, *p< 0.05). A western blot with anti-PDI antibody shows representative equal amounts of PDI in each sample. Immunoblotting 30 µg of total protein lysate from control and *db/db* mouse epididymal adipose tissue with anti-CHOP and -GRP78 antibodies of demonstrates increased levels of CHOP and no change in the levels of GRP78 in the adipose tissue from *db/db* versus control mice (representative of n=6 mice).

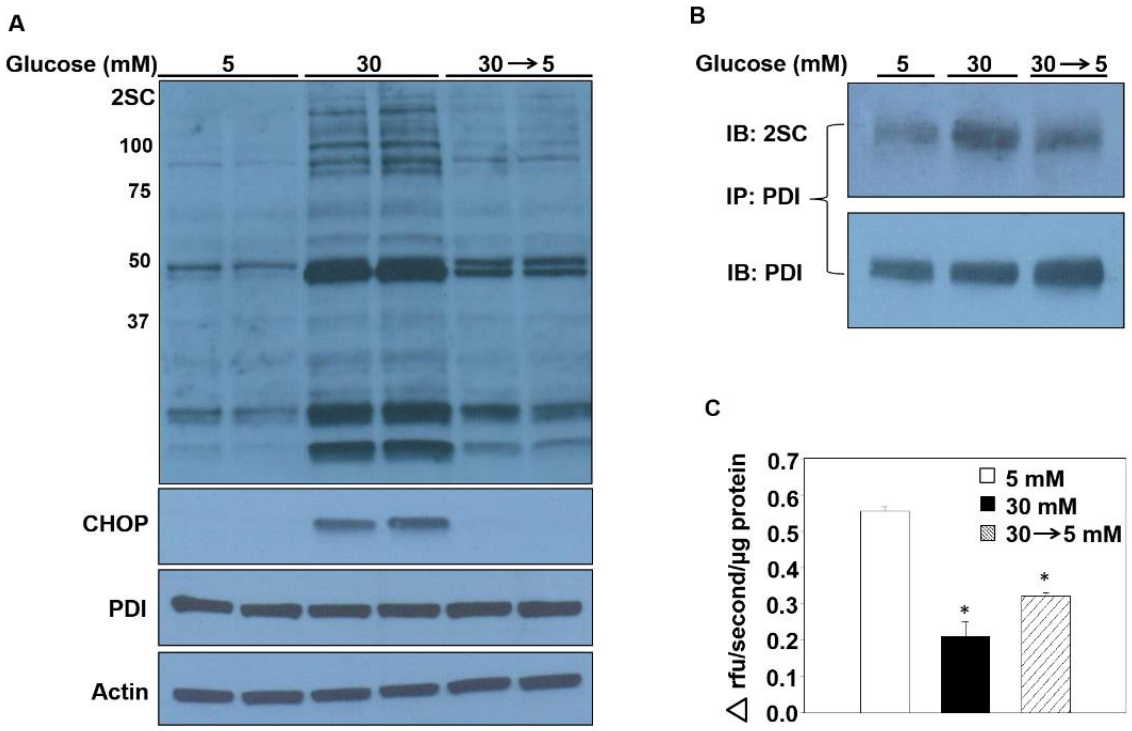

Figure 2.11: Reducing glucose concentrations rescues PDI reductase activity and ameliorates ER stress in adipocytes. (A) Adipocytes were matured in 5 mM or 30 mM glucose for 8 days or 30 mM glucose for 4 days, followed by a switch to 5 mM glucose for the remaining 4 days of maturation (30→5 mM). Western blotting was performed with 30 µg of protein using anti-2SC antibody to detect succinated proteins. A merged image of the same blot displays duplicate representative samples. Molecular weight markers are shown on the far left. An immunoblot with the identical samples was probed with anti-CHOP, -PDI and -actin antibodies to detect changes in protein expression. **(B)** Protein (300 µg) from adipocytes matured in 5 mM, 30 mM or 30→5 mM glucose was immunoprecipitated with anti-PDI antibody. After 1D electrophoresis and protein transfer a western blot was performed to detect succination using anti-2SC (upper panel), followed by reprobing with anti-PDI to verify PDI (lower panel). **(C)** Adipocytes were matured in 5 mM, 30 mM or 30→5 mM glucose. 6 µg of adipocyte cell lysate protein was incubated with 1.08 µM Di-Eosin-GSSG for 1 hr after which fluorescence was measured at λ_{ex} = 510 nm and λ_{em} =550 nm (n=3/group, mean +/- SEM, *p< 0.05).

2.3 Discussion

In this study we mechanistically demonstrate that succination of PDI, as a direct result of glucotoxicity driven mitochondrial stress, contributes to the presence of ER stress in the adipocyte. Consistent with other reports (Boden *et al.* 2014b, Han *et al.* 2013b) we document a significant increase in the protein levels of CHOP in adipocytes matured in high glucose medium, and notably this occurs in parallel with an increase in protein succination, suggesting a link between mitochondrial stress and ER stress. Niclosamide is a mild mitochondrial uncoupler that reduces mitochondrial stress by lowering the mitochondrial membrane potential and increasing the ADP:ATP ratio *in vitro*, and significantly improves glucose homeostasis in diabetic mice (Tao *et al*. 2014). In Figure 2.1 we demonstrate two novel roles for niclosamide; succination of proteins, including PDI, is decreased by directly reducing mitochondrial stress, and it prevents increased protein levels of CHOP, indicative of protection against ER stress in adipocytes matured under diabetic conditions. In addition, we detected a significant improvement in high molecular weight adiponectin secretion from adipocytes in the presence of niclosamide. Zhou *et al.* have described the requirement for normal levels of the ER chaperone disulfide-bond-A oxidoreductase-like protein to successfully combat ER stress in the adipocyte (Zhou *et al.* 2010). Our initial assessment of ER stress markers demonstrated that increased CHOP was present, however we did not observe altered PDI or Ero1 protein levels in the adipocytes matured in high glucose. Instead our findings suggest that succination-mediated inhibition of the enzyme determines

the ability of PDI to facilitate protein folding in a metabolically challenging environment.

The mitochondrial associated ER membrane (MAM) facilitates the passage of lipids and several ions through several defined channels (Arruda *et al.* 2014, Rutter *et al*. 2014). MAM enrichment, facilitating calcium transport, has been reported in hepatocytes of *ob/ob*- and high fat diet fed mice (Arruda *et al*. 2014). Excess fumarate produced in the mitochondria is transported to the cytosol and out of the cell (Lai and Gold, 1992), or it may enter the ER lumen through the MAM, facilitating the succination of ER proteins (Merkley *et al.* 2014). In this study, we have confirmed that endogenously produced fumarate increased succination of PDI in adipocytes matured in high glucose concentrations, and that succination inhibits PDI reductase activity in these adipocytes and in the adipose tissue of diabetic *db/db* mice. Similar to the inhibitory effect of S-glutathionylation and S-nitrosylation on PDI enzymatic activity (Townsend *et al.* 2009, Uehara *et al*. 2006), increasing succination of PDI is also indirectly correlated with its reductase activity. Alongside this, we specifically confirmed that the cysteine containing active-site peptides of PDI are endogenously succinated in adipocytes matured in high glucose medium. The significant reduction in PDI reductase activity contributes to disturbed protein folding by decreasing the capabilities of the major ER oxidoreductase, ultimately resulting in the pronounce CHOP levels sustained in adipocytes *in vitro* and *in vivo*.

PDI-A1 is the most abundant isoform of the PDI oxidoreductase family in

the adipocyte. Despite the fact all PDI family member (A1-A6) active-site peptides were analyzed by MS/MS mass spectrometry, the active-site peptides of PDI-A1 remained the most abundantly detected, suggesting that PDI-A1 has a major role in adipocyte ER protein folding. In addition, Muller *et al.* have demonstrated that increased expression of functional PDI-A1 alone is sufficient to preclude ER stress in HMEC-1 cells (Muller *et al.* 2013). We originally hypothesized that the N-terminal low pK_a active-site Cys55 and Cys399 of PDI would be more reactive with fumarate than the higher pK_a C-terminal active-site Cys58 and Cys402 (Lappi *et al.* 2004). However, MS/MS analysis of recombinant PDI that had been succinated *in vitro* confirmed that the C-terminal Cys58 and Cys402 are the targets of succination. The recombinant PDI mutant used was refractory to modification by fumarate, suggesting that the pK_a of at least one of the thiols is an important determinant of reactivity to succination. Importantly, mutation of the N-terminal, C-terminal or both active-site Cys of PDI to Ser decreases PDI oxidoreductase activity and increases the accumulation of PDI-substrate intermediates (Walker *et al.* 1996), suggesting that modification of the active site will promote the accumulation of misfolded proteins in the ER.

Although the ER resident protein Ero1 is susceptible to succination *in vitro* (Figure 2.6A), immunoprecipitation of Ero1 confirms that endogenous succination of Ero1 is not altered between adipocytes matured in normal or high glucose concentrations (Figure 2.6B). The reduced form of Ero1 mediates the flavin-dependent transfer of electrons to oxygen producing hydrogen peroxide and the oxidized form of Ero1. Peroxiredoxin-4 (Prx-4) is responsible for regulating

excess reactive peroxides produced in the ER via Ero1 oxidation (Tavender *et al.* 2008, Tavender *et al.* 2010). Proper functioning PDI will reduce the oxidized form of Prx-4 to allow for recycling of Prx-4 active site cysteines and continued moderation of reactive peroxide levels in the ER (Tavender *et al.* 2010, Zito *et al.* 2010). Overall, the inhibition of PDI reductase activity by 2SC may promote the accumulation of oxidized Ero1, oxidized Prx-4 and elevated hydrogen peroxide levels in the adipocyte ER and additionally contribute to oxidative stress. In other studies we have observed that oxidized thiols (sulfenic acid form) do not react with fumarate as readily as the thiolate (unpublished observations), providing an explanation for the absence of succinated, but possibly oxidized, Ero1 in our immunoprecipitations, even when the recombinant protein could be succinated *in vitro.*

High glucose conditions facilitate increased metabolic stress derived in part from fumarate, but also increased oxidative and lipotoxic stress. To determine the contribution of fumarate and protein succination to reduced PDI functionality, we knocked down fumarase expression and generated mature adipocytes with elevated levels of protein succination. Strikingly, the elevation in CHOP protein levels in FHKD adipocytes demonstrates that ER stress is a direct negative consequence of mitochondrial stress in adipocytes. In addition, Figure 2.9 suggests that half of the total decrease in PDI reductase activity in adipocytes matured in high glucose may be specifically attributed to increased succination of PDI.

Chemical chaperones, such as PBA have been employed to combat ER

stress in several rodent models of obesity and diabetes (Basseri *et al.* 2009, Özcan *et al.* 2006), as continuous ER stress ultimately culminates in cell death (Han *et al.* 2013b). The accumulation of adipose tissue macrophages as a result of hypertrophied adipocyte death is central to the chronic low-grade inflammatory response observed in obese adipose tissue (Giordano *et al.* 2013, Weisberg *et al.* 2003). We have reported that greater amounts of inflammatory cytokines are released from adipocytes matured in high glucose compared to normal glucose levels in parallel with increased protein succination (Tanis *et al.* 2015). In Figure 2.3 we show that increased inflammatory cytokine secretion occurs as a result of increased fumarate content and protein succination in the FHKD adipocyte. This data suggests that intra-organelle stress derived from elevated mitochondrial intermediary metabolism may be an early contributor to adipose tissue inflammation in diabetes.

The accumulation of the mitochondrial metabolite fumarate and resultant succination and inhibition of PDI activity uniquely links mitochondrial stress, a decreased protein folding capacity and ER stress. The reduction of ER stress in obese humans using chemical chaperones has had some success (Kars *et al.* 2010), however, we have mechanistically demonstrated that targeting mitochondrial stress is a necessary component of successfully preventing ER stress-associated increases in CHOP. Since mitochondrial stress is a product of nutritional overload, we reduced the glucose concentration to normal levels in maturing adipocytes for several days, similar to a calorie restriction intervention, and demonstrated a significant reduction in PDI succination and an improvement

in PDI reductase activity. Stanford *et al.* have described the importance of healthy adipose tissue for systemic glucose homeostasis by transplanting the subcutaneous white adipose tissue from exercised lean animals into sedentary animals fed a high fat diet, improving insulin sensitivity and blood glucose levels in the sedentary animals (Stanford *et al.* 2015). We demonstrate that a reduction in exposure to glucotoxicity limits CHOP production as a result of reduced mitochondrial stress and improved PDI reductase activity. While specific agents that prevent protein succination in adipose tissue, such as niclosamide, may have therapeutic utility, our data clearly demonstrates that simple nutritional interventions will restore ER oxidative protein folding capacity.

In summary, we find that the active-site cysteines of PDI are succinated during glucotoxicity induced mitochondrial stress, reducing PDI oxidoreductase activity and contributing to disturbed protein folding and adipocyte ER stress. The improvement in PDI enzymatic function and the reduction in ER stress as a direct result of reduced glucose concentration fortify the importance of emphasizing the link between healthy dietary consumption and proper adipocyte function in the management of Type 2 diabetes.

Chapter 3

Succination Induces Oxidative Stress and Regulates CHOP Stability in the Adipocyte.[2]

[2]Manuel AM, Walla MD, Piroli GG, Frizzell N. To be submitted to *Molecular Metabolism*

3.1 Introduction

The production of C/EBP homologous protein (CHOP) as a consequence of prolonged endoplasmic reticulum stress has been documented extensively in the adipose tissue of diabetic mouse models and type 2 diabetic patients (Boden *et al.* 2008, Kawasaki *et al.* 2012, Özcan *et al.* 2004, Schröder *et al.* 2005, Sharma *et al.* 2008). Consistent with these observations, in chapter 2 we described a prominent role for increased fumarate to elevate CHOP production during sustained ER stress. CHOP signaling is regulated by casein kinase 2 phosphorylation at Ser30, inhibiting transcriptional activation in 3T3-L1 fibroblasts and HeLa cells (Ubeda *et al*. 2003), and promoting the ubiquitination and proteasomal degradation of CHOP in macrophages (Dai *et al.* 2016). However, little is known about the mechanism regulating CHOP stability in the adipocyte during normal versus diabetic conditions. CHOP levels are increased as a result of adipogenesis and remain elevated in adipocytes matured in high glucose (Basseri *et al*. 2009, Han *et al*. 2013a, Tanis *et al.* 2015). In an extension of this observation, Tanis *et al.* highlighted the difference in CHOP levels between adipocytes matured in normal (5 mM) glucose versus high (30 mM) glucose after monitoring CHOP for up to 8 days of maturation. Interestingly, CHOP levels are transiently elevated and then decreased in adipocytes matured in 5 mM glucose in a time-dependent manner, in contrast they remain elevated in high glucose (Tanis *et al.* 2015). The sustained increase in CHOP that is unique to high glucose occurs in parallel with increased protein succination, and in the absence of continued activation of the unfolded protein response (Tanis *et al.* 2015).

Kelch-like ECH-associated protein 1 (Keap1) has recently been described as a negative regulator of CHOP stability in the LiSa-2 adipocyte cell line (Huang *et al.* 2012). In adipocytes, Keap1 and cullin3 E3 ubiquitin ligase form a supercomplex with the COP9 signalosome (CSN) (Huang *et al.* 2012), a protein complex containing metalloprotease that removes the ubiquitin (Ub)-like protein Nedd8 from cullins (Hannss *et al.* 2011). Additionally, CSN associated kinases, including casein kinase 2, phosphorylate proteasome substrates to regulate protein stability (Hannss *et al.* 2011). Huang *et al*. showed that CHOP binds the CSN/cullin3 E3 ubiquitin ligase/Keap1 supercomplex, and that this stimulates its degradation by the proteasome in adipocytes (Figure 1.2) (Huang *et al.* 2012). Using siRNA targeting the CSN1 component of the CSN reduces the formation of the supercomplex, leading to a 2-fold increase in CHOP protein levels and subsequent inhibition of adipogenesis in LiSa-2 adipocytes (Huang *et al.* 2012). Importantly, this study also confirmed that silencing the expression of Keap1 directly impairs CHOP turnover (Huang *et al.* 2012). This suggests that the modification of stress-responsive Keap1 cysteines, and subsequent Keap1 degradation, may be a significant contributor to the sustained presence of cytoplasmic and nuclear CHOP during cellular stress.

Keap1 contains 25 cysteine residues, 3 of these (Cys151, Cys273, Cys288) have been confirmed to be sensors of oxidative stress that result in the stabilization of nuclear factor (erythroid-derived 2)-like 2 (Nrf2) (McMahon *et al.* 2010, Levonen *et al.* 2004). The post-translational protein modification 2-(S-succino)cysteine (2SC) (Alderson *et al.* 2006)(Figure 1.3) has previously been

detected on the regulatory Cys151 and Cys288 of Keap1 in *fumarase* knockout mouse embryonic fibroblasts, and in neurons treated with fumaric acid esters (Adam *et al.* 2011, Linker *et al.* 2011). The nuclear accumulation of Nrf2 and transcriptional upregulation of Nrf2 target antioxidant genes, under control of the antioxidant response element (ARE), directly correlates with the succination of Keap1 (Adam *et al.* 2011, Linker *et al.* 2011). Therefore, fumarate is recognized as a physiologically relevant electrophilic activator of Nrf2 transcription. Our laboratory has established that fumarate levels and protein succination increase in adipocytes cultured in high (30 mM) versus normal (5 mM) glucose concentrations (Nagai *et al.* 2007), and in the white adipose tissue of type 2 diabetic *db/db* mice compared to lean controls (Frizzell *et al.* 2009, Thomas *et al.* 2012). In this study, I investigate if Keap1 is a target of succination in the adipocyte, similar to published studies in the *fumarase* deficient model (Adam *et al.* 2011), and I hypothesize that succination of Keap1 will prevent CHOP degradation, thereby stabilizing CHOP protein levels during diabetes.

CHOP is classically known to drive a pro-apoptotic response in damaged cells as a result of prolonged ER stress (Han *et al.* 2013b, Kim *et al.* 2008). However, our observations thus far do not support a role for CHOP-mediated apoptosis in adipocytes. Cell viability is not reduced in adipocytes matured in high glucose, even when CHOP levels are elevated (Frizzell *et al.* 2012, Tanis *et al.* 2015). In addition, the accumulation of CHOP in the absence of apoptosis has been described in the adipose tissue of obese insulin resistant patients (Diaz *et al.* 2015), and insulin resistant mice fed a high fat diet (Suzuki *et al.* 2017). As

discussed in section 1.6 above, several recent reports confirm that CHOP has alternative physiological roles distinct from apoptosis. CHOP can directly bind the promoter/enhancer region of *Ppara, Srebf1* and *Cebpa* in hepatocytes culminating in the suppression of metabolic gene expression during stress, without inducing cell death (Chikka *et al.* 2013). In addition, Prasad *et al*. have described a novel role for CHOP as an important mediator of phosphate movement into the mitochondria in adrenal cells. This results in increased steroid synthesis by stabilizing 3β-hydroxysteroid dehydrogenase type-2 protein conformation and its association with translocase outer membrane-22 during periods of stress (Prasad *et al.* 2016). While CHOP is a recognized terminus for UPR signaling, our published data coupled with the data in chapter 2 suggests that CHOP is increased even in the absence of concomitant UPR activation in high glucose. In this study, I investigated the mechanisms contributing to CHOP stability in the adipocyte, with an emphasis on the role of fumarate as a novel physiological regulator of CHOP stability. I extended these studies to examine the impact of persistent nuclear CHOP in suppressing an important anti-inflammatory response in metabolically stressed adipocytes.

3.2 Results

C/EBP homologous protein (CHOP) is upregulated in response to hyperglycemic/hyperinsulinemic driven ER stress in adipose tissue during type 2 diabetes (Boden *et al.* 2008, Özcan *et al.* 2004)(Figure 2.12C). Our earlier investigation documented prominent increases in CHOP protein levels in both adipocytes matured in normal (5 mM) and high glucose (25-30 mM) in the first 2

days of maturation (Tanis *et al.* 2015), presumably due to activation of the unfolded protein response during adipogenesis (Basseri *et al.* 2009, Han *et al.* 2013a). Remarkably, this transient increase in CHOP disappears by day 3 of maturation in normal glucose, while CHOP levels continue to increase for the duration of maturation in high glucose (Figure 3.1A)(Tanis *et al.* 2015). To determine if glucotoxicity impairs CHOP turnover versus the continuous production of more CHOP, a cycloheximide (CHX) chase experiment was performed using adipocytes matured in 5 mM or 25 mM glucose for 8 days. CHOP stability was monitored over 4 hours and both CHOP and actin total protein levels were detected by immunoblotting. Prolonged CHOP stability was observed in the absence of protein translation solely in adipocytes matured in high glucose (Figure 3.1B), and the proteasomal inhibitor MG132 was utilized as a positive control for CHOP accumulation (Diaz *et al.* 2015). Densitometric analysis of immunoblots from each time point revealed an 29.5% increase in CHOP stability in adipocytes matured in high glucose versus normal glucose after 4 hours ($n=3$, $p<0.01$)(Figure 3.1B). Previous results in chapter 2 confirmed that lentiviral knockdown of fumarase expression results in a pronounced increase in both intracellular fumarate levels and protein succination in 3T3-L1 adipocytes matured in a normal glucose concentration (Figure 2.5A, 2.5B, 2.5C, 2.6A). The CHX chase experiment was repeated using adipocytes transduced with a scrambled control or *fumarase* knockdown (FHKD) lentivirus, and cultured in 5 mM glucose to ascertain if protein succination directly inhibits CHOP degradation. Similar to adipocytes matured in high glucose, after 4 hours FHKD

adipocytes displayed a 28.5% increase in CHOP stability compared to the control (n=3, **p<0.01)(Figure 3.1C), confirming a role for succination in the regulation of CHOP turnover.

Complete silencing of Keap1 expression increases the steady state level of CHOP in LiSa-2 adipocytes (Huang *et al.* 2012), emphasizing the importance of Keap1 as a critical regulatory protein during CHOP turnover. We therefore sought to determine whether the modification of Keap1 regulatory cysteines would stabilize CHOP levels. Since Keap1 is a low abundance cytosolic protein, both control and FHKD adipocytes were transduced with a Keap1-V5 or a scrambled control lentivirus to obtain a sufficient amount of protein for molecular analyses. A significant increase in protein succination in the FHKD adipocytes was first confirmed by a western blot probed with the anti-2SC antibody (Figure 3.2A). The successful transduction using each lentivirus was verified visually following the observation of green fluorescent protein (GFP) immunofluorescence (unpublished observation), and by immunoblotting to detect both the V5 tag and Keap1 (Figure 3.2A). To determine if fumarate modifies Keap1 cysteines in the adipocyte Keap1 was immunoprecipitated from the Keap1-V5 over-expressed control and FHKD adipocytes. The immunoprecipitates were subjected to immunoblotting to detect 2SC levels, and the results demonstrated that Keap1 is succinated in the presence of excess fumarate in these adipocytes (Figure 3.2B).

Replicate Keap1-V5 immunoprecipitates from FHKD adipocytes were subjected to in gel trypsin digestion for MS/MS mass spectrometry analysis to identify the precise cysteine residue modified by fumarate. The top panel of

Figure 3.2C displays the identified MS spectrum corresponding to the succinated tryptic peptide $^{288}C^{\mathbf{2SC}}$E I L Q A D A R^{296} ($[M+2H]^{2+}$: 567.7625), containing the Keap1 regulatory Cys288 at the retention time 25.47 minutes. This result confirmed the previous observation in *Fh1*$^{-/-}$ MEFs that Cys288 is a target of succination (Adam *et al.* 2011). The mass of the analogous control precursor peptide containing the pyridylethyl (PE) cysteine modification ($[M+2H]^{2+}$: 562.2803) was detected at 16.57 minutes (lower panel, Figure 3.2C).

The antioxidant sulforaphane and the fumarate ester dimethyl fumarate (DMF) are both recognized modifiers of the redox sensitive cysteines of Keap1, resulting in activation of the Nrf2 signaling pathway (Hong *et al.* 2005, Hu *et al.* 2011, Linker *et al.* 2011). Adipocytes were treated for 3 hours with 40 µM sulforaphane or 300 µM DMF and immunoblotting demonstrated that modifying Keap1 redox sensitive cysteines preserves CHOP protein levels (Figure 3.2D and 3.2E). Heme oxygenase 1 (HOX1) is an antioxidant protein upregulated following Nrf2 transcriptional activity. Assessment of increased HOX1 protein levels confirmed activation of the Nrf2 antioxidant pathway following the modification of Keap1 by each compound (Figure 3.2D and 3.2E). Overall, this data established that the modification of Keap1 cysteines by fumarate promotes CHOP accumulation in the adipocyte.

Assessment of HOX1 levels revealed increased protein levels in both adipocytes matured in 25 mM glucose and in the adipose tissue of *db/db* mice compared to their respective controls (Figure 3.3A), concomitant with increased Keap1 modification/Nrf2 activity. Importantly, we also observed elevated HOX1

protein levels in the FHKD adipocytes (Figure 3.3A), reinforcing that succination of Keap1 promotes Nrf2 downstream signaling in the adipocyte (Adam *et al.* 2011, Linker *et al.* 2011). Given that Keap1 is succinated in the presence of excess fumarate (Adam *et al.* 2011)(Figure 3.2B, 3.2C), and that fumarate levels significantly increase in adipocytes matured in high glucose (Frizzell *et al.* 2012, Nagai *et al.* 2007), we next investigated if Keap1 is succinated in adipocytes cultured under diabetic conditions. An immunoblot confirmed the successful transduction and overexpression of the Keap1-V5 lentivirus in adipocytes matured in 5 mM or 25 mM glucose (Figure 3.3B). Surprisingly, immunoprecipitation of Keap1 (black arrow at 73 kDa) and western blotting to detect 2SC revealed that Keap1 is not succinated in adipocytes matured in high glucose (Figure 3.3C), despite confirming enrichment of Keap1-V5 in the immunoprecipitates (Figure 3.3C).

The regulatory cysteines of Keap1 are known targets of oxidation (Kobayashi *et al.* 2006) and, since Keap1 did not appear to be directly modified by fumarate in the high glucose environment; we next investigated if fumarate indirectly regulates CHOP stability by inducing oxidative stress and the oxidation of Keap1. Analysis of reactive oxygen species (ROS) utilizing the Amplex Red (hydrogen peroxide) and dichlorofluorescein (DCF) assays revealed a significant increase in ROS production in adipocytes matured in high glucose versus normal glucose (n=3, *$p<0.05$) (Figure 3.3D). Importantly, a pronounced increase in ROS levels was also observed in the FHKD adipocytes, and in adipocytes following direct DMF treatment (n=3, *$p<0.05$, **$p<0.01$) (Figure 3.3D, 3.3E). This

indicates that elevated fumarate is capable of inducing oxidative stress in the adipocyte. We have previously shown that reducing the mitochondrial membrane potential with the potent mitochondrial uncoupler carbonyl cyanide m-chlorophenyl hydrazone (CCCP) reduces fumarate levels and protein succination in adipocytes matured in 30 mM glucose (Frizzell *et al.* 2012). In addition, CCCP stimulates superoxide generation in 3T3-F442A adipocytes *in vitro* (Carriére *et al.* 2004). To confirm that oxidative stress predominantly stabilizes CHOP expression in the absence of succination we treated adipocytes matured in high glucose with 10 µM CCCP for 6 days. An immunoblot depicts reduced levels of 2SC with CCCP treatment in high glucose, while CHOP levels remained stable due to the presence of oxidative stress (Figure 3.3F). Importantly, the difference in the endogenously produced fumarate levels between FHKD and high glucose models appears to dictate which one is the more potent Keap1 modifier between fumarate and ROS. Together these results indicate that high glucose derived protein succination indirectly promotes CHOP stability through induction of oxidative stress and oxidation of Keap1 cysteines.

Our laboratory has shown that the antioxidant N-acetylcysteine (NAC) reacts slowly with fumarate to form 2SC *in vitro* (Alderson *et al.* 2006). In addition, other laboratories have shown that glutathione (GSH) has some reactivity with fumarate in *fumarase* deficient cells (Sciacovelli *et al.* 2016, Zheng *et al.* 2015). Both GSH and NAC have a similar pK_a ~9.5 and NAC is known to be a precursor for GSH synthesis (Medved *et al*. 2004, Phelps *et al.* 1992). Therefore, we investigated if NAC would reduce fumarate levels and protein

succination in adipocytes cultured in hyperglycemic/hyperinsulinemic conditions over 6-8 days. The quantification of intracellular fumarate levels following treatment of adipocytes with 0-5 mM NAC revealed that intracellular fumarate concentrations were decreased 2 and 2.65 fold with 2.5 and 5 mM NAC, respectively (n=3, *p<0.05, ***p<0.001). In parallel with this Figure 3.4B demonstrates a significant decrease in total protein succination in adipocytes matured in high glucose in the presence of 2.5 or 5 mM NAC. This suggested that the available thiol of NAC may react with endogenous fumarate to lower protein succination.

Considering that the exogenous supply of NAC may also promote the synthesis of GSH, we also measured ROS levels to examine if there was a concomitant decrease in oxidative stress. Figure 3.4C demonstrated that ROS production in 30 mM glucose was reduced in the presence of 1 mM NAC. Since ROS levels were decreased with NAC treatment, we next quantified total intracellular GSH in adipocytes matured in normal or high glucose in the presence of 5 mM NAC for 8 days, or 100 µM DMF for 24 hours (as a positive control to reduce GSH, Manuel and Frizzell, 2013). Total GSH levels were reduced by 36% in high glucose versus normal glucose (n=3, *p<0.05)(Figure 3.4D). Notably, NAC protected against glucotoxicity induced oxidative stress by improving GSH levels and reducing ROS in adipocytes cultured in high glucose (Figure 3.4C, 3.4D). An immunoblot representative of adipocytes matured in 5 mM or 25 mM glucose in the presence or absence of NAC demonstrated a significant decrease in both CHOP and HOX1 levels in the presence of NAC

(Figure 3.4E). Considering that there was no evidence for direct succination of Keap1 in high glucose conditions (Figure 3.3C), and that NAC reduces ROS levels, it appears that oxidative stress may be the direct regulator of CHOP stability in adipocytes.

In order to specifically delineate the contribution of fumarate towards the induced oxidative stress and CHOP stability, we treated FHKD adipocytes cultured in normal glucose concentrations with 5 mM or 10 mM NAC for 8 days. Interestingly, NAC administration increased protein succination and simultaneously decreased CHOP and HOX1 protein levels in FHKD adipocytes (Figure 3.5A). In contrast to NAC treatment of glucotoxic adipocytes, the treatment of FHKD adipocytes with 2.5, 5 or 10 mM NAC was not sufficient to reduce fumarate levels (Figure 3.5B). The levels of intracellular fumarate are ~5-10 mM in *fumarase* deficient cancer cells (Ternette *et al.* 2013), and fumarate increases 20-fold in FHKD adipocytes compared to adipocytes matured in 25 mM glucose (Figure 3.5C). Therefore, our data demonstrates that NAC does not react directly with the endogenously produced fumarate to reduce succination in FHKD adipocytes, and is instead acting to reduce the oxidative stress induced by fumarate excess. Further, the surprising increase in succination in the FHKD adipocytes suggested that depletion of oxidative stress might allow for increased thiol reactivity with fumarate (Figure 3.5A). To confirm if NAC was limiting thiol oxidation, and thereby promoting the availability of thiols to react with fumarate, we examined the levels of cysteine sulfenic acids. Mature FHKD adipocytes were treated with 2 mM dimedone, which covalently modifies cysteine sulfenic acids,

(Martínez-Acedo *et al.* 2014, Seo and Carroll, 2011) prior to cell lysis to assess the oxidized thiol content in the presence or absence of NAC. Immunoblotting with an antibody that detects the dimedone adduct demonstrated a significant reduction in protein oxidation upon NAC treatment (Figure 3.5D). This confirms that competition exists between fumarate and ROS for thiol reactivity within the *fumarase* depleted cells; a decrease in thiol oxidation due to NAC addition allows the excess fumarate to irreversibly modify more cysteines by succination (Figure 3.5A, 3.5D).

We have previously observed that oxidation and succination can compete for the same cysteine thiol target *in vitro* (unpublished data). Importantly, this increase in protein succination occurred in parallel with a decrease in both CHOP and HOX1 levels (Figure 3.5A), further suggesting that fumarate does not directly regulate CHOP stability and Nrf2 activation, but rather indirectly triggered these pathways through increased oxidative stress (Figure 3.3D, 3.3E). The combined data suggests that oxidative stress in the adipocyte, generated as a result of glucotoxicity or specific fumarate excess, contributes to the stabilization of CHOP protein levels since reduction of ROS promoted CHOP turnover. Interestingly, the correction of oxidative stress in the glucotoxicity model reduced fumarate mediated succination. In contrast, the correction of oxidative stress facilitated enhanced protein succination in FHKD adipocytes where fumarate levels are significantly higher.

Figure 3.6 confirms the increased presence of CHOP in parallel with 2SC in adipocytes cultured in 25 mM glucose (Figure 3.6A), and the adipose tissue

from *db/db* mice (Figure 3.6B), as well as in FHKD adipocytes (Figure 3.6C). Contrary to the established role of CHOP to promote cleaved caspase 3 mediated apoptosis (Li *et al.* 2014), cleaved caspase 3 levels were unchanged in all models (Figure 3.6A, 3.6B and 3.6C). In addition, there were no morphological changes or loss of cells observed by light microscopy, no change in nuclear content/structure (assessed by DAPI imaging of adipocytes) (Figure 3.6D), levels of cleaved caspase 3 in adipocytes matured in high glucose or FHKD adipocytes after 12 days of maturation (Figure 3.6E), or total protein content (Figure 3.6F). Therefore, we next investigated an alternative role for CHOP as it was not promoting apoptotic cell death, even in the mature hypertrophic adipocyte.

The cytosolic, mitochondrial and nuclear fractions were isolated by centrifugation and immunoblotting confirmed increased succination and organelle enrichment in each fraction (Figure 3.7A). In addition to the cytosolic accumulation, CHOP accumulates in the nuclear fraction of adipocytes matured in 25 mM glucose (Figure 3.7B), suggesting that CHOP continues to have a critical role in transcription during diabetes. Interestingly, Suzuki *et al.* elegantly demonstrated that silencing CHOP expression improves transcription of IL-13 mRNA and secretion in 3T3-L1 adipocytes, and in the adipose tissue of CHOP knockout mice fed a high fat diet (Suzuki *et al.* 2017). The improvement in IL-13, IL-4 and eotaxin secretion from the adipose tissue of CHOP knockout mice modulates an anti-inflammatory M2 macrophage phenotype leading to decreased extracellular inflammation and heightened insulin sensitivity (Suzuki *et al.* 2017). Therefore, we investigated if CHOP mediated IL-13 regulation is governed by

glucotoxicity induced oxidative stress. Conditioned medium was collected from adipocytes cultured in 5 mM or 25 mM glucose +/- 5 mM NAC for 8 days, and secreted IL-13 was quantified by ELISA (Figure 3.7C). While the levels of secreted IL-13 were reduced in adipocytes matured in high glucose by 70%, supplementation with NAC completely restored IL-13 secretion. Importantly, this data shows that oxidative stress underlies the nuclear CHOP mediated abolishment of IL-13 secretion in this *in vitro* model (Figure 3.7C).

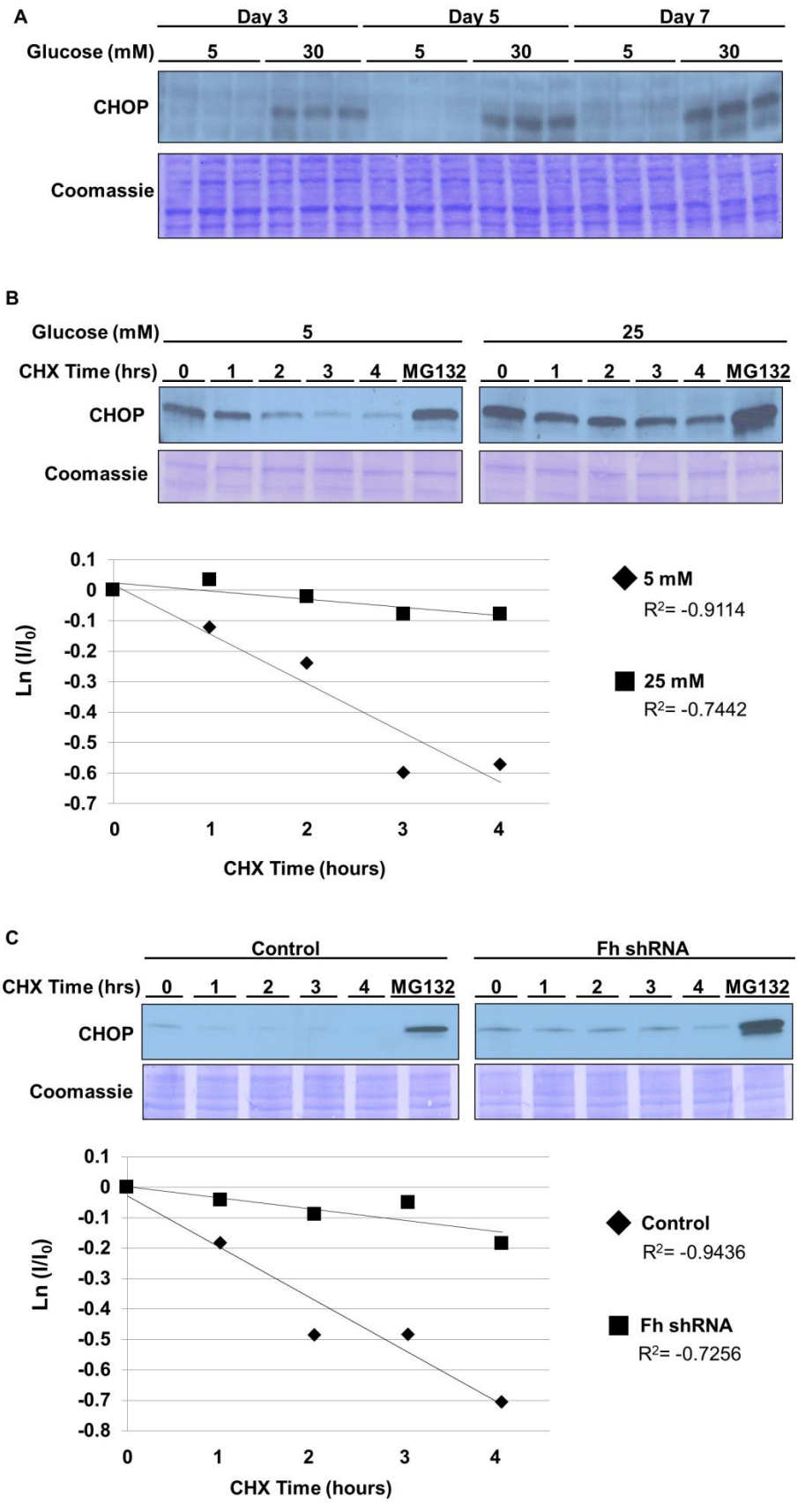

Figure 3.1: Succination regulates CHOP stability in the adipocyte. (A) Western blot probed with anti-CHOP antibody shows consistent increased CHOP levels in adipocytes matured in high glucose versus normal glucose throughout maturation. **(B)** 3T3-L1 adipocytes were matured in 5 mM or 25 mM glucose or **(C)** transduced with the scrambled control or *fumarase* knockdown lentivirus and matured in 5 mM glucose for 8 days. Each group was subjected to protein synthesis inhibition with 3.5 µg/mL cycloheximide (CHX) and the adipocytes were harvested at the indicated times after addition of CHX. CHOP protein levels over time are shown by immunoblotting with anti-CHOP antibody and Coomassie blue staining represents equal protein loading. The graphs display the natural logarithm of the relative levels of CHOP as a function of CHX chase time. n=3/group, $p<0.01$ at 4 hours.

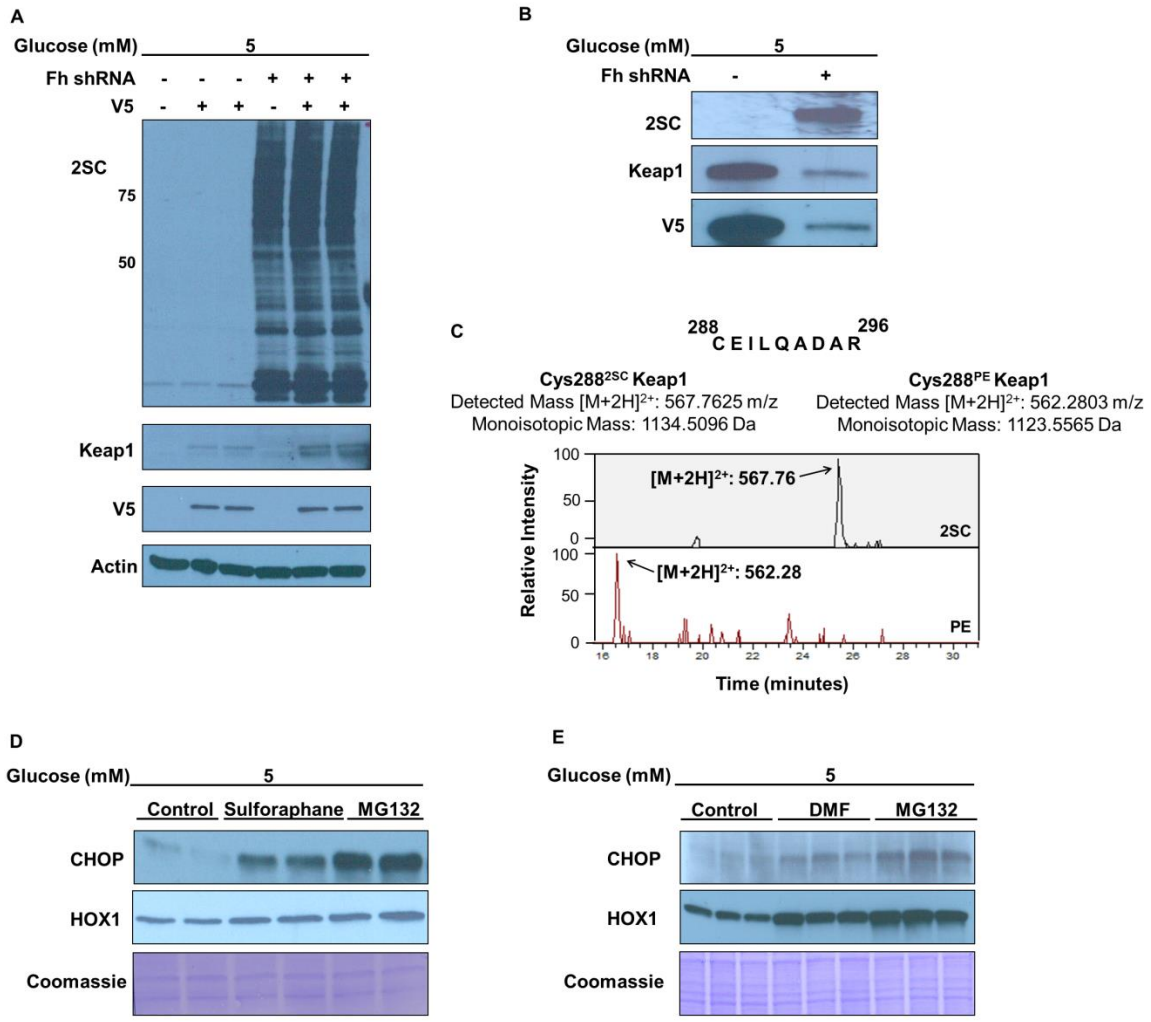

Figure 3.2: The modification of Keap1 cysteines enhances CHOP stability. **(A)** Control and *fumarase* knockdown (FHKD) adipocytes were transduced with the Keap1-V5 tagged or empty control lentivirus. Immunoblotting using the anti-2SC antibody confirms increased protein succination in adipocytes transduced with the FHKD versus the scrambled control lentivirus. The over expression of Keap1 protein was confirmed via western blotting utilizing anti-Keap1 and -V5 antibodies. **(B)** Keap1 was immunoprecipitated with anti-V5 agarose beads from 800 µg or 400 µg of protein from control or FHKD adipocytes, respectively. A western blot probed with anti-2SC antibody shows a significant increase in the amount of succinated Keap1 in the FHKD adipocytes versus the control. The blot was re-probed with anti-Keap1 and -V5 antibodies to confirm the presence of Keap1 in each immunoprecipitate sample. **(C)** MS spectra showing that the regulatory Cys288 of Keap1 is a target of succination in the FHKD adipocytes (top panel). **(D-E)** Western blots with 30 µg of protein from adipocytes matured in normal glucose and treated with 40 µM sulforaphane, 300 µM dimethylfumarate (DMF) or 10 µM MG132 for 3 hours were probed with anti-CHOP and re-probed with anti-heme oxygenase 1 antibody. Coomassie blue staining shows equal protein loading.

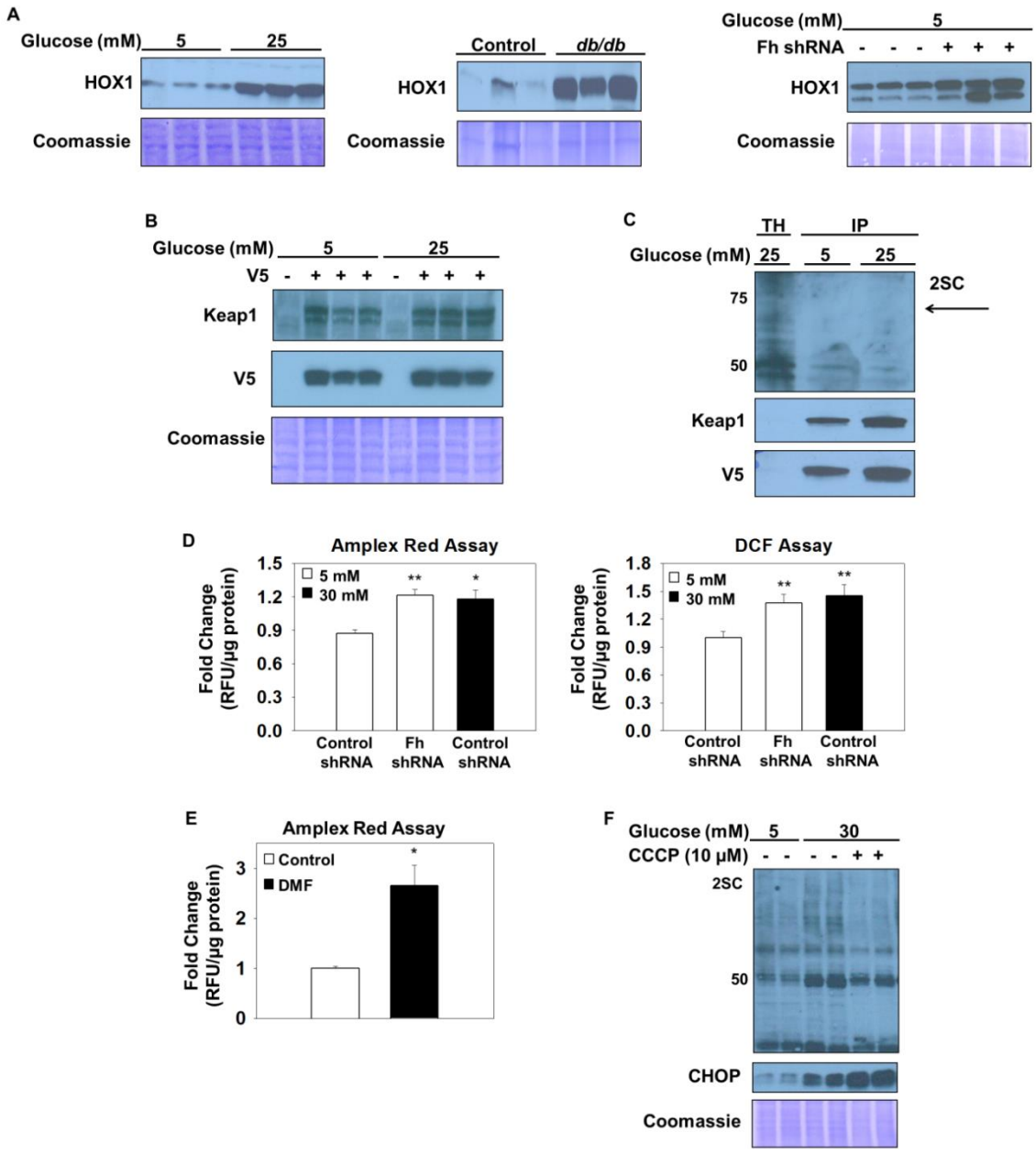

Figure 3.3: Protein succination induces oxidative stress to activate the Keap1/Nrf2 pathway and stabilize CHOP. (A) Protein from mature 3T3-L1 adipocytes, control or *db/db* epididymal adipose tissue and control or FHKD adipocytes was subjected to immunoblotting with anti-heme oxygenase 1 (HOX1) antibody. Coomassie blue staining verifies equal protein loading. **(B)** Western blotting with anti-Keap1 and -V5 antibodies validates the successful transduction of the scrambled control or Keap1-V5 tagged lentivirus into adipocytes matured in 5 mM or 25 mM glucose. **(C)** Protein (600 µg) from adipocytes matured in 5 mM or 25 mM glucose was immunoprecipitated with anti-V5 agarose beads. The eluted protein was subjected to western blotting to detect succination of the total homogenate (TH) and immunoprecipitate (IP) utilizing anti-2SC, followed by re-

probing with anti-Keap1 and -V5 antibodies. Measurement of reactive oxygen species was monitored using the Amplex Red and DCF assays according to the manufacturer's instructions outlined in the *Materials and Methods* section. **(D)** Control or FHKD adipocytes were cultured in 5 or 30 mM glucose or **(E)** 5 mM glucose and treated with 200 µM DMF. (n=3/group, mean +/- SEM, *p< 0.05, **p<0.001) **(F)** Adipocytes matured in high glucose were treated with 10 µM CCCP for 8 days. Immunoblotting with anti-2SC antibody shows decreased protein succination and anti-CHOP antibody displays increased CHOP levels in the presence of high glucose and CCCP.

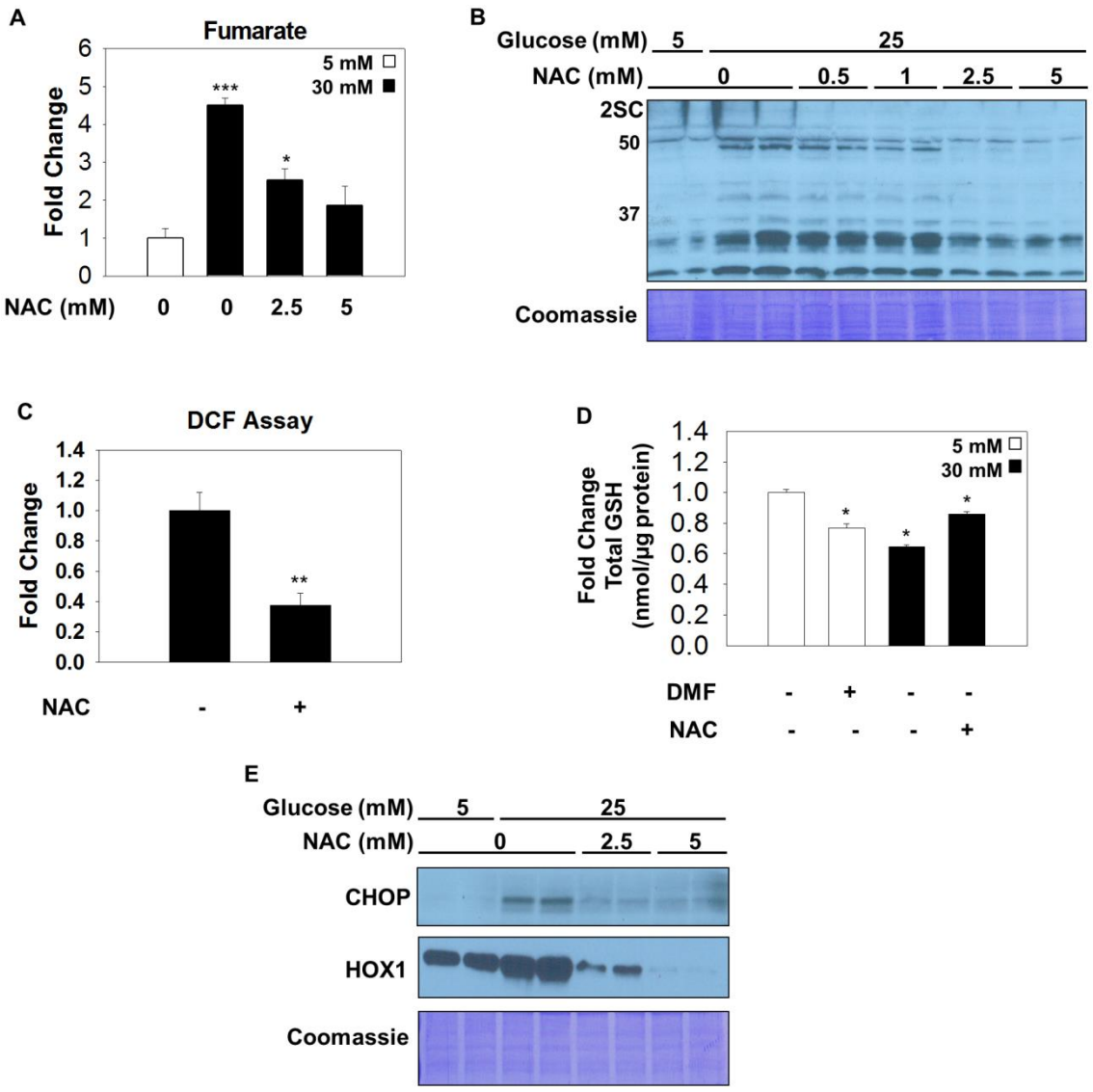

Figure 3.4: N-acetylcysteine reduces protein succination, fumarate levels and ROS production in high glucose, and reduces CHOP levels. (A) Metabolites were extracted from adipocytes matured in 5 or 25 mM glucose or 25 mM glucose treated with 5 mM NAC for 3 days as described in *Materials and Methods*. Fumarate levels are significantly increased with glucotoxicity and fumarate levels are returned back to normal with NAC. Data is normalized to total protein content (µg) (n=3/group, mean +/- SEM, *p< 0.05, ***p<0.001 vs. 5 mM glucose). **(B)** 30 µg of protein from adipocytes cultured in 5 or 25 mM glucose and treated with 0, 0.5, 1, 2.5 or 5 mM N-acetylcysteine (NAC) for 8 days was subjected to immunoblotting using anti-2SC antibody. **(C)** Reactive oxygen species were quantified by the DCF assay in adipocytes matured in 30 mM glucose with or without 1 mM NAC for 8 hours (n=4/group, mean +/- SEM, **p<0.01). **(D)** Adipocytes were treated with 100 µM dimethyl fumarate (DMF) for 24 hours or 5 mM NAC for 8 days. Total glutathione levels were quantified according to the manufacturer's instructions as described in *Materials and*

Methods (n=3/group, mean +/- SEM, *p< 0.05 vs. 5 mM glucose). **(E)** A western blot was performed with anti-CHOP and re-probed with -HOX1 antibodies to show reduced CHOP and HOX1 levels in adipocytes treated with NAC for 8 days. Coomassie staining represents equal protein loading.

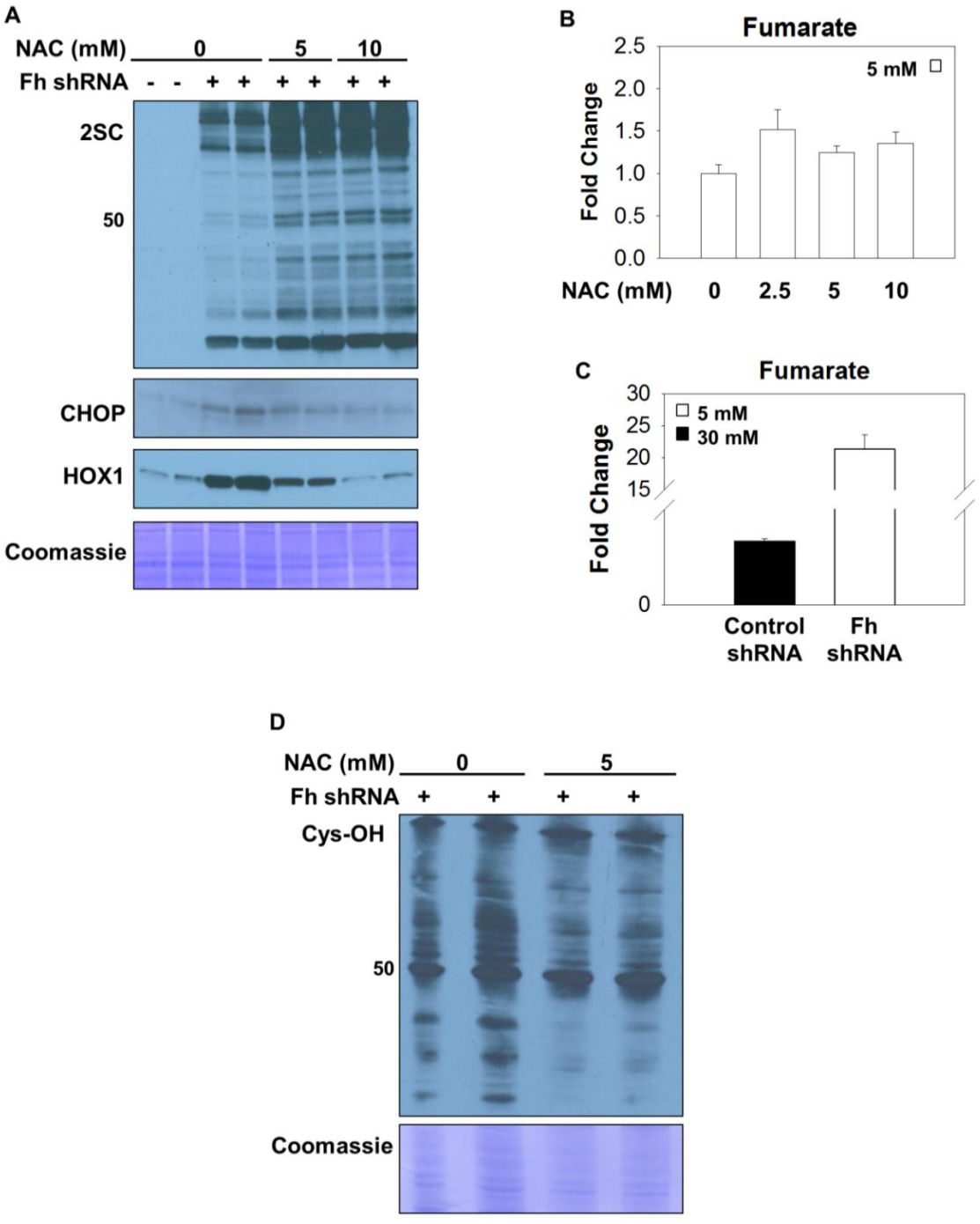

Figure 3.5: Protein oxidation regulates CHOP stability. (A) An immunoblot probed with anti-2SC, -CHOP and -HOX1 antibodies show that 5 and 10 mM N-acetylcysteine (NAC) treatment simultaneously increase protein succination and

decreases CHOP and HOX1 levels in FHKD adipocytes. **(B, C)** Metabolites were extracted from control adipocytes matured in 30 mM glucose or FHKD adipocytes cultured in 5 mM glucose and treated with 0, 2.5, 5 or 10 mM NAC for 3 days. Fumarate levels are normalized to total protein content (µg). **(D)** Dimedone labeled protein cysteine sulfenic acids are displayed with a western blot probed with anti-cysteine sulfenic acid antibody from FHKD adipocytes treated in the presence or absence of NAC.

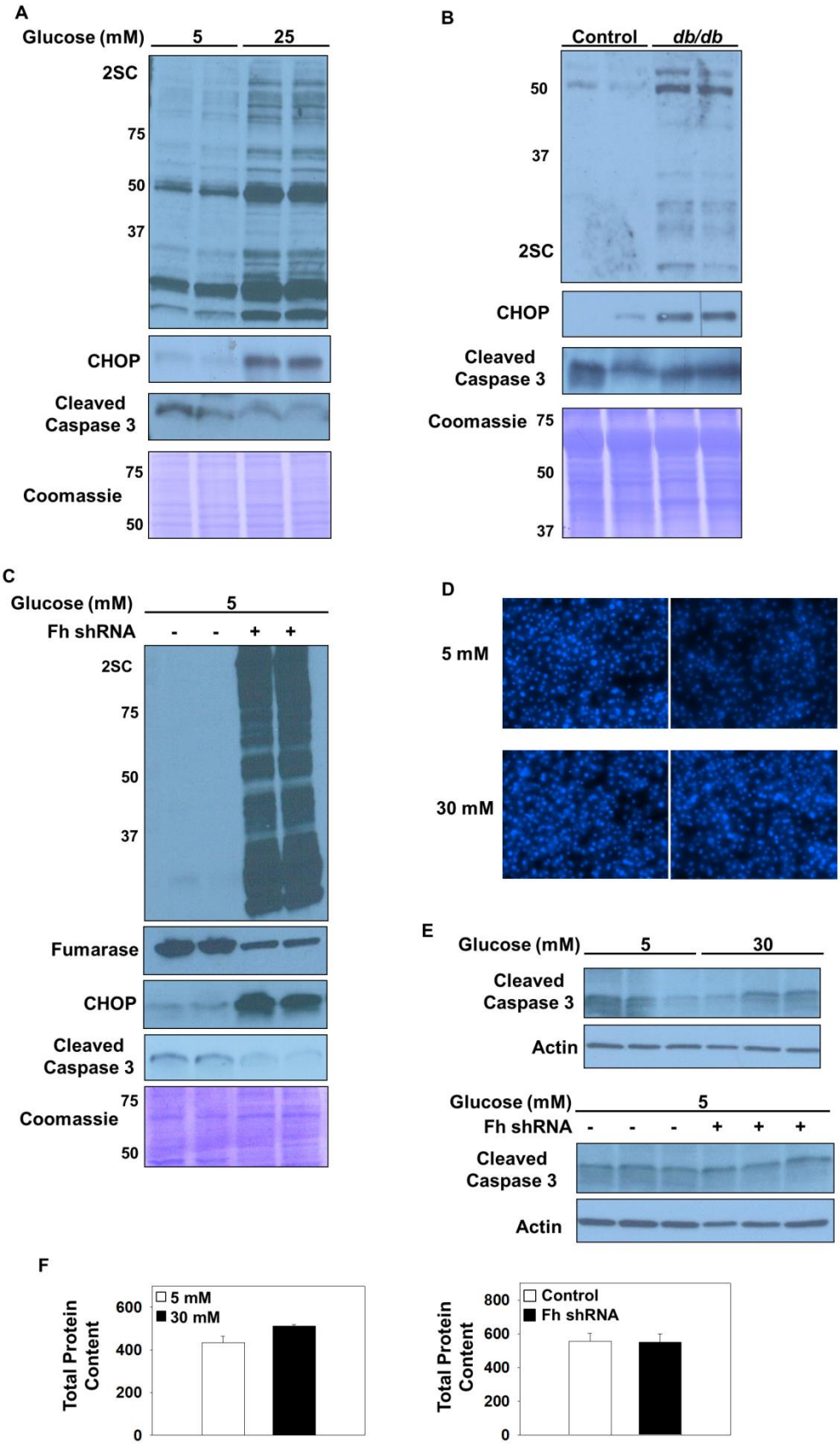

Figure 3.6: 2SC and CHOP accumulate in the absence of apoptosis. Western blots probed with anti-2SC, -CHOP and -cleaved caspase 3 antibodies with protein from **(A)** 3T3-L1 adipocytes, **(B)** control or *db/db* epididymal adipose tissue or **(C)** control or FHKD adipocytes**.** Immunoblots probed with anti-actin antibody and Coomassie staining displays equal protein loading. **(D)** DAPI imaging with the Invitrogen™ EVOS™ FL Auto Imaging System of duplicate adipocyte samples treated with 5 mM or 30 mM glucose 8 days. **(E)** Control or FHKD adipocytes were matured in 5 mM or 30 mM glucose for 12 days. An immunoblot probed with anti-cleaved caspase 3 antibody shows no evidence of increased apoptosis in adipocytes matured in high glucose concentrations or in FHKD adipocytes versus control adipocytes matured in normal glucose concentration. **(F)** The total protein content (µg) of control or FHKD adipocytes cultured in 5 mM or 30 mM glucose for 8 days was determined by the Lowry assay.

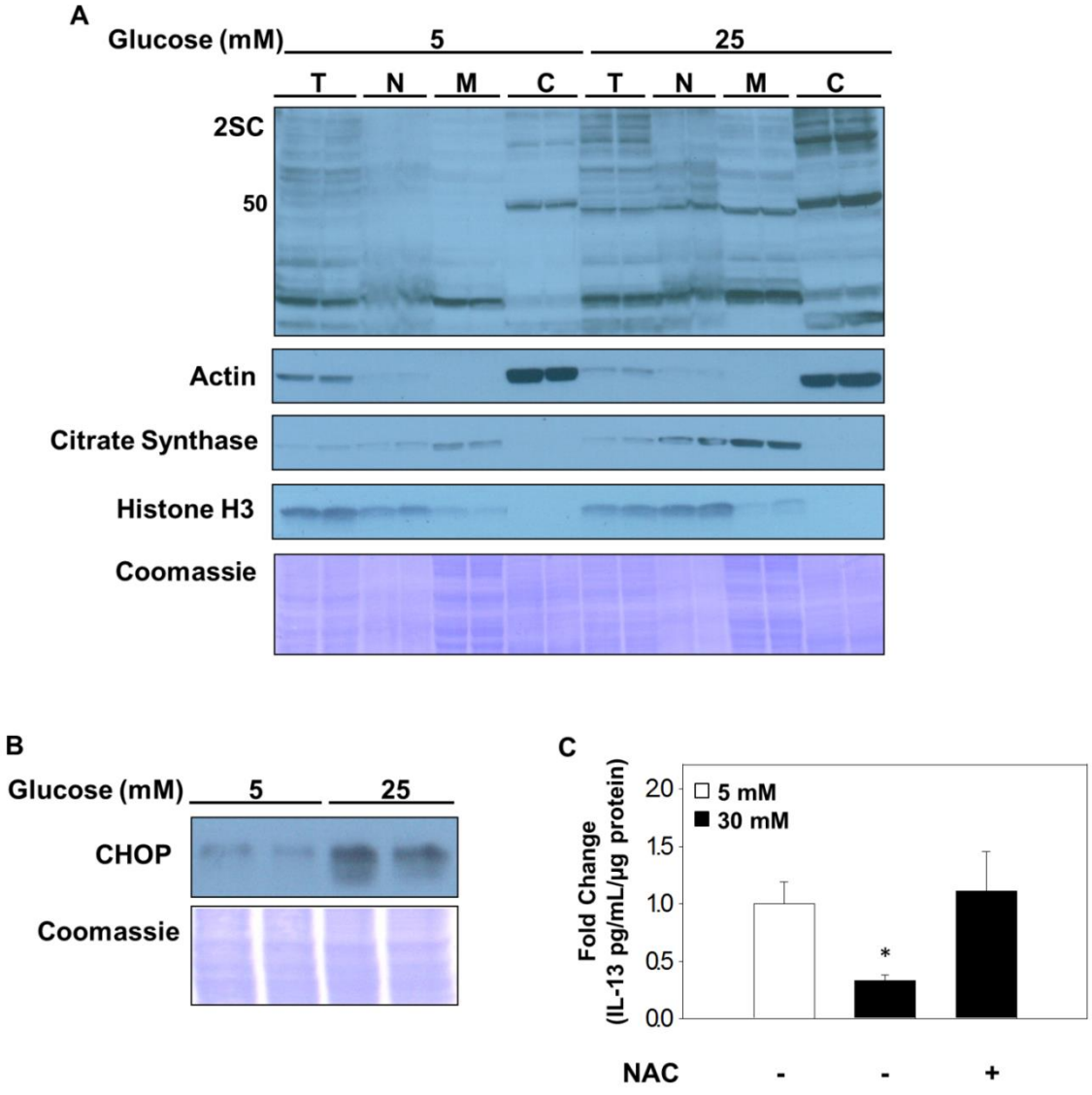

Figure 3.7: Accumulation of nuclear CHOP is associated with impaired IL-13 secretion in high glucose. (A) Protein succination increases in the total homogenate (T), nuclear (N), mitochondrial (M) and cytosolic (C) enriched fractions in adipocytes matured in 25 mM versus 5 mM glucose. Organelle enriched fractions are confirmed by immunoblotting with anti-actin (cytosolic), -citrate synthase (mitochondrial) and -histone H3 (nuclear) antibodies. **(B)** The nuclear fraction from adipocytes cultured in 5 or 25 mM glucose was isolated by centrifugation and a western blot probed with anti-CHOP antibody depicts a higher amount of CHOP in the nucleus during glucotoxicity. **(C)** Serum free medium was collected after 4 hours in adipocytes treated with normal or high glucose +/- 5 mM NAC. IL-13 levels were quantified using an IL-13 specific ELISA as described in *Materials and Methods*. (n=3/group, mean +/- SEM, *p< 0.05).

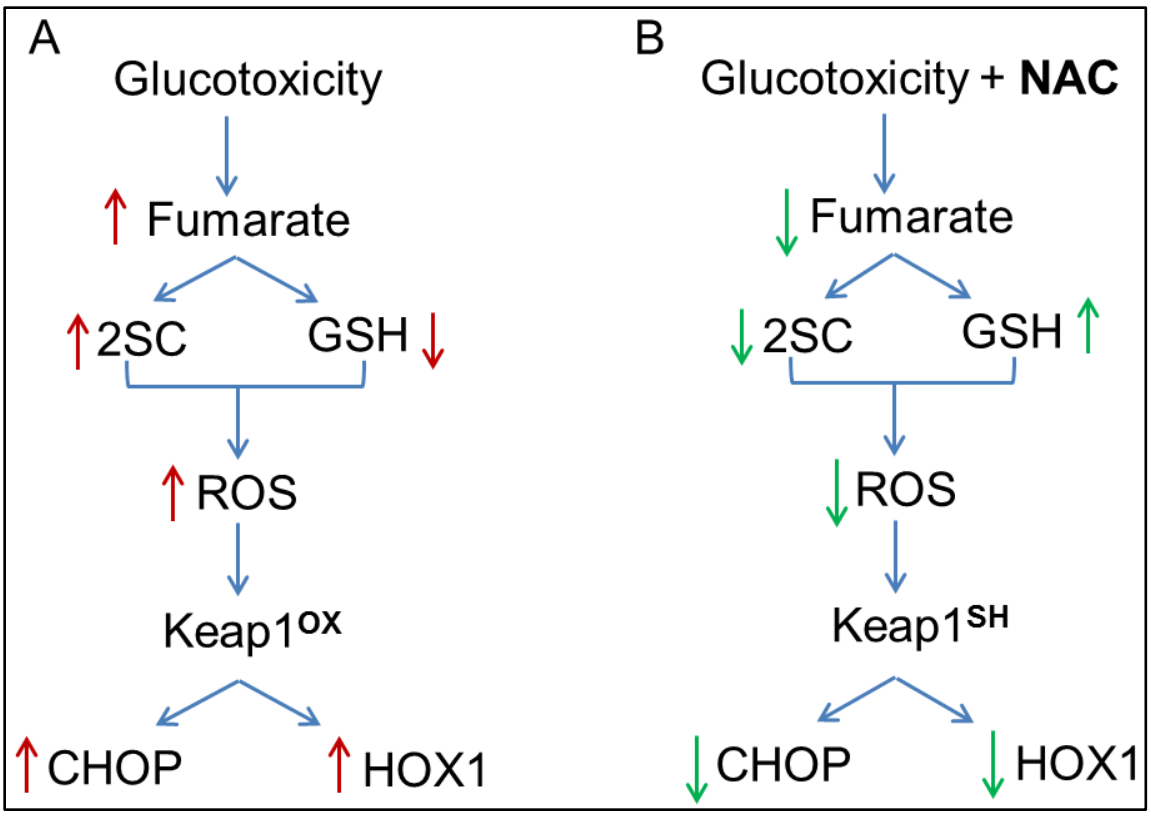

Figure 3.8: Beneficial effect of N-acetylcysteine during glucotoxicity. (A) Glucotoxicity increases fumarate levels that results in increased protein succination and reduced glutathione (GSH) concentrations. Augmented succination and lower GSH levels results in the accumulation of reactive oxygen species (ROS) that are able to react with redox sensitive cysteines on Keap1. Oxidized Keap1 is unable to sequester Nrf2 and may be unable to form the CSN supercomplex resulting in the accumulation of C/EBP homologous protein (CHOP) and increased production of heme-oxygenase 1 (HOX1). **(B)** N-acetylcysteine (NAC) decreases fumarate concentrations and protein succination and rescues the concentration of GSH in the adipocyte resulting in decreased ROS levels. In the absence of oxidative stress Keap1 is able to bind the CSN complex to promote CHOP degradation and down regulate HOX1 production by sequestering Nrf2 in the cytosol for protein turnover.

3.3 Discussion

In this study, we demonstrate that protein succination contributes to the development of oxidative stress in the adipocyte, and that oxidative stress can promote the accumulation of CHOP and the suppression of anti-inflammatory IL-13. We also show that the anti-oxidant N-acetylcysteine (NAC) resolves oxidative stress, reduces CHOP protein stabilization and improves IL-13 secretion. CHOP is known to increase during the late stages of adipogenesis to restrict prolonged adipogenic signaling after the mature adipocyte phenotype is attained (Han *et al.* 2013a). We confirmed this increase in CHOP protein levels following adipocyte maturation in high glucose, however, unlike earlier studies we compared the high glucose matured adipocytes to adipocytes matured in normal glucose (Tanis *et al.* 2015). Importantly, we noted that while CHOP protein levels did increase during early adipogenesis (1-3 days) in normal glucose, there was a decline during the later stages (3-8 days), whereas CHOP levels were increasingly elevated in high glucose (Figure 3.1A)(Tanis *et al.* 2015).

Since 3T3-L1 adipocytes matured in normal glucose differentiate normally, evidenced by the synthesis and storage of triglycerides, it suggested that CHOP accumulation in high glucose may have a role beyond the suppression of adipogenesis. Notably, sustained CHOP protein levels occur in parallel with increased protein succination (Tanis *et al.* 2015), suggesting a potential association between protein succination and impaired CHOP turnover. In Figure 3.1 we demonstrate that glucotoxicity, and more specifically protein succination, lead to decelerated CHOP turnover, implying that there is a defect in the CHOP

degradation pathway. CHOP ubiquitination and subsequent degradation is regulated by the formation of a COP9 signalosome/Cullin-3 E3 ligase/Keap1 supercomplex in adipocytes (Huang *et al.* 2012). We hypothesized that succination of Keap1 in the presence of excess fumarate (Adam *et al.* 2011, Linker *et al.* 2011) may disturb the interaction of CHOP with the degradation supercomplex, leading to the accumulation of CHOP. Immunoprecipitation of overexpressed V5 tagged Keap1 from *fumarase* knockdown (FHKD) adipocytes confirmed that Keap1 is succinated (Figure 3.2B). Further mass spectrometry analysis confirmed that the redox sensitive Cys288 in the intervening region (IVR) of Keap1 is susceptible to modification by fumarate in FHKD adipocytes (Figure 3.2C). The modification of cysteines within the IVR domain is predicted to distort the tertiary structure of Keap1, impairing substrate ubiquitination and preventing protein:protein interactions in the Cullin-E3 ligase complex (Canning *et al.* 2015). Importantly, eliminating mRNA expression and protein utilizing Keap1 siRNA stabilizes CHOP in the adipocyte (Huang *et al.* 2012), confirming that Keap1 is a vital regulatory component of CHOP turnover. In support of this, we determined that acute treatment with sulforaphane or dimethyl fumarate (DMF), both of which act to modify Keap1 regulatory thiols, confirmed the involvement of Keap1 cysteines as a regulator of CHOP protein longevity in the adipocyte (Figure 3.2D, 3.2E).

In response to oxidative stress and the oxidation of Keap1 cysteines, Nrf2 translocates into the nucleus and binds to the anti-oxidant response element (ARE) in the promotor region of the *heme-oxygenase 1* gene (Alam *et al.* 1999).

We verified that this pathway is active in the metabolically stressed adipocyte *in vitro*, as well as in the adipose tissue of *db/db* diabetic mice (Figure 3.3A). In contrast to the FHKD adipocytes, Keap1 was not directly confirmed as a target of succination in the adipocyte matured in high glucose (Figure 3.3C), despite prominent activation of the Keap1/Nrf2/HOX1 signaling pathway in the *db/db* adipose tissue and in adipocytes cultured in 25 mM glucose (Figure 3.3A). Considering that we could not detect Keap1 succination in the high glucose model where fumarate is elevated in parallel with other sources of oxidant stress, we hypothesized that Keap1 thiol oxidation was more prominent than Keap1 succination under diabetic conditions. Unpublished studies from our laboratory have demonstrated that both oxidation and succination may compete to modify the same cysteine thiols; therefore the modification generated would depend on the concentration and reactivity of the oxidant or electrophile. We have also shown that the sulfenic acid (-SOH) generated by oxidation cannot be further succinated by fumarate *in vitro*, therefore fumarate does not appear to react with already oxidized thiols.

We and others have confirmed increased ROS production in adipocytes matured in high glucose versus normal glucose (Han *et al.* 2017, Houstis *et al.* 2006, Lin *et al.* 2005)(Figure 3.3D), suggesting that oxidation, rather than succination, is indeed the principal Keap1 modification regulating CHOP stability in the adipocyte during diabetes. Importantly we also documented that ROS production is pronouncedly increased in FHKD adipocytes and adipocytes treated with dimethyl fumarate (DMF) (Figure 3.3D, 3.3E), similar to the observed

accumulation of ROS in *fumarase* deficient mouse kidney epithelial cells (Zheng *et al.* 2015). This striking data demonstrates that the remarkable increase in fumarate alone is sufficient to drive oxidative stress; and that mitochondrial derived metabolite stress and oxidant stress are inextricably linked. Furthermore, we also showed that chronic treatment with the mitochondrial uncoupler CCCP reduces protein succination, yet also increases CHOP levels (Figure 3.3F), which is likely due to CCCP stimulated superoxide production (Carriére *et al.* 2004). Therefore, although fumarate and oxidative stress occur concurrently in the adipocyte in high glucose, our data suggests that it is the increase in oxidative stress that directly contributes to impaired CHOP turnover. Moreover, protein succination indirectly contributes to CHOP stabilization through the continued induction of oxidative stress.

Considering the known increase in ROS production in adipocytes cultured in high glucose medium (Han *et al.* 2017, Houstis *et al*. 2006, Lin *et al.* 2005), we next investigated if the antioxidant N-acetylcysteine (NAC) might have a beneficial action that would also impact the levels of protein succination. NAC has been shown to attenuate the hyperglycemic pro-inflammatory response, evidenced by lower plasminogen activator inhibitor-1 (PAI-1) mRNA and protein, in the epididymal adipose tissue of diabetic mice (Lin *et al.* 2005). NAC treatment (2.5 and 5 mM) reduced the excess fumarate by 2-2.5 fold in the adipocyte matured in high glucose (Figure 3.4A). We also observed lower protein succination following NAC treatment (Figure 3.4B), consistent with the decrease in intracellular fumarate (Figure 2.1A, 2.1B) (Frizzell *et al.* 2012). Both DMF and

endogenously produced excess fumarate directly modify glutathione (GSH) in control or *fumarase* knockout mouse kidney epithelial cells, respectively (Zheng *et al.* 2015). The decrease in reduced GSH concentration due to succination in these models leads to a decrease in the GSH:GSSG ratio, elevated ROS levels and activation of several anti-oxidant response genes including HOX1 (Zheng *et al.* 2015). Figure 3.4D confirmed that DMF also lowers GSH levels in the adipocyte (Manuel and Frizzell, 2013), suggesting that increased endogenous fumarate may partially contribute to reduced total GSH levels in adipocytes matured in high glucose (Figure 3.4D). NAC, a known precursor of GSH synthesis, improved the concentration of GSH in adipocytes matured in high glucose (Figure 3.4D). In parallel, the decrease in oxidative stress also corresponded to reduced fumarate levels, although it is unclear if NAC reacts directly with fumarate, or decreases other factors related to mitochondrial stress in the adipocyte.

Hypoxia induced oxidative stress in 3T3-F442A preadipocytes is linked to the initiation of CHOP transcription (Carriére *et al.* 2004), and Diaz *et al*. have inferred that oxidative stress is associated with proteasomal dysfunction in subcutaneous adipose tissue from obese insulin resistance patients contributing to CHOP stability (Diaz *et al.* 2015). Lowering ROS levels with NAC (Figure 3.4C) diminished both HOX1 and CHOP protein levels in adipocytes matured in high glucose (Figure 3.4E), representative of a potentially renewed interaction between CHOP and the degradation supercomplex. Taken together, this demonstrates that succination contributes to reduced GSH levels and the

development of oxidative stress in adipocytes matured in hyperglycemic conditions. Limiting GSH contributes to the accumulation of ROS in the adipocyte, prompting oxidation of Keap1 and CHOP stabilization (Figure 3.8A). NAC decreases fumarate and protein succination while simultaneously increasing available GSH to scavenge ROS and prevent oxidation of Keap1. In the absence of oxidative stress, Keap1 is able to sequester target substrates such as Nrf2 (Kobayashi *et al.* 2006) and CHOP (Huang *et al.* 2012) in the cytosol, allowing them to be tagged for proteasomal degradation (Figure 3.8B).

In contrast to adipocytes matured in 25 mM glucose, NAC actually augmented protein succination in FHKD adipocytes (Figure 3.5A). Surprisingly NAC treatment also had no effect on the concentrations of endogenously produced fumarate generated in this model (Figure 3.5B). This may be related to the excessive concentration of fumarate produced in these cells, 20 fold greater than that in adipocytes matured in 25 mM glucose (Figure 3.5C). Interestingly, we still observed a significant decrease in both CHOP and HOX1 expression with NAC treatment (Figure 3.5A), despite continued increased protein succination and high fumarate levels. Assessment of protein cysteine sulfenic acid content in FHKD adipocytes (Figure 3.5D) revealed that reducing oxidative protein damage with NAC decreased thiol oxidation, which in turn down-regulates CHOP levels and Nrf2 signaling, likely by attenuating Keap1 oxidation. Remarkably, prolonged adipose tissue Nrf2 activity has been associated with decreased lipid accumulation, lipogenic gene expression and glucose tolerance while simultaneously increasing insulin resistance in the adipose tissue of *ob/ob* type 2

diabetic mice (Xu *et al.* 2012). While sustained Nrf2 activity was suspected to underlie the unhealthy phenotype in these mice, our data suggests that sustained CHOP, also regulated by Keap1 modification, may be a more significant contributor. Collectively, these results emphasize the importance of cysteine oxidation as a primary regulatory factor governing Keap1:protein interactions and CHOP stability in the adipocyte. Protein thiol oxidation indirectly correlates with succination in FHKD adipocytes (Figure 3.5A, 3.5D) confirming that oxidation and succination compete for thiol targets when fumarate levels are elevated. While fumarate levels are augmented in both of the models used (high glucose and FHKD), and it is evident that increased fumarate can further exacerbate oxidative stress, it is also clear that both models differed dramatically in response to NAC treatment. This is significant considering that knockdown models are frequently employed to model metabolite stress (Nishida *et al.* 2015, Park *et al.* 2013, Wagner *et al.* 2017), but these may not always exhibit the same concentrations observed in the disease state, producing different, perhaps more pronounced, signaling effects.

CHOP is classically known to induce apoptotic signaling via suppression of the Bcl-2 family gene transcription in the nucleus. However, the accumulation of CHOP in adipocytes due to proteasomal inhibition by MG132 has no effect on the protein levels of anti-apoptotic proteins Bcl-2 or Bax (Diaz *et al.* 2015). In addition, wild type and CHOP knockout mice fed a high fat diet display similar expression of apoptosis-related proteins Bcl-2 and CD95 and show no change in the ratio of TUNEL-positive cells to total nuclei (Suzuki *et al.* 2017). These

studies emphasize the absence of immediate CHOP-mediated apoptosis in obese adipocytes. Figure 3.6 supports these studies as we find that CHOP levels are indirectly proportional to cleaved caspase 3 protein levels in adipocytes matured in high glucose, adipose tissue from *db/db* mice and FHKD adipocytes at 8 or 12 days of adipocyte maturation. Giordano *et al*. have described increases in caspase-1 mRNA and over activation of the nucleotide-binding oligomerization domain-like receptor-3 (NLRP3) inflammasome in obese adipose tissue (Giordano *et al.* 2013). This leads to hypertrophic adipocyte death by pyroptosis, rather than CHOP induced apoptosis, in the visceral adipose tissue of *ob/ob* and *db/db* mice and subcutaneous adipose tissue of mice fed a high fat diet (Giordano *et al.* 2013).

Investigation into the functional role of CHOP in obese adipocytes led Suzuki *et al*. to determine that stabile CHOP signaling suppresses IL-13 and IL-4 mRNA transcription, promoting M1 macrophage polarization in mice after 6 weeks of high fat diet feeding (Suzuki *et al.* 2017). Eosinophils are the major source of IL-4 in the adipose tissue microenvironment while healthy adipose tissue secrets modest levels of IL-4. *CHOP* knockout mice display upregulated transcription of eotaxins and increased eosinophil recruitment resulting in increased IL-4 levels and attenuated inflammation in the adipose tissue microenvironment (Suzuki *et al.* 2017). In addition, *CHOP* knockout mice have improved insulin sensitivity after consumption of a high fat diet (Suzuki *et al.* 2017). This study emphasizes an important role for CHOP to promote adipose

tissue inflammation linked to insulin resistance during high fat diet feeding (Suzuki *et al.* 2017).

Notably, adipose tissue IL-13 secretion increases in mice fed a high fat diet for 13 weeks in response to exogenous TNFα and IL-1β inflammatory signaling (Kwon *et al.* 2014). Elevated IL-13 production observed in obese versus lean omental human adipose tissue is predicted to attenuate the inflammatory immune cell response to implement the 'low-grade' inflammation hallmark of obesity (Kwon *et al.* 2014). We confirmed that accumulation of CHOP specifically in the nuclear fraction of adipocytes matured in high glucose (Figure 3.7B) correlates with impaired IL-13 secretion during the onset of adipocyte hypertrophy (Figure 3.7C). This data suggests that CHOP may regulate IL-13 mRNA transcription at an early stage of obesity to initiate a pro-inflammatory immune cell response in the adipose tissue microenvironment. Notably, we demonstrated that NAC mediated suppression of oxidative stress (Figure 3.4C) reduced CHOP expression (Figure 3.4E) and rescued IL-13 secretion (Figure 3.7C), possibly reducing the pro-inflammatory environment. Chromatin immunoprecipitation sequencing identified GATA3, a zinc finger transcription factor, and STAT5a bound to the promotor region of IL-13 resulting in the upregulation of IL-13 mRNA transcription (Wei *et al.* 2011). Interestingly, GATA3 is expressed in white adipose tissue (Tong *et al.* 2000) and forms transcription factor complexes with C/EBPα and C/EBPβ to inhibit adipogenesis (Tong *et al.* 2005). Future studies will investigate if CHOP directly binds anti-inflammatory transcription factor complexes such as GATA3 or STAT5a (Zhu, 2015) or the

DNA promotor region to suppress IL-13 mRNA production and secretion (Figure 3.7C) (Suzuki *et al.* 2017).

In summary, we find that increased fumarate levels and protein succination are coupled to elevated oxidative stress; and that this leads to oxidative protein damage and impaired CHOP turnover in the adipocyte. Sustained CHOP protein levels in the nucleus correlates with decreased secretion of the anti-inflammatory cytokine IL-13. The improvement in IL-13 secretion following NAC treatment is a direct result of limiting oxidant-mediated CHOP stabilization, emphasizing the importance of the intracellular oxidative environment for healthy adipocyte function.

Chapter 4

Summary and Future Directions

4.1 Summary

Adipose tissue is an important endocrine organ responsible for energy storage, insulation, protection and the secretion of adipokines that help regulate systemic nutrient homeostasis. The accumulation of excess adipose tissue is associated with the secretion of pro-inflammatory cytokines and insulin resistance. Type 2 diabetes is frequently associated with obesity and ~29 million Americans are either diabetic or have pre-diabetes. Due to the growing number of individuals affected by obesity and type 2 diabetes, it is critical to understand the complex origins of disease pathology. The mechanistic studies investigated here increase our knowledge regarding the biochemical contribution of excessive caloric intake to the metabolic dysfunction known to occur in adipose tissue. Overall, I explored the contribution of nutrient excess to alterations in the post-translational regulation of protein stability and function, and how this impacts adipocyte dysfunction.

Protein succination occurs when a thioether bond is formed between the Krebs cycle intermediate fumarate and the thiol groups of cysteine residues to form S-(2-succino)cysteine (2SC) (Figure 1.3). The accumulation of fumarate and 2SC increases in adipocytes matured in high glucose and in adipose tissue from type 2 diabetic (*db/db*) mice, due to glucotoxicity driven mitochondrial stress (Frizzell *et al*. 2012) (Figure 1.4). Protein disulfide isomerase (PDI) is an abundant endoplasmic reticulum (ER) oxidoreductase that is responsible for the successful formation of disulfide bonds in the majority of proteins in the ER. In chapter 2 I identified the active site cysteines of PDI as the targets of succination

in adipocytes matured in high glucose.

The use of a *fumarase* knockdown model (FHKD) to directly increase endogenous fumarate production facilitated determination of the impact of metabolite stress on PDI activity. Direct succination of PDI active site cysteines inhibits PDI reductase activity interfering with normal protein folding and contributing to the documented increase in the unfolded protein response (UPR) and ER stress (Figure 4.1) in the adipose tissue of diabetic patients (Boden *et al*. 2014b, Hosogai *et al.* 2007). Notably, adipose tissue secretory function is not decreased for all secreted proteins. During diabetes there is increased secretion of leptin, retinol binding protein 4 (RBP4) and inflammatory proteins in parallel with adipose tissue expansion. However there are paradoxical decreases in the secretion of adipsin, omentin, vascular endothelial growth factor (VEGF) as well as the thiol dependent hormone adiponectin (Deng and Scherer, 2010). We have previously shown that the critical cysteine for adiponectin oligomerization is succinated in diabetic adipose tissue and adipocytes (Frizzell *et al.* 2009). Taken together, our data suggests that protein succination is a relevant negative regulator of protein folding and oligomerization during diabetes.

During our studies on adipocyte protein folding capacity, we noted that the protein levels of the ER stress marker C/EBP homologous protein (CHOP) were elevated, yet we found limited evidence for a pronounced up-regulation of the unfolded protein response (UPR) in diabetic conditions (versus normal glucose). This is in agreement with more recent publications documenting the presence of UPR activation in the presence of insulin, since the normal response

to insulin both *in vivo* and *in vitro* would include increased proteostasis (Boden *et al.* 2014b, Minard *et al.* 2016). Therefore, we continued to examine the persistent up-regulation of CHOP in diabetic conditions (Figure 3.1A). CHOP is a negative regulator of transcription and we confirmed that it was accumulating in the nucleus of adipocytes matured in high glucose. While increased levels of CHOP are normally associated with prolonged ER stress and the induction of apoptosis, we found no evidence for an association between CHOP and increased apoptosis (Figure 3.6).

Kelch-like ECH-associated protein 1 (Keap1) is a negative regulator of CHOP stability and Figure 3.1 demonstrates that CHOP turnover is impaired in adipocytes cultured in high glucose. The modification of Keap1 regulatory cysteines promotes the accumulation of CHOP protein levels. We identified Cys288 as the target residue for Keap1 succination in FHKD adipocytes, but surprisingly Keap1 was not directly succinated in high glucose conditions where fumarate is also increased, although to a lower extent than the FHKD model. We further demonstrated that it is oxidative stress and the accumulation of reactive oxygen species that leads to oxidation of Keap1 and the accumulation of CHOP protein levels in high glucose conditions. Interestingly, we also documented that increased fumarate promotes oxidative stress; therefore elevated fumarate can regulate Keap1/CHOP indirectly through the production of ROS. Boden *et al.* recently demonstrated the significance of adipose tissue oxidative stress in the acute development of insulin resistance in humans, independent of ER stress and inflammation (Boden *et al.* 2015). Our data elegantly demonstrates that both

oxidative stress and metabolite stress occur simultaneously, and further explains how increased fumarate levels as diabetes develops may exacerbate the existing oxidative stress. In further considering the implications of sustained CHOP levels in the nucleus, we demonstrate that CHOP may contribute to the inhibition of IL-13 production and secretion during adipocyte dysfunction (Figure 3.7C, 4.1).

In summary, the data obtained here demonstrates that elevated fumarate contributes to impaired protein folding and altered functionality in parallel with oxidative modification and inflammatory stress. Fumarate levels and protein succination are lowered following the reduction of high glucose levels, demonstrating that metabolite stress, like obesity and inflammation, can be resolved following caloric restriction.

4.2 Future Directions

It will be important to extend these studies on the role of succination in adipocyte pathophysiology to human adipose tissue. In particular, we are interested in investigating if other isomers of the PDI family, such as ERp57, are targets of succination and whether this affects protein glycosylation in the adipocyte. Continuous with our results regarding caloric restriction, it will also be beneficial to confirm that caloric restriction and/or exercise decreases protein succination and CHOP levels in the adipose tissue of type 2 diabetic mice and patients.

Our results on the increased production of ROS as a result of protein succination are insightful and exciting; suggesting that fumarate indirectly regulates the oxidative modification of proteins. Figures 3.3 and 3.4 suggest that

protein succination alone is sufficient to induce oxidative stress and activate the Keap1/Nrf2 antioxidant response pathway in the adipocyte. Interestingly, reducing protein succination with the antioxidant and glutathione precursor N-acetylcysteine (NAC) ameliorates ROS production and lessens the Keap1/Nrf2 oxidative stress response in adipocytes matured in high glucose. The precise mechanism by which NAC simultaneously reduces protein succination in the adipocyte has not been described, but it may involve the production of succinated NAC or succinated glutathione and we plan to develop methods to detect this.

We have noted in unpublished observations that oxidized thiols (sulfenic acid) will not react with fumarate *in vitro*. Figure 3.5 shows that NAC reduces protein oxidation in FHKD adipocytes (where fumarate levels are 20-fold greater than in high glucose), but simultaneously increases protein succination. Our data demonstrates that pronouncedly elevated fumarate levels, such as those observed in *fumarase* deficient renal cell carcinoma or fumaric aciduria, both contribute to and compete with the oxidative modification of proteins. While the use of antioxidants in these conditions might actually reduce oxidative stress, they are also likely to propagate the irreversible succination of other proteins. We would predict that treating adipocytes matured in high glucose with the antioxidants superoxide dismutase (SOD) or MitoQ might also decrease the amount of oxidized protein thiols and this may be more beneficial in situations where fumarate levels are not elevated to the extent that they are in models of fumarase deficiency. The combined assessment of protein oxidation, succination

and fumarate levels in adipocytes treated with SOD and MitoQ during maturation in high glucose or the *fumarase* knockdown model will further confirm whether endogenous fumarate and ROS compete to react with the same thiol targets.

Our laboratory is currently working to produce a tamoxifen inducible adipose tissue specific *fumarase* knockout mouse to delineate the whole-body ramifications of augmented adipose tissue fumarate production *in vivo*. Preliminary data generated from our laboratory demonstrates that CHOP levels increase in the white adipose tissue from another *fumarase* knockout model (Yang *et al.* 2016). We will continue to investigate several additional roles for CHOP in the regulation of metabolism and inflammation in this model and in human adipose tissue from diabetic patients. We are currently planning chromatin immunoprecipitation (ChIP) studies to detect genes directly regulated by CHOP-DNA interactions in adipocytes matured in high glucose.

Lastly, our laboratory has confirmed that succination increases on ~40 different proteins in the adipocyte during diabetes. We will continue to investigate the significance of other identified sites, and specifically pursue the stoichiometry of protein succination by multiple reaction monitoring mass spectrometry. We are committed to further understanding the quantitative significance of protein succination in the complex network of metabolic stressors occurring present during type 2 diabetes.

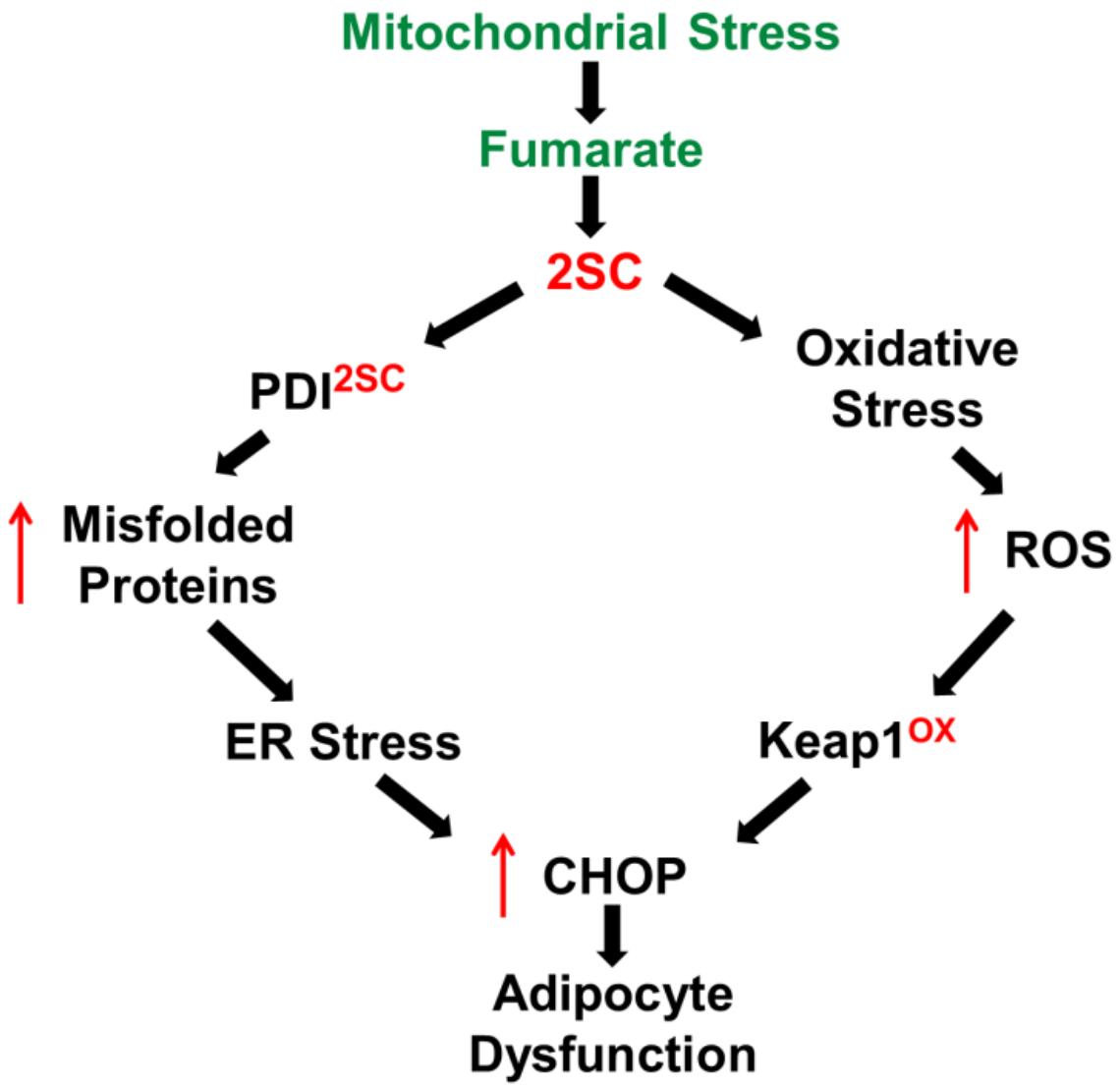

Figure 4.1. Mitochondrial stress drives adipocyte dysfunction during diabetes. The resultant accumulation of fumarate due to mitochondrial stress leads to increased protein succination. Succination of the important endoplasmic reticulum oxidoreductase protein disulfide isomerase (PDI) results in the accumulation of misfolded proteins and the ER stress markerf C/EBP homologous protein (CHOP). Additionally, succination promotes oxidative stress and the build-up of reactive oxygen species (ROS). The modification of Kelch-like ECH-associated protein 1 (Keap1) by ROS coincides with impaired CHOP turnover and the accumulation of CHOP in the nucleus. Nuclear CHOP accumulates in parallel with downregulation of IL-13 mRNA transcription and enhances adipocyte inflammation.

Chapter 5

Materials and Methods

Materials. Unless otherwise noted, all chemicals were purchased from Sigma Aldrich (St. Louis, MO). Anti-2SC antibody was prepared by Eurogentec (Fremont, CA). Insulin was purchased from Bio Ab Chem (Ladson, SC) for *in vitro* studies. Tween-20 and Criterion™ TGX™ Precast Gels were from Bio-Rad (Hercules, CA). Polyvinylidene fluoride (PVDF) was purchased from GE Healthcare (Fairfield, CT). L-glycine and sodium dodecyl sulfate (SDS) were purchased from Fisher Scientific (Waltham, MA). All materials for the Seahorse XF24 were purchased from Seahorse Bioscience (Agilent, Santa Clara, CA) except insulin, glucose and pyruvate. The CyQuant® assay was from Invitrogen (Grand Island, NY). The PROTEOSTAT® PDI assay kit was purchased from Enzo Life Sciences Inc. (Farmingdale, NY) and the Di-Eosin-GSSG was generously provided by Dr. Bulent Mutus, University of Windsor, Ontario, Canada.

Animal Models. Male *db/db* mice (BKS.Cg-Dock7^{m} +/+ Lepr^{db}/J, JAX 000642) and heterozygote control mice were purchased from Jackson Laboratories (Bar Harbor, ME). The mice were obtained at 5-6 weeks of age and allowed to acclimate 1-2 weeks with unrestricted access to food and water before initiation of experimental monitoring. Blood glucose levels were measured at 15 weeks of age after an overnight fast by collecting tail vain blood using a Bayer Contour® (Whippanny, NJ) blood glucose meter for all groups. A glucose oxidase assay was also performed to obtain values for *db/db* mice as some of these surpassed the range of the glucometer. The animals were sacrificed at 15 weeks of age using CO_2 asphyxiation and epididymal adipose tissue was removed and frozen

on dry ice.

Protein Extraction from Adipose Tissue. Adipose tissue was added to 0.5 – 5 mL radio immunoprecipitation assay (RIPA) buffer and sonicated 4 times for 30 seconds each. The tissue was incubated on ice for 10 minutes and centrifuged at 5000 rpm for 10 minutes at 4°C. A supernatant, infranatant and pellet were then visible. The infranatant volume was extracted using a needle and syringe. Acetone (9x volume) was then added to each infranatant sample. The samples were vortexed, allowed to sit on ice for 10 minutes and then centrifuged at 2000 rpm for 10 minutes at 4°C. The acetone was removed completely and the protein pellets were re-suspended in 0.5 mL of RIPA buffer and sonicated two times for 30 seconds each. The protein concentration was determined using the Lowry method.

Cell Culture. 3T3-L1 murine fibroblasts were purchased from American Type Culture Collection (Manassas, VA) and maintained up to 7 passages in Dulbecco's Modified Eagle Medium (DMEM) containing 5 mM glucose, 1% penicillin/streptomycin (CellGro, Corning Life Sciences, Tewksbury, MA) and 10% Fetal Calf Serum (FCS) (Thermo Scientific, Waltham, MA) at 37°C with 95% humidity and 5% CO_2. The medium was changed every 48 hours, with glucose supplementation at 20-24 hour intervals. At 70-80% confluence the fibroblasts were trypsinized (Thermo Scientific, Waltham, MA), neutralized with excess DMEM and collected by centrifugation at 1000 rpm for 5 minutes at 25°C. The fibroblasts were then re-suspended in DMEM for each new passage.

3T3-L1 fibroblasts were seeded at densities of 20,000, 50,000, 90,000

and 300,000 cells/ well for 24-well, 12-well, 6-well plates and 10 cm^2 petri dishes respectively. 3T3-L1 fibroblasts were induced to differentiate to adipocytes 24 hours post-confluence (~4-5 days) in DMEM with 1% penicillin/streptomycin (CellGro), 10% Fetal Bovine Serum (FBS) (Atlanta Biologicals, Flowery Branch, GA), 3-isobutyl-1 methylxanthine (0.5 mM), dexamethasome (IBMX) (0.3 µM), insulin (10 µg/mL) and glucose (30 mM) for 72 hours at 37°C with 95% humidity and 5% CO_2. The differentiation medium was removed at maturation day 0, the cells were washed with PBS and maturation DMEM containing DMEM with 1% penicillin/streptomycin (CellGro), 10% Fetal Bovine Serum (FBS) (Atlanta Biologicals, Flowery Branch, GA), 5 mM glucose/0.3 nM insulin or 30 mM glucose/3 nM insulin was applied. These conditions were selected as we have observed that adipocytes cultured in normal glucose/insulin are a more appropriate control for the high glucose/insulin (diabetic) conditions (Tanis et al. 2015). The medium was changed every 48 hours and the adipocytes were matured for 5, 8 or 12 days. Adipocytes were treated with 2 µM niclosamide upon standard medium change. 10 µM MG132 or 40 µM sulforaphane was added to the maturation medium 3 hours prior to harvest. Adipocytes matured in normal glucose and insulin concentrations were treated with 2, 4 or 6 mM dimethyl succinate for 8 days or 100 µM dimethyl fumarate for 3, 6 or 24 hours. Cells cultured in 5 mM glucose were supplemented with 5-6 mM glucose daily and 5 hours prior to protein harvest in maintain glucose levels.

Lentiviral Vector Production. The lentiviral vectors were prepared by the University of South Carolina Viral Vector Facility. Lentiviral vectors were

generated using a transient transfection protocol, as described in Kantor *et al.*, 2011. TRC2 Fh1 shRNA, clone- TRCN0000246831 or SHC202 MISSION TRC2 pLKO.5-puro non-mammalian shRNA control plasmids (Sigma/Aldrich, St. Louis, MO) were used to generate the lentiviral vectors. The vectors also contained a puromycin resistance gene. 15 µg vector plasmid, 10 µg psPAX2 packaging plasmid (Addgene #12260, Cambridge, MA), 5 µg pMD2.G envelope plasmid (Addgene #12259, Cambridge, MA) and 2.5 µg pRSV-Rev plasmid (Addgene #12253, Cambridge, MA) were transfected into 293T cells. The filtered conditioned medium was collected and stored at -80°C until use. The Keap1-V5 overexpression plasmid was kindly provided by Anil Jaiswal, University of Maryland. The plasmid sequence was validated by PCR and cloned into a lentiviral vector containing green fluorescent protein (GFP) (pLenti-CMV-KEAP1-IRES-GFP). A vector containing the Keap1-V5 sequence in the opposite orientation was used as a control. The vector was produced as described above and the filtered conditioned medium was stored following titer determination.

Lentiviral Vector Transduction. 3T3-L1 fibroblasts were incubated overnight with 150 µL of filtered conditioned medium containing *Fh1* shRNA or control lentivirus. Successfully transduced fibroblasts were selected using 1 µg/mL puromycin. The selected fibroblasts were propagated until confluent, then differentiated to adipocytes and matured for 8 days in 5 or 30 mM glucose as described above. 3T3-L1 fibroblasts or FHKD fibroblasts were differentiated as described above and transduced with the Keap1-V5 plasmid on maturation day 1. Over-expression of the Keap1 protein was monitored in adipocytes via green

fluorescent protein through 5 or 8 days of maturation. Successful maturation in both glucose concentrations was confirmed by the accumulation of lipid droplets in the adipocyte by light microscopy (Nagai *et al.* 2007, Tanis *et al.* 2015).

Seahorse Extracellular Flux Analyzer 24. 3T3-L1 fibroblasts were plated in V7-microassay plates on 0.2% gelatin at 10,000 cells per well. 150 µL of medium was added after 24 hours. Fibroblasts were differentiated as described above and matured for 2 days in 5 mM or 30 mM glucose.

An XF calibrant cartridge was hydrated 24 hours prior to analysis in XF calibrant solution pH 7.4 at 37°C with 0% CO_2. The cells were washed with 750 µL of XF assay buffer pH 7.4 and 600 µL of XF Assay Medium pH 7.4 (Agilent Technologies, Santa Clara, CA), supplemented with 5 mM or 30 mM glucose, 0.3 or 3 nM insulin, and 1 mM sodium pyruvate, was added to replace the culture media 1 hour before the analysis (Tanis 2015). 0.25 µM niclosamide was added to adipocytes by XF analyzer injection after 4 measurements of the basal oxygen consumption rate (OCR). All measurements involved a mixing (3 minutes), a wait (2 minutes) and a measure (3 minutes) period after the addition of the normal medium or the 0.25 µM niclosamide. The OCR data was normalized to the total DNA or protein content of the wells using the CyQuant® Assay (Invitrogen, Grand Island, NY) or Lowry assay, and the data was expressed in pmoles/minute/ng DNA or µg protein (Tanis *et al.* 2015).

Oil Red O Staining. 0.5 grams of Oil Red O was thoroughly mixed in 100 mL isopropanol and diluted 6:4 in nano-pure distilled water. The dye was allowed to stand for 10 minutes and filtered through Whatman No.1 filter paper. 100%

confluent 3T3-L1 fibroblasts and differentiated FHKD adipocytes were fixed for 1 hour in 4% formaldehyde. The cells were washed with PBS, stained with the Oil Red O dye for 1 hour and washed with water. The lipid droplets were visualized by brightfield microscopy and the images were obtained with an Invitrogen™ EVOS™ FL Auto Cell Imaging System (Thermo Fisher Scientific, Waltham, MA).

Amplex Red Assay. FHKD or scrambled control adipocytes were matured in 5 mM or 30 mM glucose in serum free and phenol red free medium for 2.5 hours on day 0 of maturation. The fluorescent Amplex® UltraRed Reagent was resuspended in 1 mL of sterile DMSO and diluted to a 333 µM stock in DMSO. 0.5 U/mL horseradish peroxidase and 10 µM Amplex UltraRed Reagent was added directly to the maturation medium/well. The fluorescence was recorded at 490_{ex} nm and 585_{em} nm every hour for 4 hours. Relative fluorescent units were normalized to total protein content per well following determination by the Lowry assay.

Dichlorofluorescein (DCF) Assay. FHKD or scrambled control adipocytes were matured for 2 days in 5 mM or 30 mM glucose medium. The cells were rinsed with sterile PBS and incubated for 45 minutes at 37°C with 500 µL serum free phenol red free medium and 0.0065 µg/µL DCF. The DCF containing medium was removed and the cells were returned to maturation medium with serum free, phenol red free DMEM. Relative fluorescent units were measured at 485_{ex} nm and 535_{em} nm every 30 minutes for 4 hours.

Cycloheximide Pulse Chase. 3T3-L1 control or FHKD adipocytes were matured in 5 mM or 30 mM glucose for 8 days. Adipocytes (triplicate samples/group) were

harvested at time point 0 hours and 3.5 µg/mL cycloheximide was added to four additional groups, harvested every hour for 4 hours. 10 µM MG132 was added to a separate group of adipocytes for 4 hours.

Glutathione Quantification. Adipocytes were matured for 8 days in the presence of 5 mM or 30 mM glucose with 0, 2.5 or 5 mM NAC, or 100 µM dimethyl fumarate (DMF) for 24 hours. Cells were harvested in 5% salicyclic acid sonicated, allowed to sit on ice for 10 minutes and centrifuged at 14,000 rpm, +4*C for 10 minutes. The supernatant was removed and diluted 1:5 with assay buffer and then diluted 1:6 with sample diluent buffer supplied by the commercially available kit (Arbor Assay Glutathione Fluorescent Detection Kit, Ann Arbor, MI). Total glutathione levels were quantified according to the manufacturer's instructions.

Metabolite Quantification. The quantification of fumarate was performed by GC-MS at the David H. Murdock Research Institute (DHMRI, Kannapolis, NC). Metabolite extraction was performed in an adaptation of previous methods (Piroli 2016). Adipocyte lysates harvested in methanol from confluent 10 cm^2 petri dishes were washed three times with ice-cold PBS followed by the immediate addition of 20 volumes ice-cold chloroform:methanol (2:1). The samples were vortexed and allowed to stand on ice for 10 min with intermittent vortexing prior to addition of 0.2 volumes H_2O. The samples were sonicated and allowed to stand on ice for an additional 2 min, followed by centrifugation at 3,220 x g for 20 min. The aqueous supernatant was transferred into a clean tube and dried under air. The extraction was repeated an additional time by adding equal parts of

methanol and deionized water, centrifuging, and transferring the aqueous layer into the respective tube to dry. The protein interface for each sample was removed for quantification of protein by the Lowry assay.

Prior to derivatization the extracts were resuspended in ethyl acetate and transferred to GC-MS vials. The samples were dried with N_2, and an internal standard (100 µM succinate-$^{13}C_4$, Cambridge Isotope laboratories, Inc.) was added to each of the samples and fumarate standards. The samples and standards were derivatized with 200 µl of methylamine (20 mg/ml in pyridine, M.P. Biomedicals, Solon, OH) at 30°C for 90 min, followed by drying under N_2. This was followed by the addition of 120 µl of N-methyl-N-(trimethylsilyl) trifluoroacetamide (MSTFA, Sigma, St. Louis, MO) with 1% trimethylchlorosilane (TMCS, Sigma, St. Louis, MO); the mixture was incubated at 70°C for 60 min. The derivatized product was stored in a -20°C freezer for one hour. A 100 µl aliquot of the prepared product was transferred to a deactivated glass insert in a 2 ml glass vial (Agilent Technologies, Santa Clara, CA) for GC/MS analysis. An Agilent 7890A GC system, coupled to an Agilent 5975C electron ionization (EI) mass selective detector (MSD) was used to analyze the TMS-derivatized samples. A column with dimensions 30 m × 0.25 mm I.D., 0.25 µm film thickness (Restek, Bellefonte, PA) was used, and the column operation conditions were as follows: helium carrier gas at 1.0 ml/min; GC oven temperature program of 70°C (2 min), 70-100°C (30°C/min, 1 min), 100-140°C (10°C/min, 4 min), 140-188°C (4 °C/min, 12 min), 188-280°C (5 min), with a transfer line temperature of 270°C. The GC-MS was operated under a splitless mode (inlet at 250°C). The mass

spectrometry was performed at an electron energy of -70 eV and the ion source temperature was 230°C. Selected ion monitoring (SIM) was performed for fumarate and the peak areas obtained were normalized to the added internal standard. Absolute quantitation was performed based on standard curves obtained from the normalized reference standards, and the final metabolite concentrations were normalized to the protein content of the cells.

Protein Extraction from Cells. All samples and reagents were kept on ice during protein harvest. The cells were washed 3 times with phosphate buffered saline (PBS) solution, collected in RIPA buffer and sonicated 3 times (10 seconds) at 30 second intervals. Acetone (9 volumes) was added to each sample and the samples were vortexed and incubated on ice for 10 minutes. A protein pellet was generated after centrifugation at 2000 rpm for 10 minutes at 4°C. The supernatant was removed and the protein was re-suspended in RIPA buffer and sonicated 2 times for 30 seconds. Protein concentration was determined by the Lowry method and the samples were stored at -70°C.

Intracellular Organelle Fractionation. 3T3-L1 adipocytes were matured for 8 days as described above. On ice, the cells were washed 3 times with ice cold PBS and once with homogenization buffer (detailed in Appendix A). The cells were scraped into 500 µL of homogenization buffer+ (detailed in Appendix A) and lysed using a glass homogenizer 20 times before passing each lysate through a 25 gauge needle 6 times on ice. The samples were centrifuged at 500 x g for 10 minutes at +4ºC to generate the nuclear pellet, and the supernatant was removed and re-centrifuged at 10,000 x g for 20 minutes at +4ºC to produce the

mitochondrial rich pellet and cytosolic supernatant.

Measurement of Triglycerides and Inflammatory Markers in 3T3-L1 Adipocytes. Control and FHKD adipocytes were matured in 5 mM or 30 mM glucose concentrations for 8 days and harvested in PBS. The triglyceride concentration was measured in 10 µL aliquots of cell lysates utilizing the Infinity™ Triglycerides assay kit (Thermo Fisher Scientific, Waltham, MA), according to the manufacturer's instructions. The media on scrambled control or FHKD 3T3-L1 adipocytes matured for 6 days was replaced with serum-free DMEM for 6 hrs prior to collection of conditioned media. Pro-inflammatory cytokines in serum-free conditioned media were analyzed by ELISA according to the manufacturer's instructions (Mouse Obesity ELISA, Signosis, Santa Clara, CA). Secreted IL-13 levels were determined by the abcam® Mouse ELISA kit according to the manufacturer's instructions (Interleukin-13 Mouse ELISA, abcam®, Cambridge, UK).

Western Blotting. 15-30 µg cell lysate protein and 30-100 µg mouse epididymal fat protein was diluted to 20 µL total volume with nano-pure deionized water and incubated with 5-7 µL 4X Laemmli loading buffer at 95°C for 15 minutes. The samples were centrifuged at 5000 rpm for 10 seconds and then loaded on 7.5%, 12% or 18% gels and electrophoresed at 200 volts for 60 minutes. The protein was transferred to a PVDF membrane in transfer buffer (0.1% Tris Base, 20% methanol, 79.9% nano-pure deionized water) at 250 mA for 100 minutes or 40 mM overnight at 4°C. The membrane protein loading was visualized with Ponceau Red, followed by blocking in 5% bovine serum albumin (BSA) or 5%

non-fat milk for 1 hour at room temperature, or overnight at 4°C according to the antibody manufacturer's recommendations. Primary polyclonal antibodies to actin (sc-1616), Ero1α (sc-365526), GRP78 (sc-1051) and PDI (sc-30932) were from Santa Cruz Biotechnology Inc. (Dallas, TX). Polyclonal antibodies to cleaved caspase 3 (#9664), fumarase (#4567), PPARγ (#2435) and Keap1 (#4617) were from Cell Signaling (Danvers, MA). The anti-adiponectin antibody was from R&D Systems (AF1119) and the anti-hemeoxygenase1 antibody was from Enzo Life Sciences (ADI-SPA-896D) (Farmingdale, NY). The histone-H3 antibody (05928) was from Merck Millipore (Billerica, MA). Monoclonal antibodies to PDI (MA3-019) and CHOP (MA1-250) and the anti-V5-HRP linked (MA5-15253) antibody were from Pierce (Rockford, IL). The monoclonal C/EBPα (#8178) and citrate synthase (#14309) antibodies were from Cell Signaling (Danvers, MA). The polyclonal anti-2SC antibody was prepared as described previously (Nagai et al. 2007). Chemiluminescent substrate (Thermo Pierce, Rockford, IL) was utilized followed by detection on photographic film (Denville Scientific, Metuchen, NJ). Immunoblots were stripped (62.5 mM Tris, pH 6.8, 2% SDS and 0.7% (v/v) beta mercaptoethanol) for 20 minutes at 67°C prior to re-probing with new primary antibodies. Image J software (National Institute of Health) was used to quantify band intensity by densitometry.

2-Dimensional Polyacrylamide Gel Electrophoresis. 150-200 µg of protein was acetone precipitated from wild-type or *Fh1*$^{-/-}$ MEFs, control and *db/db* adipose tissue, or total PDI immunoprecipitate were re-suspended and incubated for 10 minutes in rehydration buffer (7 M urea, 2M thiourea, 2% CHAPS, 1% IPG

buffer, and 50 mM dithiothreitol (DTT), 3.0% DeStreak, 0.5% ampholytes) at room temperature followed by centrifugation at 10,000 rpm for 5 minutes. Each sample was pipetted into an 11 inch strip and absorbed overnight into IPG strips with a pI range of 3.9-5.1, 4-7 or 3-10 (BioRad, Richmond, CA) in mineral oil. Each IPG strip was placed gel side up on the Ettan™ IGPphor II with a thick paper salt bridge soaked in 150 µL nano-pure deionized water at each end. The electrode was placed on top of the paper salt bridge that overlapped with the IGP strip and the strips were focused to 12,000-14,000 total volt hrs and frozen at -70°C. The next day, 50 mg of DTT and 125 mg of iodoacetamide were each dissolved in 5 mL of equilibration buffer. The IPG strips were allowed to thaw for 5 minutes at room temperature and incubated with 2 mL of DTT equilibration buffer for 15 minutes followed by 15 minutes incubation with 2 mL of iodoacetamide equilibration buffer. During this time the agarose sealing solution was melted in the microwave, a 4-20% 11 cm IPG+1 Criterion™ TGX™ gel was placed into the electrophoresis tank and all excess water at the top of the gel was absorbed by filter paper. Extra equilibration buffer was rinsed off the strips in 1x SDS running buffer and the strips were placed onto the gel with 300 µL agarose sealing solution pipetted around each strip. The tank was filled with 1x SDS running buffer and western blotting was performed as described above.

Protein Immunoprecipitation. 500-1000 µg adipocyte cell lysates was diluted to 500 µL total volume with immunoprecipitation buffer or PBS with 2 µL protease inhibitor, sonicated for 30 seconds and incubated (rotating) with 10 µL of washed Protein G or A agarose beads for 30 minutes. The samples were centrifuged at

5000 rpm for 5 minutes at 4°C and the supernatant transferred to a new clean tube while the beads were discarded. 4-5 µg of anti-PDI, -Ero1α or -CHOP antibodies were added to the supernatant and allowed to rotate overnight at 4°C. 15 µL of Protein G or A agarose beads were washed with 800 µL of PBS, centrifuged at 5000 rpm for 5 mins, re-suspended in 30 µL of PBS and added to each sample with 1 µL protease inhibitor. The samples incubated on the rotating wheel for 3.5 hours at room temperature, centrifuged at 5000 rpm at 4°C for 5 minutes and the supernatant was collected and frozen at -70°C. The beads were washed 4 times with PBS or PBS with 0.1% Tween-20, re-suspended in 2-4x loading buffer and boiled at 95˚C for 8 minutes to remove the bound antibody-antigen complex prior to immunoblotting. Keap1 was immunoprecipitated from control and FHKD adipocytes matured for 6 days that overexpressed the V5-Keap1 plasmid. 400-800 µg of protein was diluted in 350 µL PBS and sonicated for 30 seconds. 15 µL of V5-antigen linked agarose beads were washed 4x with PBS, the protein samples were added to the beads and incubated on the rotating wheel for 1.5 hours. The beads were washed 5 times with PBS and incubated with 2x loading buffer at 100°C for 5 minutes to remove the antibody-antigen complex.

Detection of Ero1 Succination. Ero1α immunoprecipitated from 3T3-L1 adipocytes was resolved by electrophoresis and immunoblotted with anti-2SC and anti-Ero1α antibodies. Recombinant Ero1α isolated from *Escherichia coli* strain BL21(DE3) was generously provided by Dr. Kazutaka Araki (Kyoto Sangyo University, Japan)(Araki et al. 2011). 2.77 µg protein was incubated in 0.1 M

potassium phosphate buffer with 2 mM ethylenediaminetetra acetic acid (EDTA), 100 µM diethylenetriaminepentaacetic acid (DTPA) and either 0, 1, 5 or 25 mM fumarate at 37°C for 24 hours prior to SDS-PAGE and immunoblotting with anti-2SC and anti-Ero1 antibodies.

Protein Succination Identification by Mass Spectrometry. For the identification of succination sites in PDI, 2.0 µg of recombinant PDI was incubated with 100 mM fumarate for 24 hrs at 37°C. The sites of endogenous succination of PDI were investigated following immunoprecipitation of PDI from adipocytes matured in 5 mM or 30 mM glucose for 8 days. Endogenous succination of Keap1 was identified following immunoprecipitation of the V5 tagged Keap1 protein over-expressed in FHKD adipocytes for 6 days. In all cases, samples were resolved by SDS-PAGE, and the gels were stained with Coomassie Brilliant blue. After de-staining overnight, the protein was excised from the gel and washed in 20% methanol and 7% acetic acid solution to entirely remove the Coomassie blue stain. The samples were washed with 200 µL of 100 mM ammonium bicarbonate (pH 7.4) and dehydrated via acetonitrile and vacuum centrifugation for 3 minutes. The gel pieces were allowed to rehydrate in 10 mM DTT for 30 minutes at room temperature, followed by alkylation by 170 mM 4-vinylpyridine in methanol for 30 minutes. Next, the protein samples were washed twice with 100mM ammonium bicarbonate (10 minutes) and acetonitrile (5 minutes) and completely dehydrated in the speed vacuum centrifuge for 3 minutes. The gel pieces were rehydrated on ice in 50 mM ammonium bicarbonate buffer with 2 pmol of Promega sequencing grade modified trypsin

(Promega, Madison, WI) and the protein was digested overnight at 37°C. Peptides were then extracted from the gel using 4% formic acid and 20% acetonitrile solution and were concentrated to a total volume less than 15 µL in the speed vacuum centrifuge prior to MS/MS analysis. Selected ion monitoring was performed to identify select pyridylethylated and succinated cysteine containing tryptic peptides. 1 µL of the digested samples were analyzed on a Dionex Ultimate 3000-LC system (Thermo Scientific, Rockford, IL) coupled to a Velos Pro Orbitrap mass spectrometer (Thermo Scientific, Rockford, IL). A 75-µm C18 stationary-phase LC column was used with a 60-min gradient from 2% acetonitrile in 0.1% formic acid solution (solvent A) to 70% solvent A and 30% solvent B (40% water in acetonitrile containing 0.1% formic acid). The Orbitrap was operated in data-dependent MS/MS analysis mode and excluded all ions below 200 counts. An inclusion list of up to 6 abundant isotopic masses +/- 3 amu was used to select the specific peptides for selected resonance monitoring and determination of the site of modification. To further identify specific succinated sites MRM was used to monitor select pyridylethylated and succinated tryptic peptide masses of interest (generated using Protein Calculator software) for CID (collision-induced dissociation)-MS/MS analysis. The data-dependent and CID-MS/MS data were analyzed using Proteome Discover 1.4 software with SEQUEST search engine against the uniprot_database October 2014 (*Mus musculus* 52,474 proteins). The CID-MS/MS data was sequenced manually using Thermo Xcalibur 2.2 software to confirm the modified peptides. The variable modifications of methionine oxidation, proline hydroxylation,

cysteine pyridylethylation (C^{PE}, 105.058 Da) or cysteine succination by fumarate (C^{2SC}, 116.011 Da) were considered in each data search.

PDI Reductase Activity Assays. Recombinant PDI-wild type (WT) and a mutant form of PDI (PDI^{FLFL}) were generously provided by Dr. Danyelle Townsend (Medical University of South Carolina, Charleston, SC). 13.85 µg of recombinant PDI-WT or PDI^{FLFL} was incubated in 0.1 M potassium phosphate buffer (pH 7) with 2 mM EDTA and 0, 1, 5 or 25 mM fumarate for 24 hours at 37°C. PDI reductase activity was monitored according to the PROTEOSTAT® PDI assay kit instructions (Enzo Life Sciences, Inc. Farmingdale, NY). Di-Eosin-GSSG was generously provided by Dr. Bulent Mutus, University of Windsor, Ontario, Canada. 6 µg of protein lysate from 3T3-L1 adipocytes or control and *db/db* adipose tissue was incubated with 1.06 µM Di-Eosin-GSSG, 5 µM DTT and 100 µM DTPA in 0.1 M potassium phosphate buffer, pH 7. Fluorescence was measured kinetically (30 sec intervals) on a TECAN Safire^2 microplate reader at λ_{ex}= 510 nm and λ_{em}= 550 nm.

Data Analysis. All statistical analysis were preformed using the Sigmaplot 11 software, using the student t-test (n=3, *p< 0.05, or **p<0.01, ***p<0.001). PDI reductase activity *in vitro* and glutathione measurements were analyzed using a one way ANOVA (*p<0.05, **p< 0.01).

References

Abizaid A and Horvath TL. Brain Circuits Regulating Energy Homeostasis. *Regul Pept* 149: 3–10, 2008.

Adam J, Hatipoglu E, O'Flaherty L, Ternette N, Sahgal N, Lockstone H, Baban D, Nye E, Stamp GW, Wolhuter K, Stevens M, Fischer R, Carmeliet P, Maxwell PH, Pugh CW, Frizzell N, Soga T, Kessler BM, El-Bahrawy M, Ratcliffe PJ, Pollard PJ Renal cyst formation in Fh1-deficient mice is independent of the Hif/Phd pathway: roles for fumarate in KEAP1 succination and Nrf2 signaling. *Cancer Cell* 20: 524-537, 2011.

Aguirre V., Uchida T., Yenush L., Davis R., White M.F. The c-Jun NH(2)-terminal kinase promotes insulin resistance during association with insulin receptor substrate-1 and phosphorylation of Ser(307) *J Biol Chem* 275:9047–9054, 2000.

Aguirre V., Werner E.D., Giraud J., Lee Y.H., Shoelson S.E., White M.F. Phosphorylation of Ser307 in insulin receptor substrate-1 blocks interactions with the insulin receptor and inhibits insulin action. *J Biol Chem* 277: 1531–1537, 2002

Alderson NL, Wang Y, Blatnik M, Frizzell N, Walla MD, Lyons TJ, Alt N, Carson JA, Nagai R, Thorpe SR, Baynes JW. S-(2-Succinyl)cysteine: a novel chemical modification of tissue proteins by a Krebs cycle intermediate. *Arch Biochem Biophys* 450: 1-8, 2006.

Alhusaini S, McGee K, Schisano B, Harte A, McTernan P, Kumar S, Tripathi G. Lipopolysaccharide, high glucose and saturated fatty acids induce endoplasmic reticulum stress in cultured primary human adipocytes: Salicylate alleviates this stress. *Biochem Biophys Res Commun* 397: 472-478, 2010.

Amano SU, Cohen JL, Vangala P, Tencerova M, Nicoloro SM, Yawe JC, Shen Y, Czech MP, Aouadi M. Local proliferation of macrophages contributes to obesity-associated adipose tissue inflammation. Cell Metab 19: 162-171, 2013.
Cao H. Adipocytokines in obesity and metabolic disease. *J Endocrinol* 220: T47-59, 2014.

Appenzeller-Herzog C, Ellgaard L. The human PDI family: versatility packed into a single fold. *Biochem Biophys Acta* 1783: 535-548, 2008.

Araki K, Nagata K. Functional in vitro analysis of the ERO1 protein and protein-disulfide isomerase pathway. *J Biol Chem* 286: 32705-32712, 2011.

Arruda AP, Pers BM, Parlakgül G, Güney E, Inouye K, Hotamisligil GS. Chronic enrichment of hepatic endoplasmic reticulum-mitochondria contact leads to mitochondrial dysfunction in obesity. *Nat Med* 20: 1427-1435, 2014.

Basseri S, Lhoták Š, Sharma A, Austin RC. The chemical chaperone 4-phenylbutyrate inhibits adipogenesis by modulating the unfolded protein response. *J Lipid Research* 50: 2486-2501, 2009.

Batchvarova N, Wang XZ, Ron D. Inhibition of adipogenesis by the stress-induced protein CHOP (Gadd153). *EMBO J* 14(19):4654-4661, 1995.

Blatnik, M, Frizzell, N, Thorpe, S.R, and Baynes, J.W. Inactivation of glyceraldehyde-3- phosphate dehydrogenase by fumarate in diabetes: formation of S-(2-succinyl)cysteine, a novel chemical modification of protein and possible biomarker of mitochondrial stress. *Diabetes* 57: 41- 49, 2008.

Blewett MM, Xie J, Zaro BW, Backus KM, Altman A, Teijaro JR, Cravatt BF. Chemical proteomic map of dimethyl fumarate-sensitive cysteines in primary human T cells. *Sci Signal* 9: rs10, 2016.

Boden G, Duan X, Homko C, Molina EJ, Song W, Perez O, Cheung P, Merali S. Increase in endoplasmic reticulum stress-related proteins and genes in adipose tissue of obese, insulin-resistant individuals. *Diabetes* 57: 2438-2444, 2008.

Boden G, Cheung P, Kresge K, Homko C, Powers B, Ferrer L. Insulin resistance is associated with diminished endoplasmic reticulum stress responses in adipose tissue of healthy and diabetic subjects. *Diabetes* 63: 2977-2983, 2014a.

Boden G, Cheung P, Salehi S, Homko C, Loveland-Jones C, Jayarajan S, Stein TP, Williams KJ, Liu ML, Barrero CA, Merali S. Insulin regulates the unfolded protein response in human adipose tissue. *Diabetes* 63: 912-922, 2014b.

Boden G, Homko C, Barrero CA, Stein TP, Chen X, Cheung P, Fecchio C, Koller S, Merali S. Excessive caloric intake acutely causes oxidative stress, GLUT4 carbonylation, and insulin resistance in healthy men. *Sci Transl Med* 7: 304re7, 2015.

Brownlee M. The pathobiology of diabetic complications: a unifying mechanism. *Diabetes* 54: 1615-1625, 2005.

Campbell JE, Drucker DJ. Pharmacology, physiology, and mechanisms of incretin hormone action. *Cell Metab* 17: 819-837, 2013.

Canning P, Sorrell FJ, Bullock AN. Structural basis of Keap1 interactions with Nrf2. Free Radic Biol Med 88: 101–107, 2015.

Alam J, Stewart D, Touchard C, Boinapally S, Choi AMK and Cook JL. Nrf2, a Cap'n'Collar Transcription Factor, Regulates Induction of the Heme Oxygenase-1 Gene J Biol Chem 274, 26071-26078

Cao Z, Umek R.M, McKnight S.L. Regulated expression of three C/EBP isoforms during adipose conversion of 3T3-L1 cells. *Genes & Dev* 5: 1538–1552, 1991.

Carrière A, Carmona MC, Fernandez Y, Rigoulet M, Wenger RH, Pénicaud L, Casteilla L. Mitochondrial reactive oxygen species control the transcription factor CHOP-10/GADD153 and adipocyte differentiation: a mechanism for hypoxia-dependent effect. *J Biol Chem* 279: 40462-40469, 2004.

Chang LC, Huang KC, Wu YW, Kao HL, Chen CL, Lai LP, Hwang JJ, Yang WS. The clinical implications of blood adiponectin in cardiometabolic disorders. *J Formos Med Assoc.*108: 353-366, 2009.

Chen YB, Brannon AR, Toubaji A, Dudas ME, Won HH, Al-Ahmadie HA, Fine SW, Gopalan A, Frizzell N, Voss MH, Russo P, Berger MF, Tickoo SK, Reuter VE. Hereditary leiomyomatosis and renal cell carcinoma syndrome-associated renal cancer: recognition of the syndrome by pathologic features and the utility of detecting aberrant succination by immunohistochemistry. *Am J Surg Pathol* 38: 627-637, 2014.

Cinti S., Mitchell G., Barbatelli G., Murano I., Ceresi E., Faloia E., Wang S., Fortier M., Greenberg A. S., Obin M. S. Adipocyte death defines macrophage localization and function in adipose tissue of obese mice and humans. *J. Lipid Res* 46: 2347–2355, 2005.

Circu ML, Aw TY. Reactive oxygen species, cellular redox systems, and apoptosis. *Free Radic Biol Med* 48: 749-762, 2010.

Cohen P, Spiegelman BM. Cell biology of fat storage. *Mol Biol Cell* 27: 2523-2527, 2016.

Curtis JM, Hahn WS, Stone MD, Inda JJ, Droullard DJ, Kuzmicic JP, Donoghue MA, Long EK, Armien AG, Lavandero S, Arriaga E, Griffin TJ, Bernlohr DA. Protein carbonylation and adipocyte mitochondrial function. *J Biol Chem* 287: 32967-32980.

Cusi K. The role of adipose tissue and lipotoxicity in the pathogenesis of type 2 diabetes. *Curr Diab Rep* 10: 306-315, 2010.

Dai X, Ding Y, Liu Z, Zhang W, Zou MH. Phosphorylation of CHOP (C/EBP Homologous Protein) by the AMP-Activated Protein Kinase Alpha 1 in Macrophages Promotes CHOP Degradation and Reduces Injury-Induced Neointimal Disruption In Vivo. *Circ Res* 119: 1089-1100, 2016.

DeZwaan-McCabe D, Riordan JD, Arensdorf AM, Icardi MS, Dupuy AJ, Rutkowski DT. The stress-regulated transcription factor CHOP promotes hepatic inflammatory gene expression, fibrosis, and oncogenesis. *PLoS Genet* 9: e1003937, 2013.

Den Hartigh LJ, Omer M, Goodspeed L, Wang S, Wietecha T, O'Brien KD, Han CY. Adipocyte-Specific Deficiency of NADPH Oxidase 4 Delays the Onset of Insulin Resistance and Attenuates Adipose Tissue Inflammation in Obesity. *Arterioscler Thromb Vasc Biol* 37: 466-475, 2017.

Deng Y and Scherer PE. Adipokines as novel biomarkers and regulators of the metabolic syndrome. *Ann N Y Acad Sci* 1212: E1–E19, 2010.

Díaz-Ruiz A, Guzmán-Ruiz R, Moreno NR, García-Rios A, Delgado-Casado N, Membrives A, Túnez I, El Bekay R, Fernández-Real JM, Tovar S, Diéguez C, Tinahones FJ, Vázquez-Martínez R, López-Miranda J , Malagón MM. Proteasome Dysfunction Associated to Oxidative Stress and Proteotoxicity in Adipocytes Compromises Insulin Sensitivity in Human Obesity. *Antioxid Redox Signal* 23: 597-612, 2015.

Fehse F, Trautmann M, Holst JJ, Halseth AE, Nanayakkara N, Nielsen LL, Fineman MS, Kim DD, Nauck MA. Exenatide augments first- and second-phase insulin secretion in response to intravenous glucose in subjects with type 2 diabetes. *J Clin Endocrinol Metab* 90: 5991-5997, 2005.

Finsterer J. Leigh and Leigh-like syndrome in children and adults. *Pediatr. Neurol* 39: 223-235, 2008.

Fisher-Wellman KH1, Gilliam LA, Lin CT, Cathey BL, Lark DS, Neufer PD. Mitochondrial glutathione depletion reveals a novel role for the pyruvate dehydrogenase complex as a key H2O2-emitting source under conditions of nutrient overload. *Free Radic Biol Med* 65: 1201-1208, 2013.

Frizzell N, Rajesh M, Jepson M, Nagai R, Carson JA, Thorpe SR, and Baynes JW. Succination of Thiol Groups in Adipose Tissue Proteins in Diabetes Succination Inhibits Polymerization and Secretion of Adiponectin. *J Biol Chem* 284: 25772-25781, 2009.

Frizzell N, Thomas SA, Carson JA, Baynes JW. Mitochondrial stress causes increased succination of proteins in adipocytes in response to glucotoxicity. *Biochem J* 44: 247-254, 2012.

Frohnert BI, Sinaiko AR, Serrot FJ, Foncea RE, Moran A, Ikramuddin S, Choudry U, Bernlohr DA. Increased adipose protein carbonylation in human obesity. *Obesity (Silver Spring)* 19: 1735-1741, 2011.

Fullerton MD, Galic S, Marcinko K, Sikkema S, Pulinilkunnil T, Chen ZP, O'Neill HM, Ford RJ, Palanivel R, O'Brien M, Hardie DG, Macaulay SL, Schertzer JD, Dyck JR, van Denderen BJ, Kemp BE, Steinberg GR. Single phosphorylation sites in Acc1 and Acc2 regulate lipid homeostasis and the insulin-sensitizing effects of metformin. *Nat Med* 19: 1649-1654, 2013.

Ghoreschi K, Brück J, Kellerer C, Deng C, Peng H, Rothfuss O, Hussain RZ, Gocke AR, Respa A, Glocova I, Valtcheva N, Alexander E, Feil S, Feil R, Schulze-Osthoff K, Rupec RA, Lovett-Racke AE, Dringen R, Racke MK, Röcken M. Fumarates improve psoriasis and multiple sclerosis by inducing type II dendritic cells. *J Exp Med* 208: 2291-2303, 2011.

Giordano A, Murano I, Mondini E, Perugini J, Smorlesi A, Severi I, Barazzoni R, Scherer PE, Cinti S. Obese adipocytes show ultrastructural features of stressed cells and die of pyroptosis. *J Lipid Res* 54: 2423-2436, 2013.

Gold R, Linker RA, Stangel M. Fumaric acid and its esters: an emerging treatment for multiple sclerosis with antioxidative mechanism of action. *Clin Immunol* 142: 44-48, 2012.

Gregor MF, Yang L, Fabbrini E, Mohammed BS, Eagon JC, Hotamisligil GS, Klein S. Endoplasmic reticulum stress is reduced in tissues of obese subjects after weight loss. *Diabetes* 58: 693-700, 2009.

Gregor MF, Hotamisligil GS. Inflammatory mechanisms in obesity. *Annu Rev Immunol* 29: 415–445, 2011.

Grimsrud PA, Xie H, Griffin TJ, Bernlohr DA. Oxidative stress and covalent modification of protein with bioactive aldehydes. *J Biol Chem* 283: 21837-21841, 2008.

Haase J, Weyer U, Immig K, Klöting N, Blüher M, Eilers J, Bechmann I, Gericke M. Local proliferation of macrophages in adipose tissue during obesity-induced inflammation. *Diabetologia* 57: 562-571, 2014.

Håkansson M, de Lecea L, Sutcliffe JG, Yanagisawa M, Meister B. Leptin receptor- and STAT3-immunoreactivities in hypocretin/orexin neurones of the lateral hypothalamus. *J Neuroendocrinol* 11: 653-663, 1999.

Han CY, Umemoto T, Omer M, Den Hartigh LJ, Chiba T, LeBoeuf R, Buller CL, Sweet IR, Pennathur S, Abel ED, Chait A. NADPH oxidase-derived reactive oxygen species increases expression of monocyte chemotactic factor genes in cultured adipocytes. *J Biol Chem* 287: 10379–10393, 2012.

Han CY. Roles of Reactive Oxygen Species on Insulin Resistance in Adipose Tissue. *Diabetes Metab J* 40: 272-279, 2016.

Han J, Murthy R, Wood B, Song B, Wang S, Sun B, Malhi H, Kaufman RJ. ER stress signalling through eIF2 and CHOP, but not IRE1, attenuates adipogenesis in mice. *Diabetologia* 56: 911–924, 2013a.

Han J, Back SH, Hur J, Lin YH, Gildersleeve R, Shan J, Yuan CL, Krokowski D, Wang S, Hatzoglou M, Kilberg MS, Sartor MA, Kaufman RJ. ER-stress-induced transcriptional regulation increases protein synthesis leading to cell death. *Nat Cell Biol* 15: 481-490, 2013b.

Hannss R, Dubiel W. COP9 signalosome function in the DDR. *FEBS Lett* 585: 2845-2852, 2011.

Hauner H. The mode of action of thiazolidinediones. *Diabetes Metab Res Rev* 18: S10-15, 2002.

Hatahet F, Ruddock LW. Protein disulfide isomerase: a critical evaluation of its function in disulfide bond formation. *Antioxid Redox Signal* 11: 2807-2850, 2009.

Hawkins HC, Freedman RB. The reactivities and ionization properties of the active-site dithiol groups of mammalian protein disulphide-isomerase. *Biochem J* 275: 335-339, 1991.

Hoehn KL. Identification of a novel mitochondrial uncoupler that does not depolarize the plasma membrane. *Mol Metab.* 3:114-123, 2013.

Hong F, Freeman ML, Liebler DC. Identification of sensor cysteines in human Keap1 modified by the cancer chemopreventive agent sulforaphane. *Chem Res Toxicol* 18: 1917-1926, 2005.

Hosogai N, Fukuhara A, Oshima K, Miyata Y, Tanaka S, Segawa K, Furukawa S, Tochino Y, Komuro R, Matsuda M, Shimomura I. Adipose tissue hypoxia in obesity and its impact on adipocytokine dysregulation. *Diabetes* 56: 901-911, 2007.

https://www.cdc.gov/diabetes/data/

https://www.cdc.gov/obesity/data/index.html

Hu C, Eggler AL, Mesecar AD, van Breemen RB. Modification of keap1 cysteine residues by sulforaphane. *Chem Res Toxicol* 24: 515-521, 2011.

Huang X, Ordemann J, Müller JM, Dubiel W. The COP9 signalosome, cullin 3 and Keap1 supercomplex regulates CHOP stability and adipogenesis. *Biol Open* 1:705-710, 2012.

Inaba K, Masui S, Iida H, Vavassori S, Sitia R, Suzuki M. Crystal structures of human Ero1α reveal the mechanisms of regulated and targeted oxidation of PDI. *EMBO J.* 29: 3330-43, 2010.

Jauhiainen A, Thomsen C, Strömbom L, Grundevik P, Andersson C, Danielsson A, Andersson MK, Nerman O, Rörkvist L, Ståhlberg A, Åman P, Jiao P, Ma J, Feng B, Zhang H, Diehl JA, Chin YE, Yan W, Xu H. FFA-induced adipocyte inflammation and insulin resistance: involvement of ER stress and IKKβ pathways. *Obesity (Silver Spring)* 19: 483-491, 2011.

Jauhiainen A, Thomsen C, Strömbom L, Grundevik P, Andersson C, Danielsson A, Andersson MK, Nerman O, Rörkvist L, Ståhlberg A, Åman P. Distinct cytoplasmic and nuclear functions of the stress induced protein DDIT3/CHOP/ GADD153. *PLoS One* 7: e33208, 2012.

Kantor B, Bayer M, Ma H, Samulski J, Li C, McCown T, Kafri T. Notable reduction in illegitimate integration mediated by a PPT-deleted, nonintegrating lentiviral vector. *Mol Ther* 19: 547-556, 2011.

Karala AR, Lappi AK, Ruddock LW. Modulation of an active-site cysteine pK_a allows PDI to act as a catalyst of both disulfide bond formation and isomerization. *J Mol Biol* 396: 883-892, 2010.

Kars M, Yang L, Gregor MF, Mohammed BS, Pietka TA, Finck BN, Patterson BW, Horton JD, Mittendorfer B, Hotamisligil GS, Klein S. Tauroursodeoxycholic Acid may improve liver and muscle but not adipose tissue insulin sensitivity in obese men and women. *Diabetes* 59: 1899-1905, 2010.

Kaul N, Forman HJ. Activation of NF kappa B by the respiratory burst of macrophages. *Free Radic Biol Med* 21: 401–405. 1996.

Kawakami M, Murase T, Ogawa H, Ishibashi S, Mori N, Takaku F, Shibata S. Human recombinant TNF suppresses lipoprotein lipase activity and stimulates lipolysis in 3T3-L1 cells *J. Biochem* 101: 331–338, 1987.

Kawasaki N, Asada R, Saito A, Kanemoto S, Imaizumi K. Obesity-induced endoplasmic reticulum stress causes chronic inflammation in adipose tissue. *Sci Rep* 2: 799, 2012.

Kenwood BM, Weaver JL, Bajwa A, Poon IK, Byrne FL, Murrow BA, Calderone JA, Huang L, Divakaruni AS, Tomsig JL, Okabe K, Lo RH, Cameron Coleman G, Columbus L, Yan Z, Saucerman JJ, Smith JS, Holmes JW, Lynch KR, Ravichandran KS, Uchiyama S, Santos WL, Rogers GW, Okusa MD, Bayliss DA,

Kerins MJ, Vashisht A, Liang BX, Duckworth SJ, Praslicka BJ, Wohlschlegel JA, Ooi A. Fumarate mediates a chronic proliferative signal in fumarate hydratase

inactivated cancer cells by increasing transcription and translation of ferritin genes *Mol Cell Biol* doi: 10.1128/MCB.00079-17. [Epub ahead of print], 2017.

Kim I, Xu W, Reed JC. Cell death and endoplasmic reticulum stress: disease relevance and therapeutic opportunities. *Nat Rev Drug Discov* 7: 1013-1030, 2008.

Klett D, Cahoreau C, Villeret M, Combarnous Y. Effect of pharmaceutical potential endocrine disruptor compounds on protein disulfide isomerase reductase activity using di-eosin-oxidized-glutathione. *PLoS One* 5: e9507, 2010.

Kobayashi A, Kang M, Okawa H, Ohtsuji M, Zenke Y, Chiba T, Igarashi K, and Yamamoto M. Oxidative Stress Sensor Keap1 Functions as an Adaptor for Cul3-Based E3 Ligase To Regulate Proteasomal Degradation of Nrf2. *Mol Cell Biol* 24: 7130-7139, 2004.

Kobayashi A, Kang MI, Watai Y, Tong KI, Shibata T, Uchida K, Yamamoto M Oxidative and electrophilic stresses activate Nrf2 through inhibition of ubiquitination activity of Keap1. *Mol Cell Biol* 26: 221-229, 2006.

Lai RK, Goldman P. Organic-acid profiling in adipocyte differentiation of 3T3-F442A cells—Increased production of Krebs cycle acid metabolites. *Metab Clin Exp* 41: 545–547, 1992.

Lappi AK, Lensink MF, Alanen HI, Salo KE, Lobell M, Juffer AH, Ruddock LW. A conserved arginine plays a role in the catalytic cycle of the protein disulphide isomerases. *J Mol Biol* 335: 283-295, 2004.

Lee DF, Kuo HP, Chen CT, Wei Y, Chou CK, Hung JY, Yen CJ, Hung MC. IKKbeta suppression of TSC1 function links the mTOR pathway with insulin resistance. *Int J Mol Med* 22: 633-638, 2008.

Lee SA, Yuen JJ, Jiang H, Kahn BB, Blaner WS. Adipocyte-specific overexpression of retinol-binding protein 4 causes hepatic steatosis in mice. *Hepatology* 64: 1534-1546, 2016.

Lefterova MI, Mullican SE, Tomaru T, Qatanani M, Schupp M, Lazar MA. Endoplasmic reticulum stress regulates adipocyte resistin expression. *Diabetes* 58: 1879-1886, 2009.

Levonen AL, Landar A, Ramachandran A, Ceaser EK, Dickinson DA, Zanoni G, Morrow JD, Darley-Usmar VM. Cellular mechanisms of redox cell signalling: role of cysteine modification in controlling antioxidant defences in response to electrophilic lipid oxidation products. *Biochem J* 378: 373-382, 2004.

Li X, Huang HY, Chen JG, Jiang L, Liu HL, Liu DG, Song TJ, He Q, Ma CG, Ma

D, Song HY, Tang QQ. Lactacystin inhibits 3T3-L1 adipocyte differentiation through induction of CHOP-10 expression. *Biochem Biophys Res Commun* 350: 1-6, 2006.

Li Y, Guo Y, Tang J, Jiang J, Chen Z. New insights into the roles of CHOP-induced apoptosis in ER stress. *Acta Biochim Biophys Sin (Shanghai)* 46: 629-640, 2014.

Lin Y, Berg AH, Iyengar P, Lam TK, Giacca A, Combs TP, Rajala MW, Du X, Rollman B, Li W, Hawkins M, Barzilai N, Rhodes CJ, Fantus IG, Brownlee M, Scherer PE. The hyperglycemia-induced inflammatory response in adipocytes: the role of reactive oxygen species. *J Biol Chem* 280: 4617-4626, 2005.

Linker RA, Lee DH, Ryan S, van Dam AM, Conrad R, Bista P, Zeng W, Hronowsky X, Buko A, Chollate S, Ellrichmann G, Brück W, Dawson K, Goelz S, Wiese S, Scannevin RH, Lukashev M, Gold R. Fumaric acid esters exert neuroprotective effects in neuroinflammation via activation of the Nrf2 antioxidant pathway. *Brain* 134: 678-692, 2011.

Linker RA, Gold R. Dimethyl fumarate for treatment of multiple sclerosis: mechanism of action, effectiveness, and side effects. *Curr Neurol Neurosci Rep*. 13: 394, 2013.

Liu M, Zhou L, Xu A, Lam KS, Wetzel MD, Xiang R, Zhang J, Xin X, Dong LQ, Liu F. A disulfide-bond A oxidoreductase-like protein (DsbA-L) regulates adiponectin multimerization. *Proc Natl Acad Sci U S A.* 105: 18302-18307, 2008.

Liu M, Liu F. Transcriptional and post-translational regulation of adiponectin. *Biochem J.* 425: 41-52, 2010.

Liu M, Chen H, Wei L, Hu D, Dong K, Jia W, Dong LQ, Liu F. Endoplasmic reticulum (ER) localization is critical for DsbA-L protein to suppress ER stress and adiponectin down-regulation in adipocytes. *J Biol Chem* 290: 10143-10148, 2015.

Llamas-Velasco M, Requena L, Adam J, Frizzell N, Hartmann A, Mentzel T. Loss of Fumarate Hydratase and Aberrant Protein Succination Detected With S-(2-Succino)-Cysteine Staining to Identify Patients With Multiple Cutaneous and Uterine Leiomyomatosis and Hereditary Leiomyomatosis and Renal Cell Cancer Syndrome. *Am J Dermatopathol* 38: 887-891, 2016.

Long JZ, Svensson KJ, Bateman LA, Lin H, Kamenecka T, Lokurkar IA, Lou J, Rao RR, Chang MR, Jedrychowski MP, Paulo JA, Gygi SP, Griffin PR, Nomura DK, Spiegelman BM. The Secreted Enzyme PM20D1 Regulates Lipidated Amino Acid Uncouplers of Mitochondria. *Cell* 166: 424-435, 2016.

Luethy JD, Holbrook NJ. Activation of the gadd153 promoter by genotoxic agents: a rapid and specific response to DNA damage. *Cancer Res* 52: 5-10, 1992.

Lumeng CN, Bodzin JL, Saltiel AR. Obesity induces a phenotypic switch in adipose tissue macrophage polarization. *J Clin Invest* 117: 175-184, 2007.

Malhi H, Kropp EM, Clavo VF, Kobrossi CR, Han J, Mauer AS, Yong J, Kaufman RJ. C/EBP homologous protein-induced macrophage apoptosis protects mice from steatohepatitis. *J Biol Chem* 288: 18624-18642, 2013.

Maris M, Overbergh L, Gysemans C, Waget A, Cardozo AK, Verdrengh E, Cunha JP, Gotoh T, Cnop M, Eizirik DL, Burcelin R, Mathieu C. Deletion of C/EBP homologous protein (Chop) in C57Bl/6 mice dissociates obesity from insulin resistance. *Diabetologia* 55: 1167-1178, 2012.

Martínez-Acedo P, Gupta V, Carroll KS. Proteomic analysis of peptides tagged with dimedone and related probes. *J Mass Spectrom* 49: 257-265, 2014.

McMahon, M, Lamont,D.J, Beattie,K.A, Hayes,J.D, Keap1 perceives stress via three sensors for the endogenous signaling molecules nitricoxide, zinc, and alkenals. *Proc. Natl. Acad. Sci* 107: 18838–18843, 2010.

Medved I, Brown MJ, Bjorksten AR, Murphy KT, Petersen AC, Sostaric S, Gong X, McKenna MJ. N-acetylcysteine enhances muscle cysteine and glutathione availability and attenuates fatigue during prolonged exercise in endurance-trained individuals. *J Appl Physiol* 97: 1477-85, 2004.

Merkley ED, Metz TO, Smith RD, Baynes JW, Frizzell N. (2014). The succinated proteome. *Mass Spectrom Rev* 33: 98-109, 2014.

Miglio G, Sabatino AD, Veglia E, Giraudo MT, Beccuti M, Cordero F. A computational analysis of S-(2-succino)cysteine sites in proteins. *Biochim Biophys Acta* 1864: 211-218, 2016.

Miller RA, Chu Q, Xie J, Foretz M, Viollet B, Birnbaum MJ. Biguanides suppress hepatic glucagon signalling by decreasing production of cyclic AMP. *Nature* 494: 256-260, 2013.

Minard AY, Wong MK, Chaudhuri R, Tan SX, Humphrey SJ, Parker BL, Yang JY, Laybutt DR, Cooney GJ, Coster AC, Stöckli J, James DE. Hyperactivation of the Insulin Signaling Pathway Improves Intracellular Proteostasis by Coordinately Up-regulating the Proteostatic Machinery in Adipocytes. *J Biol Chem* 291: 25629-25640, 2016.

More VR, Xu J, Shimpi PC, Belgrave C, Luyendyk JP, Yamamoto M, Slitt AL.

Keap1 knockdown increases markers of metabolic syndrome after long-term high fat diet feeding. *Free Radic Biol Med* 16: 85-94, 2013.

Morley TS, Xia JY, Scherer PE. Selective enhancement of insulin sensitivity in the mature adipocyte is sufficient for systemic metabolic improvements. *Nat Commun* 6:7906, 2015.

Muller C, Bandemer J, Vindis C, Camaré C, Mucher E, Guéraud F, Larroque-Cardoso P, Bernis C, Auge N, Salvayre R, Negre-Salvayre A. Protein disulfide isomerase modification and inhibition contribute to ER stress and apoptosis induced by oxidized low density lipoproteins. *Antioxid Redox Signal* 18: 731-742, 2013.

Nagai R, Brock JW, Blatnik M, Baatz JE, Bethard J, Walla MD, Thorpe SR, Baynes JW, Frizzell N. Succination of Protein Thiols During Adipocyte Maturation: A Biomarker of Mitochondrial Stress. *J Biol Chem* 282: 34219–34228, 2007.

Nishida Y, Rardin MJ, Carrico C, He W, Sahu AK, Gut P, Najjar R, Fitch M, Hellerstein M, Gibson BW, Verdin E. SIRT5 Regulates both Cytosolic and Mitochondrial Protein Malonylation with Glycolysis as a Major Target. *Mol Cell* 59: 321-332, 2015.

Ooi A, Wong JC, Petillo D, Roossien D, Perrier-Trudova V, Whitten D, Min BW, Tan MH, Zhang Z, Yang XJ, Zhou M, Gardie B, Molinié V, Richard S, Tan PH, Teh BT, Furge KA. An antioxidant response phenotype shared between hereditary and sporadic type 2 papillary renal cell carcinoma. *Cancer Cell* 20: 511-523, 2011.

Oyadomari S, Mori M. Roles of CHOP/GADD153 in endoplasmic reticulum stress. *Cell Death Differ* 11: 381-389, 2004.

Özcan U, Cao Q, Yilmaz E, Lee AH, Iwakoshi NN, Ozdelen E, Tuncman G, Görgün C, Glimcher LH, Hotamisligil GS. Endoplasmic reticulum stress links obesity, insulin action, and type 2 diabetes. *Science* 306: 457-461, 2004.

Özcan U, Yilmaz E, Özcan L, Furuhashi M, Vaillancourt E, Smith R, Görgün C, Hotamisligil G. (2006). Chemical chaperones reduce ER stress and restore glucose homoeostasis in a mouse model of type 2 diabetes. *Science* 313: 1137-1140, 2006.

Ozes ON, Akca H, Mayo LD, et al: A phosphatidylinositol 3kinase/Akt/mTOR pathway mediates and PTEN antagonizes tumor necrosis factor inhibition of insulin signaling through insulin receptor substrate-1. *Proc Natl Acad Sci USA* 98: 4640-4645, 2001.

Papadopoulou A, D'Souza M, Kappos L, Yaldizli O. Dimethyl fumarate for multiple sclerosis. *Expert Opin Investig Drugs* 19: 1603-1612, 2010.

Park J, Chen Y, Tishkoff DX, Peng C, Tan M, Dai L, Xie Z, Zhang Y, Zwaans BM, Skinner ME, Lombard DB, Zhao Y. SIRT5-mediated lysine desuccinylation impacts diverse metabolic pathways. *Mol Cell* 50: 919-930, 2013.

Peng H, Li H, Sheehy A, Cullen P, Allaire N, Scannevin RH. Dimethyl fumarate alters microglia phenotype and protects neurons against proinflammatory toxic microenvironments. *J Neuroimmunol* 299: 35-44, 2016.

Perry RJ, Zhang D, Zhang XM, Boyer JL, Shulman GI. Controlled-release mitochondrial protonophore reverses diabetes and steatohepatitis in rats. *Science* 347: 1253-1256, 2015.

Phelps DT, Deneke SM, Daley DL, Fanburg BL. Elevation of glutathione levels in bovine pulmonary artery endothelial cells by N-acetylcysteine. *Am J Respir Cell Mol Biol* 7: 293-9, 1992.

Piroli GG, Manuel AM, Walla MD, Jepson MJ, Brock JW, Rajesh MP, Tanis RM, Cotham WE, Frizzell N. Identification of protein succination as a novel modification of tubulin. *Biochem J* 462: 231-245, 2014.

Piroli GG, Manuel AM, Clapper AC, Walla MD, Baatz JE, Palmiter RD, Quintana A, Frizzell N. Succination is increased on select proteins in the brainstem of the Ndufs4 knockout mouse, a model of Leigh syndrome. *Mol Cell Proteomics* 15: 445-461, 2015.

Pollard PJ, Brière JJ, Alam NA, Barwell J, Barclay E, Wortham NC, Hunt T, Mitchell M, Olpin S, Moat SJ, Hargreaves IP, Heales SJ, Chung YL, Griffiths JR, Dalgleish A, McGrath JA, Gleeson MJ, Hodgson SV, Poulsom R, Rustin P, Tomlinson IP. Accumulation of Krebs cycle intermediates and over-expression of HIF1alpha in tumours which result from germline FH and SDH mutations. *Hum Mol Genet* 14: 2231-9223, 2005.

Pollard PJ, Spencer-Dene B, Shukla D, Howarth K, Nye E, El-Bahrawy M, Deheragoda M, Joannou M, McDonald S, Martin A, Igarashi P, Varsani-Brown S, Rosewell I, Poulsom R, Maxwell P, Stamp GW, Tomlinson IP. Targeted inactivation of fh1 causes proliferative renal cyst development and activation of the hypoxia pathway. *Cancer Cell* 11: 311-319, 2007.

Quintana A, Kruse SE, Kapur RP, Sanz E, Palmiter RD. Complex I deficiency due to loss of Ndufs4 in the brain results in progressive encephalopathy resembling Leigh syndrome. *Proc Natl Acad Sci U S A*. 107: 10996-1001, 2010.

Rahman S, Blok RB, Dahl HH, Danks DM, Kirby DM, Chow CW, Christodoulou J,

Thorburn DR. Leigh syndrome: clinical features and biochemical and DNA abnormalities. *Ann Neurol.* 39: 343-351, 1996.

Ranjit S, Boutet E, Gandhi P, Prot M, Tamori Y, Chawla A, Greenberg AS, Puri V, Czech MP. Regulation of fat specific protein 27 by isoproterenol and TNF-α to control lipolysis in murine adipocytes. *J Lipid Res* 52: 221-236, 2011.

Raturi A, Mutus B. Characterization of redox state and reductase activity of protein disulfide isomerase under different redox environments using a sensitive fluorescent assay. *Free Radic Biol Med* 43: 62-70, 2007.

Rehman MB, Tudrej BV, Soustre J, Buisson M, Archambault P, Pouchain D, Vaillant-Roussel H, Gueyffier F, Faillie JL, Perault-Pochat MC, Cornu C, Boussageon R. Efficacy and safety of DPP-4 inhibitors in patients with type 2 diabetes: Meta-analysis of placebo-controlled randomized clinical trials. *Diabetes* Metab 43: 48-58, 2017.

Ron D, Walter P. Signal integration in the endoplasmic reticulum unfolded protein response. *Nat Rev Mol Cell Biol* 8: 519-529, 2007.

Rosen ED, Hsu CH, Wang X, Sakai S, Freeman MW, Gonzalez FJ, Spiegelman BM. C/EBPalpha induces adipogenesis through PPARgamma: a unified pathway. *Genes Dev* 16: 22-26, 2002.

Rosen ED, Spiegelman BM. What we talk about when we talk about fat. *Cell* 156: 20-44, 2014.

Ruecker N, Jansen R, Trujillo C, Puckett S, Jayachandran P, Piroli GG, Frizzell N, Molina H, Rhee KY, Ehrt S. Fumarase Deficiency Causes Protein and Metabolite Succination and Intoxicates Mycobacterium tuberculosis.*Cell Chem Biol* 24: 306-315, 2017.

Ruhoy IS, Saneto RP. The genetics of Leigh syndrome and its implications for clinical practice and risk management. *Appl Clin Genet.* 7: 221-234, 2014.

Rushmore TH, Morton MR, Pickett CB. The antioxidant responsive element. Activation by oxidative stress and identification of the DNA consensus sequence required for functional activity. *J Biol Chem* 266: 11632–11639, 1991.

Rutkevich LA, Cohen-Doyle MF, Brockmeier U, Williams DB. Functional relationship between protein disulfide isomerase family members during the oxidative folding of human secretory proteins. *Mol Biol Cell* 21: 3093-3105, 2010.

Rutter GA, Pinton P. Mitochondria-associated endoplasmic reticulum membranes in insulin signaling. *Diabetes* 63: 3163-3165, 2014.

Samuel Varman T, Shulman Gerald I. Mechanisms for Insulin Resistance: Common Threads and Missing Links. *Cell* 148: 852-871, 2012.

Satoh K, Zhang L, Zhang Y, Chelluri R, Boufraqech M, Nilubol N, Patel D, Shen M, Kebebew E. Identification of Niclosamide as a Novel Anticancer Agent for Adrenocortical Carcinoma. *Clin Cancer Res* [Epub ahead of print], 2016.

Scaiewicz V, Nahmias A, Chung RT, Mueller T, Tirosh B, Shibolet O. CCAAT/Enhancer-Binding Protein omologous (CHOP) Protein Promotes Carcinogenesis in the DEN-Induced Hepatocellular Carcinoma Model. *PLoS One* 8: e81065, 2013.

Schmidt MM, Dringen R. Fumaric acid diesters deprive cultured primary astrocytes rapidly of glutathione. *Neurochem Int* 57:460-467, 2010.

Schröder M, Kaufman RJ. The mammalian unfolded protein response. *Annu Rev Biochem* 74: 739-789, 2005.

Schwenger KJ, Allard JP. Clinical approaches to non-alcoholic fatty liver disease. *World J Gastroenterol* 20: 1712-1723, 2014.

Sciacovelli M, Gonçalves E, Johnson TI, Zecchini VR, Henriques da Costa AS, Gaude E, Drubbel AV, Theobald SJ, Abbo S, Tran M, Rajeeve V, Cardaci S, Foster S, Yun H, Cutillas P, Warren A, Gnanapragasam V, Gottlieb E, Franze K, Huntly B, Maher ER, Maxwell PH, Saez-Rodriguez J, Frezza C. Fumarate is an epigenetic modifier that elicits epithelial-to-mesenchymal transition. *Nature* 537: 544–547, 2016.

Seo YH, Carroll KS. Quantification of protein sulfenic acid modifications using isotope-coded dimedone and iododimedone. *Angew Chem Int Ed Engl* 50: 1342-1345, 2011.

Sha H, He Y, Yang L, Qi L. Stressed out about obesity: IRE1α-XBP1 in metabolic disorders. *Trends Endocrinol Metab* 22: 374-381, 2011.

Sharma NK, Das SK, Mondal AK, Hackney OG, Chu WS, Kern PA, Rasouli N, Spencer HJ, Yao-Borengasser A, Elbein SC. Endoplasmic reticulum stress markers are associated with obesity in nondiabetic subjects. *J Clin Endocrinol Metab* 93: 4532-4541, 2008.

Shi H, Kokoeva M, Inouye K, Tzameli I, Yin H, Flier JS. TLR4 links innate immunity and fatty acid–induced insulin resistance. *J Clin Invest* 116: 3015–3025, 2006.

Smith U, Kahn BB. Adipose tissue regulates insulin sensitivity: role of adipogenesis, de novo lipogenesis and novel lipids. *J Intern Med* 280: 465-475,

2016.

Solinas G, Naugler W, Galimi F, Lee MS, Karin M. Saturated fatty acids inhibit induction of insulin gene transcription by JNK-mediated phosphorylation of insulin-receptor substrates. *Proc Natl Acad Sci U S A.* 103: 16454-16459, 2006.

Solinas G, Karin M. JNK1 and IKKβ: molecular links between obesity and metabolic dysfunction. *FASEB J* 24:2596–2611, 2010.

Solinas G, Becattini B. JNK at the crossroad of obesity, insulin resistance, and cell stress response. *Mol Metab* 6: 174-184, 2016.

Song Z, Xiaoli AM, Zhang Q, Zhang Y, Yang ES, Wang S, Chang R, Zhang ZD, Yang G, Strich R, Pessin JE, Yang F. Cyclin C regulates adipogenesis by stimulating transcriptional activity of CCAAT/enhancer binding protein alpha. *J Biol Chem* pii: jbc.M117.776229, 2017.

Song B, Scheuner D, Ron D, Pennathur S, Kaufman RJ. Chop deletion reduces oxidative stress, improves beta cell function, and promotes cell survival in multiple mouse models of diabetes. *J Clin Invest* 118: 3378-3389, 2008.

Stanford KI, Middelbeek RJ, Townsend KL, Lee MY, Takahashi H, So K, Hitchcox KM, Markan KR, Hellbach K, Hirshman MF, Tseng YH, Goodyear LJ. A novel role for subcutaneous adipose tissue in exercise-induced improvements in glucose homeostasis. *Diabetes* 64: 2002-2014, 2015.

Starkov AA, Fiskum G, Chinopoulos C, Lorenzo BJ, Browne SE, Patel MS, Beal MF. Mitochondrial alpha-ketoglutarate dehydrogenase complex generates reactive oxygen species. *J Neurosci* 24: 7779–7788, 2004.

Stemmer K, Kotzbeck P, Zani F, Bauer M, Neff C, Müller TD, Pfluger PT, Seeley RJ, Divanovic S. Thermoneutral housing is a critical factor for immune function and diet-induced obesity in C57BL/6 nude mice. *Int J Obes (Lond)* 39: 791-797, 2015.

Stephens TW, Basinski M, Bristow PK, Bue-Valleskey JM, Burgett SG, Craft L, Hale J, Hoffmann J, Hsiung HM, Kriauciunas A, MacKellar W, Rosteck PR, Jr, Schoner B, Smith D, Tinsley FC, Zhang XY, Heiman M. The role of neuropeptide Y in the antiobesity action of the obese gene product. *Nature* 377:530–532, 1995.

Sun S, Ji Y, Kersten S, Qi L. Mechanisms of inflammatory responses in obese adipose tissue. *Annu Rev Nutr* 32: 261-286, 2012.

Suzuki T, Gao J, Ishigaki Y, Kondo K, Sawada S, Izumi T, Uno K, Kaneko K, Tsukita S, Takahashi K, Asao A, Ishii N, Imai J, Yamada T, Oyadomari S,

Katagiri H. ER Stress Protein CHOP Mediates Insulin Resistance by Modulating Adipose Tissue Macrophage Polarity. *Cell Rep* 18: 2045-2057, 2017.

Tanis RM, Piroli GG, Day SD, Frizzell N. The effect of glucose concentration and sodium phenylbutyrate treatment on mitochondrial bioenergetics and ER stress in 3T3-L1 adipocytes. *Biochim Biophys Acta* 1853: 213-221, 2015.

Tanaka T, Yoshida N, Kishimoto T, Akira S. Defective adipocyte differentiation in mice lacking the C/EBPbeta and/or C/EBPdelta gene. *EMBO J* 16: 7432–7443, 1997.

Tanti JF, Gremeaux T, van Obberghen E, Le Marchand-Brustel Y. Serine/threonine phosphorylation of insulin receptor substrate 1 modulates insulin receptor signaling. *Jrnl of Biol Chem* 269: 6051–6057, 1994.

Tao H, Zhang Y, Zeng X, Shulman GI, Jin S. Niclosamide ethanolamine-induced mild mitochondrial uncoupling improves diabetic symptoms in mice. *Nat Med.* 20: 1263-1269, 2014.

Tavender TJ, Sheppard AM, Bulleid NJ. Peroxiredoxin IV is an endoplasmic reticulum-localized enzyme forming oligomeric complexes in human cells. *Biochem J* 411: 191-199, 2008.

Tavender TJ, Bulleid NJ. Peroxiredoxin IV protects cells from oxidative stress by removing H2O2 produced during disulphide formation. *J Cell Sci* 123: 2672-2679, 2010.

Ternette N, Yang M, Laroyia M, Kitagawa M, O'Flaherty L, Wolhulter K, Igarashi K, Saito K, Kato K, Fischer R. Inhibition of Mitochondrial Aconitase by Succination in Fumarate Hydratase Deficiency. *Cell Rep* 3: 689-700, 2013.

Thiessen A, Schmidt MM, Dringen R. Fumaric acid dialkyl esters deprive cultured rat oligodendroglial cells of glutathione and upregulate the expression of heme oxygenase 1. *Neurosci Lett* 475: 56-60, 2010.

Thulé PM, Umpierrez G. Sulfonylureas: a new look at old therapy. *Curr Diab Rep* 14: 473, 2014.

Tian XY, Ganeshan K, Hong C, Nguyen KD, Qiu Y, Kim J, Tangirala RK, Tontonoz P, Chawla A. Thermoneutral Housing Accelerates Metabolic Inflammation to Potentiate Atherosclerosis but Not Insulin Resistance. *Cell Metab* 23: 165-178, 2016.

Tiganis T. Reactive oxygen species and insulin resistance: the good, the bad and the ugly. *Cell* 32: 82–89, 2011.

Tomlinson IP, Alam NA, Rowan AJ, Barclay E, Jaeger EE, Kelsell D, Leigh I, Gorman P, Lamlum H, Rahman S, Roylance RR, Olpin S, Bevan S, Barker K, Hearle N, Houlston RS, Kiuru M, Lehtonen R, Karhu A, Vilkki S, Laiho P, Eklund C, Vierimaa O, Aittomäki K, Hietala M, Sistonen P, Paetau A, Salovaara R, Herva R, Launonen V, Aaltonen LA. Germline mutations in FH predispose to dominantly inherited uterine fibroids, skin leiomyomata and papillary renal cell cancer. *Nat. Genet* 30: 406–410, 2002.

Tong, Q., G. Dalgin, H. Xu, C. N. Ting, J. M. Leiden, and G. S. Hotamisligil. Function of GATA transcription factors in preadipocyte-adipocyte transition. *Science* 290:134-138, 2000.

Tong Q, Tsai J, Tan G, Dalgin G, Hotamisligil GS. Interaction between GATA and the C/EBP family of transcription factors is critical in GATA-mediated suppression of adipocyte differentiation. *Mol Cell Biol* 25: 706-715, 2005..

Tontonoz P, Hu E, Spiegelman BM. Stimulation of adipogenesis in fibroblasts by PPAR gamma 2, a lipid-activated transcription factor. *Cell* 79: 1147-1156, 1994

Townsend DM, Manevich Y, He L, Xiong Y, Bowers RR Jr, Hutchens S, Tew KD. Nitrosative stress-induced s-glutathionylation of protein disulfide isomerase leads to activation of the unfolded protein response. *Cancer Res* 69: 7626-7634, 2009.

Tu BP, Weissman JS. The FAD- and O(2)-dependent reaction cycle of Ero1-mediated oxidative protein folding in the endoplasmic reticulum. *Mol Cell* 10: 983-94, 2002.

Ubeda M, Wang XZ, Zinszner H, Wu I, Habener JF, Ron D. Stress-induced binding of the transcriptional factor CHOP to a novel DNA control element. *Mol Cell Biol* 16: 1479-1489, 1996.

Uehara T, Nakamura T, Yao D, Shi ZQ, Gu Z, Ma Y, Masliah E, Nomura Y, Lipton SA. S-nitrosylated protein-disulphide isomerase links protein misfolding to neurodegeneration. *Nature* 441: 513-517, 2006.

Unger RH, Scherer PE, Holland WL. Dichotomous roles of leptin and adiponectin as enforcers against lipotoxicity during feast and famine. *Mol Biol Cell* 24: 3011–3015, 2013.

Wagner GR, Bhatt DP, O'Connell TM, Thompson JW, Dubois LG, Backos DS, Yang H, Mitchell GA, Ilkayeva OR, Stevens RD, Grimsrud PA, Hirschey MD. A Class of Reactive Acyl-CoA Species Reveals the Non-enzymatic Origins of Protein Acylation. *Cell Metab* 25: 823-837, 2017.

Walker KW, Lyles MM, Gilbert HF. Catalysis of oxidative protein folding by mutants of protein disulfide isomerase with a single active-site cysteine.

Biochemistry 35: 1972-1980, 1996.

Wang ND, Finegold MJ, Bradley A, Ou CN, Abdelsayed SV, Wilde MD, Taylor LR, Wilson DR, Darlington GJ. Impaired energy homeostasis in C/EBP alpha knockout mice. *Science* 269: 1108–1112, 1995.

Weisberg S, McCann D, Desai M, Rosenbaum M, Leibel R, and Ferrante A. Obesity is associated with macrophage accumulation in adipose tissue. *J Clin Invest* 112: 1796–1808, 2003.

Wei G, Abraham BJ, Yagi R, Jothi R, Cui K, Sharma S, Narlikar L, Northrup DL, Tang Q, Paul WE, Zhu J, Zhao K. Genome-wide analyses of transcription factor GATA3-mediated gene regulation in distinct T cell types. *Immunity* 35: 299-311, 2011.

White UA and Stephens JM. Transcriptional factors that promote formation of white adipose tissue. *Mol Cell Endocrinol* 318: 10–14, 2010.

Xiao F, Gordge MP. Cell surface thiol isomerases may explain the platelet-selective action of S-nitrosoglutathione. *Nitric Oxide* 25: 303-308, 2011.

Xiong Y, Manevich Y, Tew KD, Townsend DM. S-Glutathionylation of Protein Disulfide Isomerase Regulates Estrogen Receptor α Stability and Function. *Int J Cell Biol* 2012: 273549-273558, 2012.

Xu H, Barnes GT, Yang Q, Tan G, Yang D, Chou CJ, Sole J, Nichols A, Ross JS, Tartaglia LA, Chen H. Chronic inflammation in fat plays a crucial role in the development of obesity-related insulin resistance. *J Clin Invest* 112: 1821-1830, 2003.

Xu J, Kulkarni SR, Donepudi AC, More VR, Slitt AL. Enhanced Nrf2 activity worsens insulin resistance, impairs lipid accumulation in adipose tissue, and increases hepatic steatosis in leptin-deficient mice. *Diabetes* 61: 3208-3218, 2012.

Xue M, Qian Q, Adaikalakoteswari A, Rabbani N, Babaei-Jadidi R, Thornalley PJ. Activation of NF-E2-related factor-2 reverses biochemical dysfunction of endothelial cells induced by hyperglycemia linked to vascular disease. *Diabetes* 57: 2809-2817, 2008.

Xue M, Rabbani N, Momiji H, Imbasi P, Anwar MM, Kitteringham N, Park BK, Souma T, Moriguchi T, Yamamoto M, Thornalley PJ. Transcriptional control of glyoxalase 1 by Nrf2 provides a stress-responsive defence against dicarbonyl glycation. *Biochem J* 443: 213-222, 2012.

Yang M, Soga T, Pollard PJ, Adam J. The emerging role of fumarate as an

oncometabolite. *Front Oncol* 2:85, 2012.

Yang M, Ternette N, Su H, Dabiri R, Kessler BM, Adam J, Teh BT, Pollard PJ. The Succinated Proteome of FH-Mutant Tumours. *Metabolites* 4: 640-654, 2014.

Yeh W.C, Cao Z, Classon M, McKnight S.L. Cascade regulation of terminal adipocyte differentiation by three members of the C/EBP family of leucine zipper proteins. *Genes & Dev* 9: 168–181, 1995.

Zhang J, Nadtochiy SM, Urciuoli WR, Brookes PS. The cardioprotective compound cloxyquin uncouples mitochondria and induces autophagy. *Am J Physiol Heart Circ Physiol.* 310: H29-38, 2016.

Zhou L, Liu M, Zhang J, Chen H, Dong LQ, Liu F. DsbA-L alleviates endoplasmic reticulum stress-induced adiponectin downregulation. *Diabetes* 59: 2809-2816, 2010.

Zhu J. T helper 2 (Th2) cell differentiation, type 2 innate lymphoid cell (ILC2) development and regulation of interleukin-4 (IL-4) and IL-13 production. *Cytokine* 75: 14-24, 2015.

Zito E, Melo EP, Yang Y, Wahlander Å, Neubert TA, Ron D. Oxidative protein folding by an endoplasmic reticulum-localized peroxiredoxin. *Mol Cell* 40: 787-797, 2010.

Appendix A

Buffer Preparations

Radio Immunoprecipitation buffer

50 mM Tris-HCl pH 7.4, 150 mM NaCl, 2mM EDTA, 0.5% sodium deoxycholate, 0.1% SDS, 1% Triton-X. Dissolve in 200 mL with DI water and store at +4. On the day of use, add 2 mM sodium orthovanadate, 2 mM sodium fluoride and protease inhibitor cocktail at 1:1000 dilution.

Sigma Rabbit anti-PDI antibody - IP buffer

Dissolve 10 mM Tris-Base pH 8, 0.1 mM EDTA, 150 mM NaCl and 0.25% Tween-20 in nano-pure water. Add 2 µL protease inhibitor/ sample on the day of use.

10x Wash buffer

200 mM Tris-HCl pH 7.4 in 1 mL DI water. 0.05% Tween-20 was added to 1x wash buffer.

10x Transfer buffer

250 mM Tris- HCl and 1920 mM glycine dissolved in 1 mL DI water.

1x Transfer buffer

700 mL DI water, 200 mL methanol and 100 mL 10x Transfer buffer

10X SDS running buffer

250 mM Tris-HCl, 1920 mM glycine and 1% SDS was added to 1 mL DI water.

Stripping buffer

Add 3.785 grams Tris-Base to ~400 mL nano-pure water pH 6.8. Dissolve 10 grams SDS and bring the final volume to 500 mL with nano-pure water. Before stripping add 7 µL beta-mercaptoethanol/1 mL stripping buffer used.

4x Laemmli loading buffer

Dissolve 0.969 grams Tris-Base in 10 mL nano-pure water and pH 6.8. Add 2.468 grams DTT, 3.2 grams SDS, 16 mL glycerol and ~8 milligrams bromophenol blue for color. Store at -20ºC.

Homogenization buffer for intracellular organelle separation

Dissolve 0.0484 grams Tris-Base in 30 mL nano-pure water and pH 7.4. Add 0.084 grams MOPS, 0.0156 grams DTPA, 0.0152 grams EGTA and 2.74 grams sucrose. Bring the total volume to 40 mL with nano-pure water. Immediately before use, add 2 mM sodium orthovanadate, 2 mM sodium fluoride and protease inhibitor cocktail at 1:1000 dilution (homogenization buffer+).

Coomassie Stain

Stir 400 mL nano-pure water, 100 mL glacial acetic acid and 500 mL methanol for 10 mins. Add 2.5 grams Coomassie Brilliant Blue R-250 (*Do not use G-250*) and stir for at least 2 hours at room temperature. Filter staining solution using a 0.45 µm Zap Cap and vacuum aspirator.

Coomassie Destain

Mix 100 mL methanol, 830 mL nano-pure water and 70 mL acetic acid

Appendix B

3T3-L1 Cell Culture Methods

- Put on gloves and spray your hands with 70% alcohol!
- All cell culture experiments should be done in the cell culture fume hood.
- Do NOT open any sterile cell culture plate, container, medium, insulin, glucose…. (etc.) outside of the cell culture fume hood.
- All glass and plastic pipette tips should be autoclaved and dried before using for cell culture experiments.
- NEVER touch the tip of your cell culture pipettes on another surface!!!! (e.g., the bottle of medium, the side of the cell culture plate, the surface of the fume hood….etc.). If the pipette tip does touch another surface throw out the pipette tip and replace it with a new clean tip.
- Clean the fume hood surface where you will be working with 70% alcohol prior to use.
- Every piece of equipment you will need (pipettes, tubes, medium… etc.) should be cleaned with 70% alcohol before placing the item into the cell culture fume hood.

Thawing 3T3-L1 fibroblasts

1) Place the 1L container of 1g/L glucose DMEM +FCS medium in the cell culture water bath for ~15 minutes.

2) When the FCS medium is warm take the bottle out of the water bath and wipe off any residual water on the outside of the bottle. Then spray the outside of the bottle with 70% alcohol and wipe with a paper towel. Place the bottle into the fume-hood.

3) Clean one 15 mL tube, one T-75cm^2 flask, the 1000 µL pipette and the mechanical pipette with 70% alcohol and place in the fume-hood. You will also need a few 10 mL sterile pipettes located in the top drawer next to the cell culture freezer.

4) Pipette 6 mL of FCS into the 15 mL tube and 10 mL of FCS into the T-75cm^2 flask. Now the work station is set-up and you are ready to get out the vial of cells.

5) Slowly pull the rack out of the nitrogen tank and remove one vial of (P2 or P3) 3T3-L1 fibroblasts from the box. Leave the vial of cells on the countertop while you return the rack of boxes to the liquid nitrogen tank.

6) Allow the vial of cells to thaw at room temperature in the cell culture fume hood, ~10 minutes. Immediately after the cells have thawed, pipette the cells from the vial into the 6 mL of FCS in the 15 mL tube. Centrifuge (located in the Frizzell lab) the 15 mL tube containing the cells at 1000 rpm for 5 minutes at room temperature. A 15 mL balance tube of water is located next to the centrifuge in the Frizzell lab. After centrifugation there will be a SMALL white pellet on the bottom of the 15 mL tube containing the cells.

7) Aspirate all of the medium on top of the pellet using the glass pipettes located in the tall metal cylinder in the fume hood. **DO NOT DISTURB THE CELL PELLET.**

8) Re-suspend the cell pellet in 5 mL of FCS medium by pipetting up and down ~3 times or just until the pellet is completely dissolved.

9) Pipette all 5 mL of re-suspended cells into the 10 mL of FCS in the T-75cm flask. Gently swirl the medium in the flask to mix all the cells into the medium evenly. Label the flask (P3) 3T3-L1 fibroblasts and today's date. Place the flask into the cell culture incubator.

Cell Culture- Passaging Cells

1L container of 1g/L glucose DMEM +FCS medium and sterile PBS warmed to ~37°C in the cell culture water bath

Trypisin- let thaw in the cell culture water bath

15 mL tube	mechanical pipette
new flask	200 µL and 1000 µL pipettes
correct number of plates	Sterile 10 mL cell culture pipettes

1) When the PBS and FCS medium is warm take the bottles out of the water bath and wipe off any residual water on the outside of the bottle. Then spray the outside of the bottle with 70% alcohol and wipe with a paper towel. Place the bottle into the cell culture fume hood.

2) Clean all tools with 70% alcohol and place them into the cell culture fume hood.

3) Place the flask of cells into the cell culture fume hood.

4) Turn the flask upside down and gather all of the medium into the back corner of the flask. Aspirate the FCS medium from the flask and pipette a sufficient amount of sterile PBS onto the cells in the flask. Gently swirl the PBS around the flask to wash the cells and aspirate the PBS.

5) Pipette trypsin onto the flask and place the flask back into the cell culture incubator for ~3 minutes.

    a. 25 cm^2 flask; 1.5 mL trypsin
    b. 75 cm^2 flask; 4 mL trypsin
    c. 150 cm^2 flask; 6 mL trypsin

6) Gently tap the bottom of the flask and use the microscope the make sure the cells have detached from the flask and are floating in the trypsin medium.

7) Pipette enough FCS into the flask to bring the total volume of cells to 12 mL (use the FCS to wash the cells completely off the bottom of the flask). Pipette all of the cells/trypsin/FCS into the 15 mL tube and centrifuge at 1000 rpm for 5 minutes at room temperature. A 15 mL balance tube of water is located next to the centrifuge in the Frizzell lab. After centrifugation there will be a small white pellet on the bottom of the 15 mL tube containing the cells.

8) Aspirate all of the medium on top of the pellet. **DO NOT DISTURB THE CELL PELLET!**

9) Re-suspend the cell pellet in FCS medium by pipetting up and down ~3 times or just until the pellet is completely dissolved.

10) Cell Density: pipette 15 µL of cells into the hemocytometer and place on the microscope. Count the number of cells in each quadrant of the hemocytometer and calculate the average number of cells/ quadrant.

    Example:

    Average 50 cells/0.1 µL = 500 cells/ 1 µL (concentration of cell in the 15 mL tube)

    If you want to plate 50,000 cells/ well…

50,000/500 cells/µL = 100 µL of cells should be pipetted onto each well

11) Pipette FCS medium onto each well and a new flask. Pipette the desired density of cells directly into each well and the flask. Gently swirl/mix the cells and medium thoroughly. Label each plate and the flask with today's date, the passage number and type of the cell. Place the flask into the cell culture incubator.

Cell Culture – Feeding Cells

*Place the tip of the cell culture pipette close to the wall of each well and slowly drip/pipette the cell culture medium down the side of each well.

24-well plate; 500 µL/well 6-well plate; 3 mL/well

12-well plate; 1 mL/well 10 cm2 petri dish; 10 mL/dish

3T3-L1 Fibroblasts

Medium: 1g/L glucose DMEM + 10% Fetal Calf Serum + 1% (100x) Penicillin/streptomycin

1) Plated fibroblasts are fed every 48 hours until 100% confluent.

2) Wait 24 hours after wells are 100% confluent before differentiation

Differentiation

Medium: 1 g/L glucose DMEM + 10% Fetal Bovine Serum + 1% (100x) Penicillin/streptomycin

1/1000 dilution Dexamethasome 1/100 dilution 1mg/mL insulin

1/1000 dilution IBMX 25 mM glucose

1) Slowly aspirate fibroblast medium (FCS)

2) Add a sufficient amount of sterile PBS to each well, gently swirl plate and aspirate PBS off each well

3) Add differentiation medium to each well and place the cells back into the cell culture incubator for 3 days.

3T3-L1 Adipocyte Maturation

Sterile 1 M glucose and 172 nM insulin stocks must be pre-made

5mM glucose medium: 1 g/L glucose DMEM + 10% Fetal Bovine Serum + 1% (100x) Penicillin/streptomycin + 0.3 nM insulin

25 mM glucose medium: 1 g/L glucose DMEM + 10% Fetal Bovine Serum + 1% (100x) Penicillin/streptomycin + 3 nM insulin + 20 mM glucose

1) Slowly aspirate differentiation medium

2) Add a sufficient amount of sterile PBS to each well, gently swirl plate and aspirate PBS off each well

3) Add maturation medium to each well and place the cells back into the cell culture incubator for 2 days

4) The maturation medium must be changed every 48 hours throughout the duration of the experiment

Harvesting Cells

1) Label the correct number of 1.5 mL eppendorf tubes (immediately freeze samples after harvest) or 15 mL tubes (immediately acetone precipitate after harvest).

2) Add 2 mM NaF, 2 mM sodium orthovanadate (SOV) and 1:1000 protease inhibitor to RIPA buffer (RIPA+ buffer).

    a. Stocks of 500 mM NaF and 500 mM SOV and protease inhibitor are all found in the -20 freezer.
    b. Boil the SOV for ~ 7 minutes in the 95°C heating block before you add it to the RIPA buffer. Discard the boiled SOV after use in the trash can. NaF and protease inhibitor may be re-frozen to use again in the -20°C freezer.
    c. You will need 200 µL of RIPA+ buffer/ well on a 6-well plate

d. You will need 500 µL of RIPA+ buffer/ 10 cm plate

3) Place PBS on ice
   a. A stock container of PBS should already be made up in the +4 fridge
   b. You will need total ~100 mL PBS/ 6 well plate
   c. You will need total ~30 mL PBS/ 10 cm plate

4) Wash cell scraper with alcohol pad (wash scraper between each different groups of samples)

5) Take your ice bucket to the cell culture room and remove one 6-well plate from the cell culture incubator. Place the plate IMMEDIATELY on ice and bring the ice bucket back to your lab bench.

6) Discard the cell culture medium into the 1L waste container

7) Wash each well 3x with ICE COLD PBS. Discard PBS into the waste container after each wash.

8) Tilt the plate on ice and pipette off the residual PBS

9) Add 200 µL of RIPA+ buffer to each well and rock the plate around so the buffer covers the entire well. Open your labeled eppendorf tubes.

10) Tilt the plate downward and scrape the cells toward the bottom of the well into the RIPA+ buffer. Keep the plate tilted, do NOT lay the plate flat again

11) Pipette the cells into the open tubes and place immediately on ice.

12) Freeze the samples in the -80°C freezer or sonicate and acetone precipitate the sample.

Appendix C

List of Manuscripts Derived from Dissertation Work

Peer-Reviewed Journal Articles

1. Allison M. Manuel, Michael D. Walla, Boris Kantor, Gerardo G. Piroli, Norma Frizzell. Succination Promotes Oxidative Stress and CHOP Stability in the Adipocyte. *Molecular Metabolism* (In preparation)

2. Gerardo G. Piroli*, Allison M. Manuel*, Tulsi Patel, Michael D. Walla, Jingtian Wang, Liang Shi, Scott A. Lanci, Ashley Galloway, Pavel I. Ortinski, Deanna S. Smith, Norma Frizzell. Protein Succination by Dimethylfumarate Mediates Neuroprotective Responses Independent of Keap1 Activation. *Mol. Cell Proteomics* (In preparation)

3. Manuel AM, Walla MD, Faccenda A, Martin SL, Tanis RM, Piroli GG, Adam J, Kantor B, Mutus B, Townsend DM, Frizzell N. (2017) Succination of Protein Disulfide Isomerase Links Mitochondrial Stress and Endoplasmic Reticulum Stress in the Adipocyte During Diabetes. *Antioxid Redox Signal* PMID: 28376661

4. Piroli GG, Manuel AM, Clapper AC, Walla MD, Baatz JE, Palmiter RD, Quintana A, and Frizzell N. (2015) Succination is increased on select proteins in the brainstem of the Ndufs4 knockout mouse, a model of Leigh syndrome. *Mol. Cell Proteomics* 15: 445-461 PMID: 26450614

5. Piroli GG, Manuel AM, Walla MD, Jepson MJ, Brock JW, Rajesh MP, Tanis RM, Cotham WE, Frizzell N. (2014) Identification of Protein Succination as a Novel Modification of Tubulin. *Biochem J* 462: 231-45. PMID: 24909641

6. Manuel AM, Frizzell N. (2013) Adipocyte protein modification by Krebs cycle intermediates and fumarate ester-derived succination. *Amino Acids* 45: 1243-1247. PMID: 23892396

Literature Review

7. Manuel AM, Frizzell N (2014) What KEAPS Adipocytes Stressed During Diabetes? *IMARS Highlights* 9: 9-13

Appendix D

Antioxidants and Redox Signaling Reprint Permission from Website

4. Retention of Rights
4.1. Author(s) retain the right to self-archive the Author Accepted Manuscript version of their Contribution on their own personal website. Author(s) may also deposit their Author Accepted Manuscript version of the Contribution in any repository, provided it is only made publicly available 12 months after the official publication** or later. The Author(s) may not archive or deposit the final published version (Version of Record), which is published on Liebertpub.com and in the Journal. Furthermore, the Author(s) may only post their Manuscript version provided acknowledgment is given to the original source of publication and a link to the published Contribution in the Journal is inserted. The link must be provided by inserting the Digital Object Identifier (DOI) of the Contribution in the following sentence: "Final publication is available from Mary Ann Liebert, Inc.: http://dx.doi.org/[insert DOI]".

**For purposes of Clause #4, "Official publication" refers to the final published version (version of record) of the Contribution published within an issue of the Journal.
4.2. Mary Ann Liebert, Inc., hereby licenses back to the Author(s) the following rights with respect to the final published version (Version of Record) of the Contribution:
4.2A.The right to send or transmit individuals copies of the Contribution to research colleagues upon their specific request provided no fee is charged, and further provided that there is no systematic distribution of the Contribution (e.g. posting on listservs, repository, website or automated delivery). Posting the final published version on the open internet is not permitted.
4.2B.The right to re-use the Contribution or parts thereof for any publication authored or edited by the Author(s) (excluding journal articles) where such re-use material constitutes less than half of the total material in such publication. In such case, any modifications should be accurately noted. Posting the final published version on the open internet is not permitted.
4.2C.The right to include the Contribution in teaching or training duties at the Author(s) institution/employer including course packs, oral presentation, in-house training, and use in theses/dissertations. The Contribution may not be used in seminars outside of normal teaching obligations (e.g. commercial seminars). Posting the final published version on the open internet is not permitted.

Norma Frizzell
norma.frizzell@uscmed.sc.edu
+1 (803) 216-3521
Payment Method: n/a

Order Details

Antioxidants & redox signaling

Order detail ID:	70580269
Order License Id:	4132640769978
ISSN:	1557-7716
Publication Type:	e-Journal
Volume:	
Issue:	
Start page:	
Publisher:	MARY ANN LIEBERT, INC.

Permission Status: Granted
Permission type: Republish or display content
Type of use: Thesis/Dissertation

Requestor type	Academic institution
Format	Print, Electronic
Portion	chapter/article
Title or numeric reference of the portion(s)	Entire article
Title of the article or chapter the portion is from	Succination of Protein Disulfide Isomerase Links Mitochondrial Stress and Endoplasmic Reticulum Stress in the Adipocyte During Diabetes
Editor of portion(s)	N/A
Author of portion(s)	Manuel AM, Walla MD, Faccenda A, Martin SL, Tanis RM, Piroli GG, Adam J, Kantor B, Mutus B, Townsend DM, Frizzell N.